MODIFIED NANOSTRUCTURED METAL AND METAL OXIDE INCORPORATED REDUCED GRAPHENE-BASED NANOCOMPOSITE FOR ELECTROCHEMICAL SENSOR APPLICATIONS

MARLINDA BINTI AB RAHMAN

FACULTY OF SCIENCE
UNIVERSITY OF MALAYA
KUALA LUMPUR

2017

MODIFIED NANOSTRUCTURED METAL AND METAL OXIDE INCORPORATED REDUCED GRAPHENE-BASED NANOCOMPOSITE FOR ELECTROCHEMICAL SENSORS APPLICATIONS

MARLINDA BINTI AB RAHMAN

THESIS SUBMITTED IN FULFILMENT OF THE REQUIREMENTS FOR THE DEGREE OF DOCTOR OF PHILOSOPHY

DEPARTMENT OF PHYSICS
FACULTY OF SCIENCE
UNIVERSITY OF MALAYA
KUALA LUMPUR

2017

UNIVERSITY OF MALAYA

ORIGINAL LITERARY WORK DECLARATION

Name of Candidate: **MARLINDA BINTI AB RAHMAN**

Registration/Matric No: **SHC130073**

Name of Degree: **DOCTOR OF PHILOSOPHY**

Title of ~~Project Paper/Research Report/Dissertation~~/Thesis ("this Work"):

MODIFIED NANOSTRUCTURED METAL AND METAL OXIDE INCORPORATED REDUCED GRAPHENE-BASED NANOCOMPOSITE FOR ELECTROCHEMICAL SENSOR APPLICATIONS

Field of Study: **EXPERIMENTAL PHYSICS**

I do solemnly and sincerely declare that:

(1) I am the sole author/writer of this Work;
(2) This Work is original;
(3) Any use of any work in which copyright exists was done by way of fair dealing and for permitted purposes and any excerpt or extract from, or reference to or reproduction of any copyright work has been disclosed expressly and sufficiently and the title of the Work and its authorship have been acknowledged in this Work;
(4) I do not have any actual knowledge nor do I ought reasonably to know that the making of this work constitutes an infringement of any copyright work;
(5) I hereby assign all and every rights in the copyright to this Work to the University of Malaya ("UM"), who henceforth shall be owner of the copyright in this Work and that any reproduction or use in any form or by any means whatsoever is prohibited without the written consent of UM having been first had and obtained;
(6) I am fully aware that if in the course of making this Work I have infringed any copyright whether intentionally or otherwise, I may be subject to legal action or any other action as may be determined by UM.

Candidate's Signature Date:

Subscribed and solemnly declared before,

Witness's Signature Date:

Name:

Designation:

ABSTRACT

The selection and development of an active sensing material is very important in order to sense target analytes for variety of electrochemical sensor. Currently, fabrications of functional nanostructured pave more attention in the sensor nanotechnology. It is due to their high surface-to-volume ratio that plays a key role for an efficient transport of electrons and optical excitation. Thus, the aim of this work is on developing and preparing novel reduced graphene oxide based metal and metal oxide with modified nanostructure materials for electrochemical sensors performance. This research work was divided into three parts. The first part is the synthesis, characterization and fabrication of nitrite sensing consists of flower-like zinc oxide (ZnO) nanostructure and reduced functionalized graphene oxide (rFGO) was prepared via a hydrothermal route. The nanocomposite was deposited on the surface of a glassy carbon electrode and studied using impedance spectroscopy. It exhibits excellent electrocatalytic activity toward the oxidation of nitrite over working potential of 0.9 V (vs. Ag/AgCl), it displayed a higher current and lower over potential (reduced by up to ~200 mV) than controlled electrodes. The amperometric current is linearly related to the concentration of nitrite in the 10 μM to 8 mM range, and the detection limit is 33 μM. The second part of this work is synthetic method for the preparation of reduced graphene oxide–gold nanorods in an aqueous medium for electrochemical sensing of dihydronicotinamide adenine dinucleotide (NADH). The gold nanorods (AuNRs) had an average length of 44 ± 3 nm and a width of 12 ± 2 nm. The electrochemical characteristics of the gold nanorod-reduced graphene oxide/glassy carbon electrode (AuNR-RGO/GCE) were studied using cyclic voltammogram, and the NADH sensing was studied using chronoamperogram. The amperometric current increased linearly when the NADH concentration was increased in the range of 1–31 μM, and the lowest detection limit (LOD) was estimated to be 0.22 μM (S/N = 3). The third part of this

work is the preparation of myoglobin-modified gold nanorods incorporating reduced graphene oxide (RGO) were fabricated and deposited on a glassy carbon electrode (GCE) to obtain a sensor for nitric oxide (NO). The AuNRs have an average length of 38 ± 3 nm and a width of 11 ± 1 nm. The GCE modified with the nanohybrid is shown to be a viable sensor for the determination of NO by linear sweep voltammetry. Its electrocatalytic response toward the oxidation of NO is distinctly enhanced compared to other electrodes. The sensor, best operated at a working voltage of 0.85 V (vs. SCE), showed two linear response ranges (from 10 to100 μM, and from 100 to 1000 μM), with a detection limit of 5.5 μM. Furthermore, it exhibits excellent selectivity for NO over common interferents such as $NaNO_3$, and also over electroactive species such as ascorbate, dopamine, glucose, and uric acid. These excellent electrocatalytic properties, wide linear range, low detection limit, high sensitivity, and rapid response time make these modified nanostructures as potential candidate for practical applications.

ABSTRAK

Pemilihan dan pembuatan bahan pengesan yang aktif adalah sangat penting untuk mengesan bahan kimia yang pelbagai bagi penderia elektrokimia. Pada masa ini, fabrikasi sub-fungsi struktur-nano mempelopori dalam bidang nanoteknologi penderia. Ini kerana nisbah permukaan-isipadu yang tinggi memainkan peranan penting untuk pengangkutan elektron dan pengujaan optik yang cekap. Justeru, kajian ini bertujuan untuk membangunkan dan menyediakan graphene oksida novel terturun berasaskan logam dan logam oksida dengan bahan-bahan nanostruktur yang diubah suai untuk prestasi penderia elektrokimia. Kerja penyelidikan ini dibahagikan kepada tiga bahagian. Bahagian pertama adalah sintesis, pencirian dan fabrikasi pengesan nitrit yang terdiri daripada nanostruktur bunga zink oksida (ZnO) graphene oksida berfungsi terturun (rFGO) telah disediakan melalui kaedah hidroterma. Nanokomposit yang telah diendapkan ke atas permukaan elektrod karbon berkaca dan dikaji menggunakan impedans spektroskopi. Ia mempamerkan aktiviti elektrokatalitis yang sangat baik ke arah pengoksidaan bahan nitrit. Pada keupayaan kerja iaitu 0.9 V (vs Ag/AgCl), ia memaparkan arus yang lebih tinggi dan keupayaan lampau yang lebih rendah (menurun sehingga ~ 200 mV) daripada elektrod kawalan. Arus amperometrik berkadar terus dengan kepekatan nitrit dalam julat 10 μM ke 8 mM, dan had pengesanan ialah 33 μM. Bahagian kedua kajian ini adalah kaedah sintetik bagi penyediaan graphene oksida terturun–emas nanorod dalam medium akueus dan diaplikasikan dalam mengesan elektrokimia dihydronicotinamide adenine dinucleotide (NADH). Emas nanorod (AuNRs) mempunyai panjang purata 44 ± 3 nm dan lebar seluas 12 ± 2 nm. Pencirian elektrokimia elektrod karbon berkaca graphene oksida terturun–emas nanorod (AuNR-RGO/GCE) telah dikaji menggunakan kitaran voltammetrik, dan NADH pengesan telah dikaji menggunakan kaedah kronoamperometrik. Arus amperometrik yang kini meningkat secara terus apabila kepekatan NADH bertambah dalam julat 1 – 31 μM dan

had pengesanan terendah dianggarkan ialah 0.22 μM (S/N = 3). Bahagian ketiga kajian ini adalah pengubahsuaian mioglobin-emas nanorod yang digabungkan dengan graphene oksida terturun (RGO) telah direka dan diendapkan ke atas elektrod karbon berkaca (GCE) untuk mengesan nitrik oksida (NO). AuNRs ini mempunyai satu panjang purata 38 ± 3 nm dan lebar seluas 11 ± 1 nm. GCE yang telah diubahsuai dengan nanohibrid menunjukkan satu pengesan yang berdaya maju bagi mengesan NO melalui kaedah voltammetrik ayunan lurus. Tindak balas elektrokatalitis terhadap pengoksidaan NO meningkat berbanding dengan elektrod lain. Penderia terbaik dikendalikan pada voltan keupayaan 0.85 V (vs SCE), dengan mempamerkan dua tindak balas terus dalam julat (dari 10 μM sehingga 100, dan dari 100 ke 1000 μM), dengan had pengesanan ialah 5.5 μM. Selain itu, ia mempamerkan selektiviti yang sangat baik untuk NO mengatasi interferensi yang umum seperti $NaNO_3$, dan juga pelbagai elektroaktif seperti askorbat, dopamine, glukosa dan asid urik. Sifat-sifat elektrokatalitis yang sangat baik, rangkaian lurus yang luas, had pengesanan yang rendah, kepekaan yang tinggi dan masa tindak balas yang cepat menjadikan pengubahsuaian nanostruktur ini sebagai calon yang berpotensi untuk aplikasi praktikal.

ACKNOWLEDGEMENTS

I am grateful to Allah, our Lord and Cherisher for granting me a chance and the ability to successfully complete this PhD journey. This PhD journey was a truly life-changing experience for me. Indeed, without His Help and Will, nothing is accomplished.

First and foremost, I would like to express my sincere thanks to my beloved parents, Mr. Ab Rahman Mohamad and Umi Kethom Abd Rahman, and also my families, especially to my husband Mr. Mohd Faris Anuar for their supportive, understanding and unconditional love within my studies. I could not get to where I stand now without their support.

I would like to express my deepest gratitude to my supportive supervisor, Dr. Huang Nay Ming for his continuous support, encouragement and also guidance of this research. Many thanks go to Dr. Alagasamy Pandikumar and Dr. Subramaniam Jayabal for their helpful discussion throughout the PhD journey. I am also grateful to my former head Low Dimensional Materials Research Centre, Prof. Datin Dr. Saadah Abdul Rahman for providing me opportunities and encouragement during my studies at Department of Physics, University of Malaya.

Special thanks go to my colleagues, lab members and staff at Low Dimensional Materials Research Centre (LDMRC), Department of Physics, who helped me throughout my research and study at University of Malaya. Many thanks go to my colleagues for helping and assisting me in my experiments since the first time I am in solid state laboratory.

Finally, I am gratefully to acknowledge the financial support and laboratory facilities from Postgraduate Research Grant (PPP) (PG121-2014B) from the University of

Malaya. Moreover, I would like to convey thanks to Ministry of Higher Education Malaysia for providing me with MyPhD fund.

TABLE OF CONTENTS

LIST OF FIGURES

LIST OF TABLES

LIST OF ABBREVIATIONS

AA	:	Ascorbic acid
Ag/AgCl	:	Silver/silver chloride
AuNR-rGO	:	Gold nanorod-reduced graphene oxide
AuNR-rGO/GCE	:	Gold nanorod-reduced graphene oxide/glassy carbon electrode
ATP	:	Adenosine-5′-triphosphate
CA	:	Chronoamperometry
$C_{14}H_{25}N_2Na_3O_9Si$	:	N-(trimethoxysilylpropyl) ethylenediamine triacetic acid trisodium salt
$CH_3(CH_2)_{15}N(Br)(CH_3)_3$	:	Cetytrimethylammonium bromide
$C_{21}H_{27}N_7Na_2O_{14}P_2.xH_2O$	:	β-Nicotinamide adenine dinucleotide disodium salt hydrate
CNT	:	Cabon nanotube
CR-GO	:	Chemically reduced graphene oxide
CTAB	:	Cetyl trimethylammonium bromide
CV	:	Cyclic voltammetry
DA	:	Dopamine
DMSO	:	Dimethyl sulfoxide
EDX	:	Energy dispersive X-rays
EIS	:	Electrochemical impedance spectroscopy
ESR	:	Equivalent series resistance
ET	:	Electron transfer
FESEM	:	Field emission scanning electron microscopy
$Fe(CN)_6^{3-}/Fe(CN)_6^{4-}$	:	Ferricyanide

FGO	:	Functionalized graphene oxide
FGS	:	Functionalized graphene sheets
FTIR	:	Fourier transform infrared spectroscopy
f-ZnO@rFGO	:	Flower-like zinc oxide/reduced functionalized graphene oxide
GCE	:	Glassy carbon electrode
GO	:	Graphene oxide
GOD	:	Glucose oxidase
GR/PPy/CS	:	Graphene/polypyrrole/chitosan
GSNO	:	S-nitrosoglutathione
HAC	:	Heteratom-enriched activated carbon
$HAuCl_4.3H_2O$	:	Hydrogen tetrachloroaurate (III) hydrate
Hb/Au/GACS	:	Hemoglobin graphene with biocompatible chitosan
Hb–CPB	:	Hemoglobin–cetylpyridinium bromide
HEX	:	Hexokinase
HRTEM	:	High resolution transmission electron microscopy
LOD	:	Limit of detection
LSV	:	Linear sweep voltammogram
LSPR	:	Localized surface plasmon resonance
Mb	:	Myoglobin
Mb-AuNRs/RGO	:	Myoglobin-gold nanorod/reduced graphene oxide
MGNFs	:	Multilayer graphene nanoflake films
MWCNTs	:	Multi-wall carbon nanotubes
NADH	:	Dihydronicotinamide adenine dinucleotide
NaH_2PO_4	:	Sodium dihydrogen phosphate

Na_2HPO_4	:	Disodium hydrogen phosphate
$NaNO_2$	:	Sodium nitrite
$NH_2NH_2 \cdot xH_2O$	:	Hydrazine hydrate
NiTSPc	:	Nickel tetrasulfonated phthalocyanine
ODA	:	Octadecylamine
*o*PD	:	*o*-phenylenediamine
PAM	:	Polyacrylamide
PBS	:	Phosphate buffer solution
P_3MT	:	Poly-(3-methylthiophene)
PEDOT	:	Poly-(3,4-ethylenedioxythiophene)
PEI/[(PSS/PAH)$_2$/PSS/AuNP]^3	:	Poly-(ethylenimine)/[(poly(sodium 4-styrenesulfonate)/poly(allylamine hydrochloride))$_2$/poly(sodium 4-styrenesulfonate)/gold nanoparticles]^3
PG	:	Pyrolytic graphite
RD-UMEs	:	Ring disk ultramicroelectrodes
rFGO	:	Reduced functionalized graphene oxide
RCF	:	Relative centrifugal force
RGO	:	Reduced graphene oxide
RSD	:	Relative standard deviation
SCE	:	Saturated calomel electrode
SD	:	Standard deviation
SPCEs	:	Screen-printed carbon electrodes
SWCNT	:	Single-walled Carbon Nanotubes
SWV	:	Square wave voltammetry
TETA-silane	:	Triethylenetetraamine-silane

TPDT	:	N^1-[3-(trimethoxysilyl)propyl]diethylenetriamine
UA	:	Uric acid
UV-vis	:	Ultraviolet-visible
XPS	:	X-ray photoelectron
XRD	:	X-ray diffraction
$Zn(CH_3COO)_2 \cdot 2H_2O$	:	Zinc acetate dehydrate

LIST OF SYMBOLS

i–t	:	Current-time
$I_{D/}\, I_G$	:	D- Raman peak/G- Raman peak
i_{LA}	:	Anodic limiting current
i_{LC}	:	Cathodic limiting current
R_{ct}	:	Charge transfer resistance
V	:	Voltage
w	:	Angular frequency
Z_{real}	:	Real phase
Z_{imag}	:	Imaginary phase

LIST OF APPENDICES

CHAPTER 1: INTRODUCTION

1.1 Research Background

A growing variety of biosensors have significant impacts on our everyday life. Key issues to take into consideration toward the integration of biosensing platforms include the demand for minimal costs and the potential for real time monitoring, particularly for point-of-care applications where simplicity must also be considered. In light of these developmental factors, electrochemical approaches are the most promising technologies due to their simplicity, high sensitivity and specificity.

1.2 Sensors

Sensors are the devices, which are composed of an active sensing material with a signal transducer. The role of these two important components in sensors is to transmit the signal without any amplification from a selective compound or from a change in a reaction. These devices produce any one of the signals as electrical, thermal or optical output signals which could be converted into digital signals for further processing (Yogeswaran & Chen, 2008). The sensor can be classified based on the output signals. An electrochemical sensor is able to produce an electrical output signal into digital signal through a series of principal stages via the electrochemical reduction/oxidation process (Frey et al., 2006). Typically, electrochemical sensors have more advantage over the others because the electrodes can detect the materials which are present within the host without any damage. On the other hand, sensors can be broadly classified into two categories such as chemo sensors and biosensors.

The selection and development of an active sensing material is very important in order to sense a target of analyte or set of analytes to prove the sensitivity and selectivity. Recent development in the nanotechnology has given more attention on new materials and devices of desirable properties that useful for variety of electrochemical sensor. Basically, the response obtained in electrochemical sensors is attributed from the

interaction between chemistry and electricity which are based on potentiometric, amperometric, and conductivity measurements. Currently, fabrications of functional nanostructured become new trend in the sensor nanotechnology. It is due to their high surface-to-volume ratio that plays a key role for an efficient transport of electrons and optical excitation. In the fabrication of chemically modified electrochemical sensors, the detection of analytes take into consideration of two main factors; the enhancement in electrocatalytical activity and high selectivity of analytes in the presence of potential interference species (Stetter, 2004).

Graphene-based nanocomposite materials are the most commonly used as the modified electrode due to its excellent electrical conductivity and large surface area (Zhang et al., 2010). The presence of oxygen-containing functional groups and certain amount of defects in the graphene-based nanocomposite materials play a vital role in the electrochemical sensors which makes redox reaction occurs effectively (Pandikumar et al., 2014). However, making composite with metals, metal oxides, metal organic frameworks, polymers, clay, zeolite, and carbonaceous materials acquire excellent electrochemical performance which lead to better detection of target analytes in the presence of interfering species.

Among them, these metal oxide and noble metal nanostructures on graphene forms composite materials have reveals promotional benefits in improving electrochemical properties. The remarkable properties of metal or metal oxide nanostructures incorporated on graphene depicts high electrocatalytic activity, excellent conductivity, and selectivity which makes nanostructures decorated graphene an ideal choice to be used as an electroactive material in electrochemical sensors. In addition, the absence of interfering oxidation and reduction peaks in graphene based nanocomposite with metal or metal oxide nanostructures in the electrochemical sensor shows promising anti-interference effect.

1.3 Scope of Research

As the title of thesis suggests the aim to develop and prepare novel reduced graphene oxide-based nanocomposite material Au and ZnO with nanostructures to achieve an enhanced performance of electrochemical sensors. The key motivation behind this doctoral work is to overcome the limitation of bare electrode in detection of target analytes. Hence, this work is prepared to provide an effective way to resolve this issue by introducing suitable surface modification on the working electrode. The modified electrode is prepared through a simple method using reduced graphene oxide-based nanocomposite materials consisting noble metal, Au nanorods and metal oxide flower-like zinc oxide nanocomposite for electrochemical sensors. This doctoral work also features an effort to understand the relationship between the as-prepared nanocomposite materials and their enhanced electrochemical sensor performance, which could provide guidelines for electrochemical sensor designs in the future.

1.4 Research Objectives

1) To synthesize reduced graphene oxide-based metal and metal oxide nanocomposites consisting gold nanorods and flower-like zinc oxide through the facile method.

2) To investigate morphological nature and evaluate the electrocatalytic activities of reduced graphene oxide-based metal and metal oxide nanocomposites for electrochemical sensors.

3) To study method for the detection of analyte that affects the performance of electrochemical sensors.

4) To understand the laboratory scale fabrication of electrochemical sensors by using the modified reduced graphene oxide-based metal and metal oxide electrodes.

1.5 Outline of Thesis

The structure of this thesis can be summarized as follows.

Chapter 1 begins with the history of the sensor followed by a brief discussion on electrochemical sensor. Then the scopes of the research are highlighted and ended with the objectives of this thesis.

Chapter 2 serves a comprehensive literature review on the background and working principles of electrochemical sensor. This chapter also discussed a thorough literature review on sensor components, remaining challenges for electrochemical sensor and possible application for electrochemical sensor.

Chapter 3 presents the synthetic protocol adopted for the preparation of reduced graphene oxide-based metal and metal oxide nanocomposite materials and its characterization techniques including X-ray photoelectron spectroscopy (XPS), X-ray diffraction (XRD), UV-vis absorption spectroscopy, field-emission scanning electron microscopy (FESEM), High resolution transmission electron microscopy (HRTEM), Fourier transform infrared spectroscopy (FTIR), Raman and photoluminescence (PL) spectroscopic techniques.

Chapter 4 discusses the electrocatalytic activities of flower-like zinc oxide/reduced functionalized graphene oxide (*f*-ZnO@rFGO) nanocomposite toward nitrite ions and an emphasis on the relationship of the rFGO and flower-like zinc oxide content on the electrochemical performance. The analytical performance of *f*-ZnO@rFGO nanocomposite modified electrode in the detection of nitrite ions was discussed.

Chapter 5 demonstrates the preparation, characterization and electrocatalytic performance of reduced graphene oxide–gold (AuNR-RGO) nanorod as a promising material for detection of NADH analyte. The presence of Au nanorods on the reduced graphene oxide sheets helped the enhancement oxidation of NADH. Furthermore, the synergetic effects of the Au nanorods and effective charge transfer process improved the elctrocatalytic performance of electrochemical sensor towards detection NADH analyte.

Chapter 6 reports the preparation and characterization of myoglobin-gold nanorods/reduced graphene oxide (Mb-AuNRs/RGO) nanohybrid. The relationship of the myoglobin and Au nanorods content on reduced graphene oxide with respect to the oxidation of nitric oxide was investigated. The modification with myoglobin and Au nanorods on reduced graphene oxide successfully improve the effective charge transfer towards the detection of nitric oxide analyte.

Chapter 7 summarizes the entire doctoral works that have been presented in this thesis. The proposed future works in electrochemical sensor to improve the sensitivity and selectivity towards variety important analytes with graphene based metal and metal oxide nanostructures are parented in the end of this chapter.

CHAPTER 2: LITERATURE REVIEW

2.1 Historical Overview of Electrochemical Sensor

An overview of analytical chemistry development demonstrates that electrochemical sensors represent the most rapidly growing class of chemical sensors. The history of electrochemical sensors starts basically with the development of the glass electrode by Cremer in 1906 (Cremer, 1906). Haber and his student Klemensiewicz took up the idea in 1909 and made the basis for analytical applications (Haber & Klemensiewicz, 1909). The former wanted to introduce the device as "Haber electrode" causing protests of Cremer. The latter should be given full appreciation of the invention of the glass electrode though Haber dominates the literature (Lubert & Kalcher, 2010). The first amperometric sensor was developed by Clark (Clark, 1956) .The "Clark sensor" electrode was introduced in the 1950s (Astrup & Severinghaus, 1986). Oxygen entering the system through a gas-permeable membrane is reduced to water at a noble metal cathode. Clark (1962) also described the first glucose biosensors in 1962, using his oxygen electrode to determine the depletion of oxygen by the action of glucose oxidase on glucose (Clark et al., 1962). Another important milestone was the invention of a valinomycin-based potassium ion-selective electrode (ISE) in 1970 (Pioda et al., 1970).

2.2 Working Principle of Chemical Sensors

A chemical sensor can be defined as a device that provides continuous information about its environment. Ideally, a chemical sensor provides a certain type of response directly related to the quantity of a specific chemical species. All chemical sensors consist of a transducer, with transforms the response into a detectable signal on modern instrumentation, and a chemically selective layer, which isolates the response of the analyte from its immediate environment. The electrochemical sensors operate by reacting with the analyte of interest by oxidizing or reducing the target gas at a working electrode and producing an electrical signal proportional to the analyte concentration as

shown in Figure 2.1. The outcome response is continuous and reversible. The electrochemical sensor consists of a transduction element covered by a recognition layer. The recognition layer may be chemical or biological materials. The recognition layer is then interacts with target analyte. The transduction element translates the chemical changes into electrical signals. This electrical signal which is related to the concentration of an analyte that been detected.

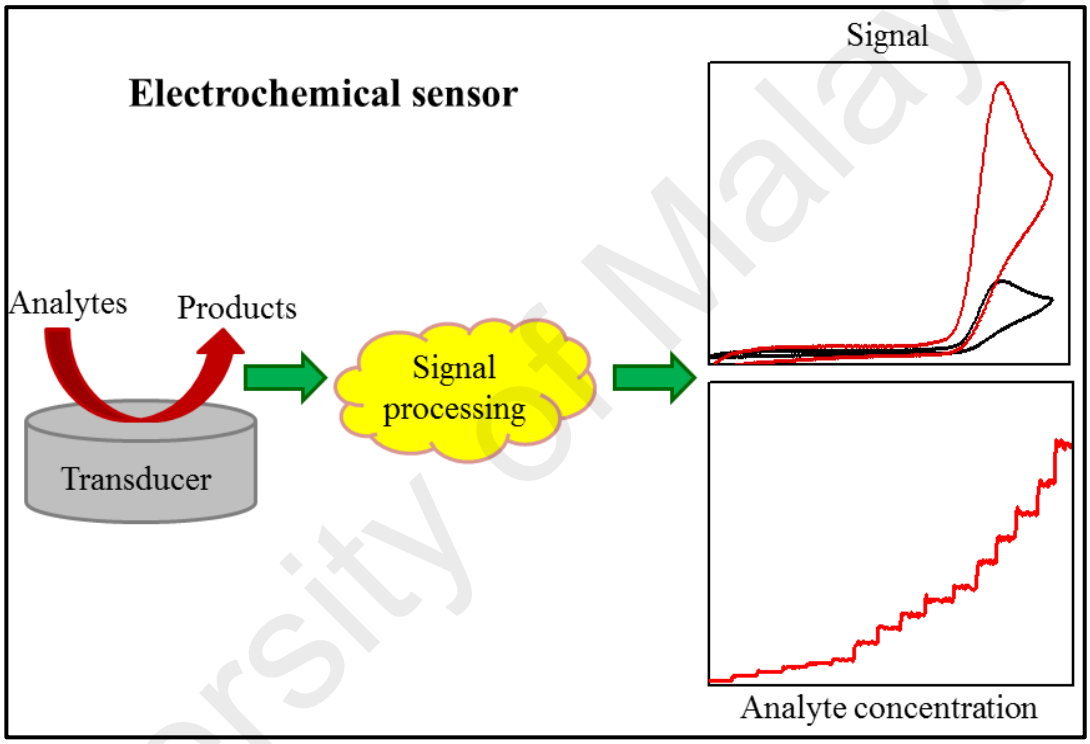

Figure 2.1: Schematic diagram of working principal of electrochemical sensor.

A typical electrochemical sensor consists of a sensing electrode (or working electrode), reference electrode and a counter electrode (auxiliary electrode) in the electrolyte, Figure 2.2.

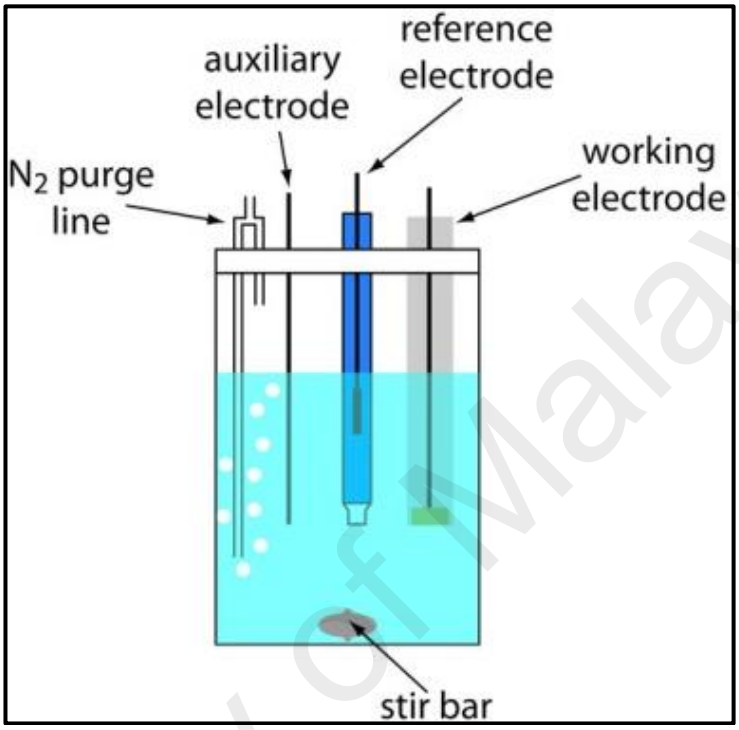

Figure 2.2: Schematic diagram of the three reference electrodes design for electrochemical sensor. (https://chem.libretexts.org)

The development of all voltammetric techniques has been based predominantly on carbonaceous materials as working electrodes. Carbon–based working electrode materials include all allotropic forms of carbons such as graphite, glassy carbon, amorphous carbon, fullerenes, nanotubes, and are all used as important electrode materials in electroanalytical chemistry.

2.3 Principles and Methods of Experimental Evaluation

Electrochemistry provides powerful analytical techniques encompassing the advantages of instrumental simplicity, moderate cost and portability. Modern electrochemical methods are sensitive, selective, rapid and facile techniques applicable to biomedical fields, and indeed in most areas of analytical chemistry. A number of

electrochemical strategies have been explored in the development of nanomaterials based electrochemical sensors for biomedical applications. The electrochemical sensors can use a range of modes of detection such as potentiometric, voltammetric and conductimetric. Each principle requires a specific design of the electrochemical cell.

The voltammogram provides an electroanalytical method, the premise of which is that current is linearly dependent upon the concentration of the electroactive species (analyte) involved in a chemical or biological recognition process (at a scanned or fixed potential). The voltammogram implies a varying voltage voltammetric techniques have been extremely useful in measuring blood levels, metabolites and the urinary excretion of drugs following low doses, especially when coupled with chromatographic methods (Morrin, 2012; Newman & Turner, 2005). Cyclic voltammogram (CV) and linear sweep voltammogram (LSV) have received great interest as they can be used for the elucidation of electrode processes and redox mechanisms (Meng et al., 2012). Differential pulse voltammogram (DPV) (Shah & Chen, 2012) and square wave voltammogram (SWV) (Chatterjee & Chen, 2012) are particularly useful in the determination of trace amounts of electroactive compounds in pharmaceuticals and biological fluids. Stripping voltammetry has also been widely utilized due to its ability to preconcentrate analytes for ultrasensitive detection (Chen et al., 2009). Amperogram is another common electrochemical technique which has been widely employed in electrochemical sensors and biosensors.

2.3.1 Cyclic Voltammogram (CV)

The cyclic voltammogram (CV) is a well-established dynamic electrochemical method to determine oxidation and reducible substances in a solution. On a working electrode the potential is changed linearly with time. A current response depending on the scan rate ($V.s^{-1}$) is recorded. The current density is an indicator of the amount of substances which are oxidized or reduced and the corresponding peak potential is a characteristic for the redox process but also influenced by the electrode material. CV is often carried out in electrochemical cells with micrometer dimensions. For these designs mostly micro-electrode arrays are used to minimize the diffusion effects (Schwarz et al., 2000). The CV consists of cycling the potential of an electrode, which is immersed in an unstirred solution, and measuring the resulting current. The potential of this working electrode is controlled versus a reference electrode such as a saturated calomel electrode (SCE) or a silver/silver chloride electrode (Ag/AgCl). A cyclic voltammogram is obtained by measuring the current at the working electrode during the potential scan. The current can be considered the response signal to the potential excitation signal. The voltammogram is a display of current (vertical axis) versus potential (horizontal axis). Because the potential varies linearly with time, the horizontal axis can also be thought of as a time axis (Kissinger & Heineman, 1983).

A typical cyclic voltammogram is shown in Figure 2.3 for a glassy carbon working electrode in a solution containing 3 mM $Fe(CN)_6^{3-}/Fe(CN)_6^{4-}$ as the electroactive species in 0.1 M KCl in water as the supporting electrolyte. The potential first to scan from -0.20 V to +0.50 V versus Ag/AgCl at which point the scan direction is reversed, causing a scan back to the original potential of 0.20 V with the scan rate is 50 mV/s.

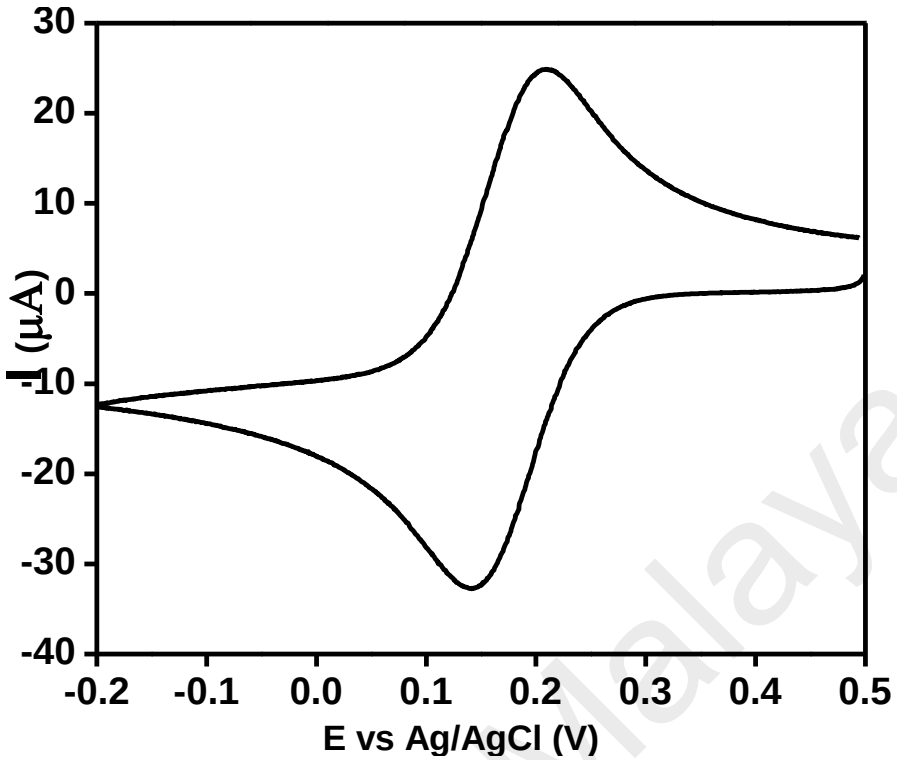

Figure 2.3: CV of a glassy carbon working electrode in a solution containing 3 mM $Fe(CN)_6^{3-}$/$Fe(CN)_6^{4-}$ in 0.1 M KCl.

The initial potential (E_i) of -0.20 V is applied, when the electrode becomes a sufficiently strong oxidant, $Fe(CN)_6^{4-}$, which has been accumulating adjacent to the electrode, can now be oxidized by the electrode process. Equation 2.1 has shown the half chemical equation for the oxidation process:

$$Fe(CN)_6^{4-} \rightarrow Fe(CN)_6^{3-} + e \qquad (2.1)$$

The anodic current rapidly increases until the surface concentration of $Fe(CN)_6^{4-}$ is diminished, causing anodic current peak at ~0.21 V.

When the potential is sufficiently negative to reduce $Fe(CN)_6^{3-}$, cathodic current is occurs at the electrode process as shown in the equation 2.2:

$$Fe(CN)_6^{3-} + e \rightarrow Fe(CN)_6^{4-} \qquad (2.2)$$

The electrode is now a sufficiently strong reductant to reduce $Fe(CN)_6^{3-}$. The cathodic current increases rapidly until the concentration of $Fe(CN)_6^{3-}$ at the electrode surface is substantially diminished, causing the cathodic current peak at ~0.14 V.

Simply stated, in the forward scan $Fe(CN)_6^{3-}$ is electrochemically generated from $Fe(CN)_6^{4-}$ by the oxidation as indicated the anodic current. In the reverse scan this $Fe(CN)_6^{3-}$ is reduced back to $Fe(CN)_6^{4-}$ as indicated by the cathodic current.

2.3.2 Linear Sweep Voltammogram (LSV)

The linear sweep voltammogram is simply cyclic voltammogram without a vertex potential and reverse scan. The LSV involves scanning the potential of the working electrode linearly with time at rates typically, in the range of 10 mV/s to 1000 V/s. The current is plotted as a function to potential to yield a voltammogram.

The diagnostic criteria are developed whereby variation of peak current and peak potential with sweep rate and initial concentration can be used to characterize the mechanism. Figure 2.4 is shown a typical linear sweep voltammogram for ion O and ion R for the reduction and oxidation reactions.

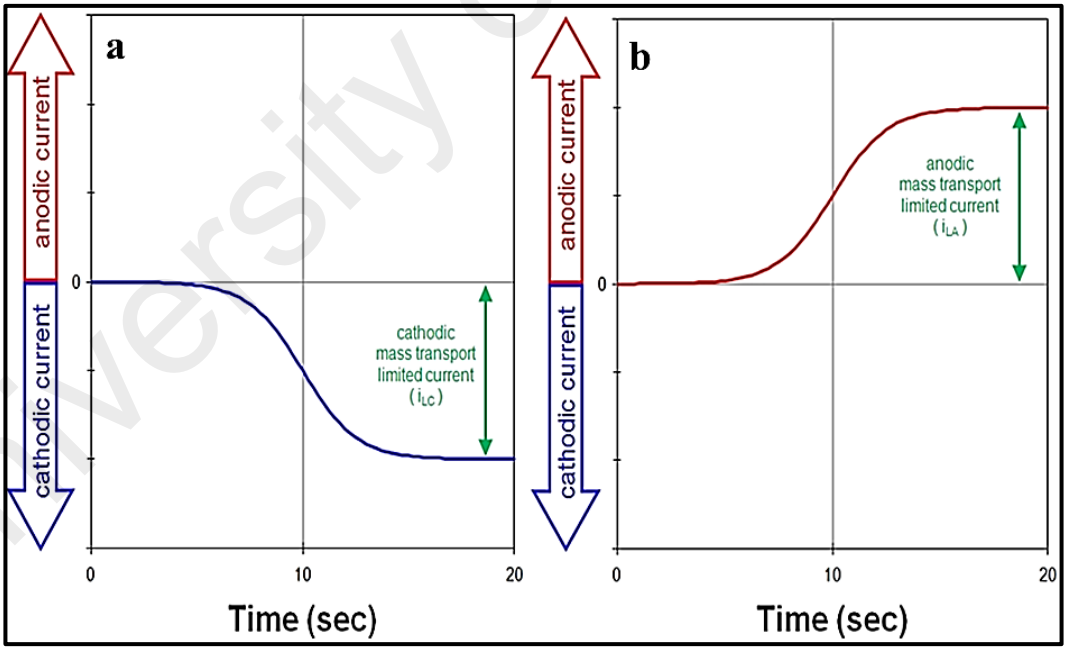

Figure 2.4: A voltammogram plot of current versus potential for cathodic current (a) and anodic current (b).
(Cite: https://www.pineresearch.com/shop/knowledgebase/rotating-electrode-theory)

At the start of the experiment (Figure 2.4 (a)), the bulk solution contains only ion O, so at potentials well positive of the redox potentials, there is no net conversion of ion O to R. As the redox potential is approached, there is a net cathodic current which increases exponentially with potential due to the exponential potential dependence of the rate of heterogeneous electron transfer. The current eventually reaches a maximum value (limiting current) once the applied potential is sufficiently negative relative to the standard electrode potential. At such a negative potential, any oxidized form of the molecule or ion O that reaches the surface of the electrode is immediately converted to the reduced form R as shown in the equation 2.3 below:

$$O + n\,e^{-} \rightarrow R \qquad (2.3)$$

As O is converted to R, concentration gradients are set up for both O and R, and diffusion occurs down these gradients (O diffuses towards the electrode, and R diffuses in the opposite direction. After the (cathodic) peak potential is reached, the current decays as a result of the depletion of O in the interfacial region. The rate of electrolysis (and hence the current) now depends on the rate of mass transport of O from the bulk solution to the electrode surface; that is, it is dependent on the rate of diffusion of O, so the time dependence is $t^{-½}$. The peak is therefore asymmetric. The maximum current observed in this circumstance is called the cathodic limiting current (i_{LC}).

Figure 2.4 (b) the electrode potential is slowly swept in the positive direction and an anodic current is observed. The anodic current eventually reaches a maximum value when the potential is sufficiently positive relative to the standard electrode potential. At this point, any of the reduced form (R) that reaches the electrode surface is immediately converted to the oxidized form (O) as shown in the equation 2.4 below:

$$R \rightarrow O + n\,e^{-} \qquad (2.4)$$

The observed current is the result of electrons flowing into the electrode. The maximum current observed is called the anodic limiting current (i_{LA}).

2.3.3 Chronoamperogram (CA)

Chronoamperogram is a technique where the potential of the working electrode is stepped for a specified period of time. In CA, the working electrode is held at a constant potential while the current as a function of time is monitored. The current plot is then related to the concentration of the analyte present. In the electrochemical cell containing electroactive species, the CA measurements are carried out recording reduction or oxidation currents between the working electrode and the counter electrode when controlled potentials are applied at the working electrode with respect to the reference electrode which may also serve as the auxiliary electrode (Eggins, 2008; Thévenot et al., 2001). The resulting current is directly correlated to the bulk concentration of the electroactive species or its production or consumption rate within the adjacent biocatalytic layer coated on the working electrode, such steady-state currents are usually proportional to the bulk analyte concentration (Thévenot et al., 2001). An example of a sample curve for detection of adenosine-5′-triphosphate (ATP) by using amperometric measurements with a detection limit of 10 nmol/l (Kueng et al., 2004) is shown in Figure 2.5.

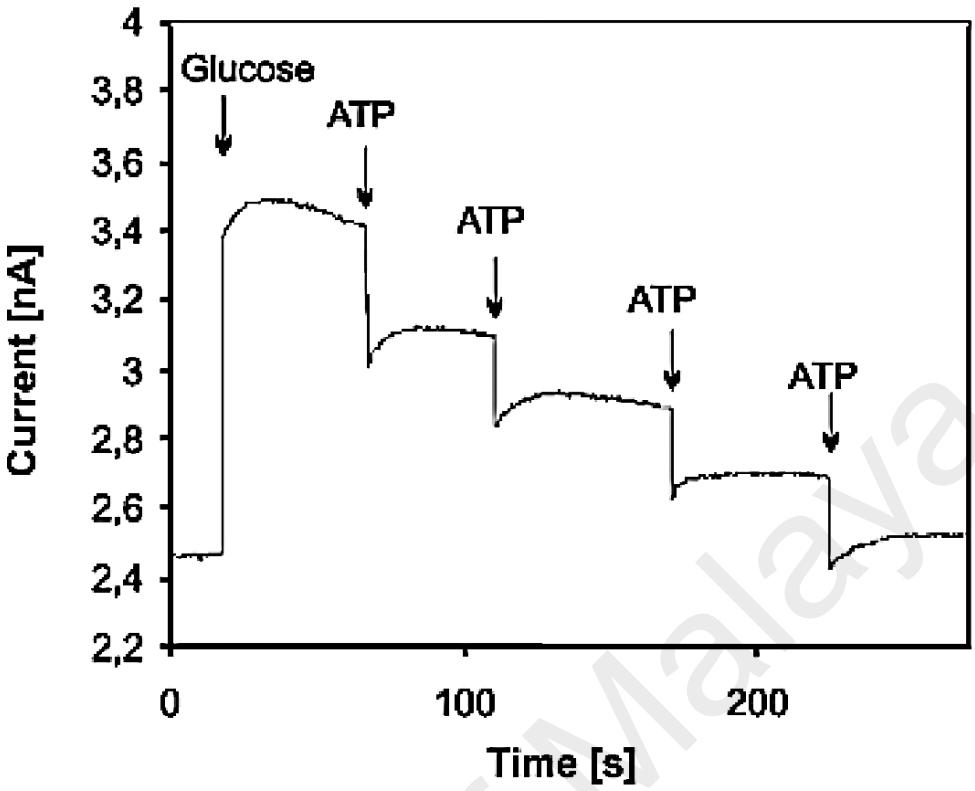

Figure 2.5: A sample amperometric measurement: According to Kueng et al. (2004) this is a typical hydrodynamic response of their biosensor to glucose followed by several injections of ATP measured in phosphate buffer at 650 mV in reference to Ag/AgCl. The change in current response is proportional to the ATP concentration as glucose is consumed at the glucose oxidase (GOD) and hexokinase (HEX) modified electrode surface (Kueng, et al., 2004).

2.3.4 Electrochemical Impedance Spectroscopy (EIS)

Electrochemical impedance spectroscopy is a powerful tool to evaluate the electrochemical system and it's useful for research and development of new electrode materials. It is used to investigate any intrinsic material property or specific processes that could influence the conductivity/resistivity or capacitivity of an electrochemical system. It can accurately measure error-free kinetic and mechanistic information using a variety of techniques and output formats. During an impedance measurement, a frequency response analyzer is used to impose small amplitude of potential in a range of fixed frequency (generally from 100 kHz to 10 mHz). The used of the small amplitude is to ensure minimal perturbation of the electrochemical test system, reducing errors caused by the measurement technique. By varying the excitation frequency of the

applied potential over a range of frequencies, one can calculate the complex impedance, sum of the real and imaginary impedance components, of the system as a function of the frequency (*i.e.* angular frequency, *w*). Therefore, EIS combines the analysis of both real and imaginary components of impedance, namely the electrical resistance and reactance, as shown in Equation 2.5 (Patolsky et al., 1999).

$$Z\ (j\omega) = \frac{U\ (j\omega)}{I\ (j\omega)} = Z_r(\omega) + jZ_i(\omega)\ ;\ \omega = 2\pi f \qquad (2.5)$$

This method is especially valuable because it enables the equivalent series resistance (ESR) of the electrode materials and the charge transfer resistance (R_{ct}) of the system to be separately evaluated. The Nyquist plot is used as to evaluate the phase relation between the imaginary phase ($-Z_{imag}$) and the real phase (Z_{real}) of the impedances as shown in Figure 2.6.

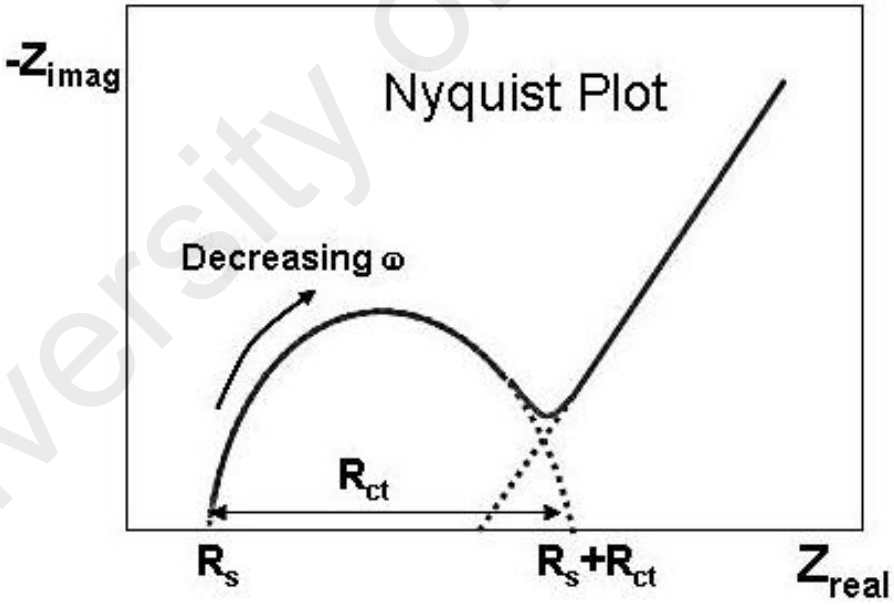

Figure 2.6: Example of complex plane diagram of an EIS measurement (Pacios et al., 2011).

For electrochemical sensing, EIS techniques are useful to monitor changes in electrical properties arising from biorecognition events at the surfaces of modified electrodes. For example, changes in the conductance of the electrode can be measured

as a result of protein immobilization and antibody-antigen reactions on the electrode surface (Katz & Willner, 2003; Patolsky et al., 1999; Pei et al., 2001).

2.4 Materials for electrochemical sensors

The discussions in the earlier sections have shown the performance of an electrochemical sensor is highly dependent on the material used as the sensing electrode. Materials ranging from carbon composites (Céspedes et al., 1996), beads or microspheres (Solé et al., 2001), molecular imprinted polymers (MIP) (Merkoci & Alegret, 2002) or quantum dots (Merkoçi et al., 2005) are playing an important role in these sensing systems.

2.4.1 Graphene-Based Nanocomposite Material

Graphene-based nanomaterials have captured great interest among physicists, chemists and materials scientists alike. Graphene is a two-dimensional (2-D) sheet of carbon atoms in a hexagonal configuration with atoms bonded by sp^2 bonds. These bonds and this electron configuration are the reasons for the extraordinary properties of graphene, which include a very large surface area [at 2630 m^2/g, it is double that of single-walled carbon nanotubes (SWCNTs)], a tunable band gap, room-temperature Hall effect, high mechanical strength (200 times greater than steel), and high elasticity and thermal conductivity (Geim & Novoselov, 2007).

The discovery of graphene in 2004, added a new dimension to electrochemical biosensor research (Novoselov et al., 2004). Since the historical application by Sir Humphrey Davy of graphite electrodes for electrochemical production of alkali metals, carbon materials have been widely used in both analytical and industrial electrochemistry due to their low cost, wide potential window, relatively inert electrochemistry, and electrocatalytic activity for a variety of redox reactions (McCreery, 2008).The use of graphene can avoid the problems associated with metal

alloy NP and CNT. The unique properties of graphene (fast electron transportation, high thermal conductivity, excellent mechanical flexibility and good biocompatibility) give it potential applicability in electrochemical biosensors (Allen et al., 2009; Brownson & Banks 2010; Pumera, 2010).

The most important property of graphene is its excellent electrical conductivity. The various forms of graphene-based materials include thermally reduced graphene oxide (TRGO), chemically reduced graphene oxide (CRGO), and electrochemically reduced graphene oxide (ERGO), contains oxygen-containing functional groups and certain amounts of defects (Kampouris & Banks, 2010; Wu et al., 2013). The rapid electron transfer takes place at the surface of edge planes and defects when compared to the basal planes for the electrochemical sensors fabricated with graphene based materials (Brownson et al., 2012; Yuan et al., 2013). The presence of these structural defects in the chemically modified graphene can be exploited for electrochemical sensor applications.

Based on Zhou et al. (2009) reported graphene exhibits a wide electrochemical potential window of ca. 2.5 V in 0.1 M PBS (pH 7.0) (Zhou et al., 2009), which is comparable to that of graphite, glassy carbon (GC), and even boron-doped diamond electrodes (McCreery, 2008; Niwa et al., 2006), and the charge-transfer resistance on graphene as determined from AC impedance spectra is much lower than that graphite and GC electrodes (Zhou et al., 2009). The electron transfer behavior studies of graphene using cyclic voltammogram (CV) of redox couples, such as $[Fe(CN)_6]^{3-/4-}$ and $[Ru(NH_3)_6]^{3+/2+}$, are reported, which exhibit well-defined redox peaks (Tang et al., 2009; Yang et al., 2009). Both anodic and cathodic peak currents in the CVs are linear with the square root of the scan rate, which suggest that the redox processes on graphene-based electrodes are predominantly diffusion controlled (Lin et al., 2009). The peak-to-peak potential separations (ΔEp) in CVs for most one-electron-transfer redox

couples are quite low, very close to the ideal value of 59 mV, for example, 61.5 – 73 mV (10 mV/s) for $[Fe(CN)_6]^{3-/4-}$ (Wang et al., 2009; Yang et al., 2009) and 60 – 65 mV (100 mV/s) for $[Ru(NH_3)_6]^{3+/2+}$ (Tang et al., 2009), much smaller than that on GC (McCreery, 2008). The peak-to-peak potential separation is related to the electron transfer (ET) coefficient (Nicholson, 1965), and a low ΔEp value indicates a fast ET for a single-electron electrochemical reaction (Shang et al., 2008) on graphene.

Historically, several electrochemical sensors based on graphene and graphene composites for bioanalysis and environmental analysis have been developed. Shan et al. (2009) reported the first graphene-based glucose biosensor with graphene/polyethylenimine-functionalized ionic liquid nanocomposites modified electrode which exhibits wide linear glucose response (2 to 14 mM, R = 0.994), good reproducibility (relative standard deviation of the current response to 6 mM glucose (Shan et al., 2009). Zhou et al. (2009) reported a glucose biosensor based on chemically reduced graphene oxide (CR-GO) (M. Zhou, et al., 2009). The graphene (CR-GO)-based biosensor exhibits substantially enhanced amperometric signals for sensing glucose: wide linear range (0.01 – 10 mM), high sensitivity (20.21 μA mM cm^{-2}) and low detection limit of 2.00 μM (S/N = 3). Zhou et al. (2009) also studied the electrochemical behavior of hydrogen peroxide on graphene (chemically reduced graphene oxides, CR-GO) modified electrode, which shows a remarkable increase in electron transfer rate compared with graphite/GC and bare GC electrodes (Zhou et al., 2009). Kang et al. (2009) employed biocompatible chitosan to disperse graphene and construct glucose biosensors (Kang et al., 2009). It was found that chitosan helped to form a well-dispersed graphene suspension and immobilize the enzymemolecules, and the graphene-based enzyme sensor exhibited excellent sensitivity (37.93 μA mM^{-1} cm^{-2}) and long-term stability for measuring glucose. Tang et al. (2009) studied the electrochemical behavior of NADH on graphene (chemically reduced graphene oxides,

CR-GO) modified electrode, which shows a remarkable increase in electron transfer rate compared with graphite/GC and GC electrodes (Tang et al., 2009). Shan et al. (2010) reports a graphene/AuNPs/chitosan composites film based biosensor which exhibited good electrocatalytical activity toward H_2O_2 and O_2 (Shan et al., 2010). Wu et al. (2009) reports GOD/graphene/ PtNPs/chitosan based glucose biosensor with a detection limit of 0.6 mM glucose (Wu et al., 2009). These enhanced performances were attributed to the large surface area and good electrical conductivity of graphene, and the synergistic effect of graphene and metal nanoparticles.

2.4.2 Graphene-based Metal Oxide Nanocomposite

There great demand for the synthesis of graphene–semiconductor nanomaterial composites because of their promise in electronics, optics, and energy-based applications. Although graphene-metal based nanocomposites were investigated widely with its enhancement of composite features for the detection of sensor, other alternative cost-effective materials were still explored to replace metal. Thus, this leads to metal oxides being studied in achieving this target since it is high in abundance, cost-effective, and "green". The addition of these metal oxide nanostructures on graphene forms composite materials that exposes promotional benefits in refining electrochemical properties which cannot be achieved by either component alone. To date, various kinds of semiconductor nanomaterials have been synthesized and supported on graphene-based templates, which include TiO_2 (Du et al., 2010; Zhang et al., 2010), ZnO (Wu et al., 2010; Yin et al., 2010), SnO_2 (Wang et al., 2011; Zhang et al., 2010), MnO_2 (Chen et al., 2010; Yan et al., 2010), Co_3O_4 (Chen & Wang, 2010; Yan et al., 2010), Fe_3O_4 (Liang et al., 2010; Shen et al., 2010), Fe_2O_3 (Singh et al., 2009; Zhu et al., 2011), NiO (Son et al., 2010), Cu_2O (Wu et al., 2010; Wu et al., 2011), RuO_2 (Kim et al., 2010; Wu et al., 2010), CdS (Guo et al., 2010; Wang et al., 2010), and CdSe (Kim et al., 2010; Li et al., 2011; Lin et al., 2010). The synthetic methods for preparation of these graphene–

semiconductor nanomaterial composites include in-situ crystallization (Cao et al., 2010; He & Gao, 2010; Strom et al., 2010), solution mixing (Liu et al., 2010; Yang et al., 2010; Yang et al., 2010), microwave-assisted growth (Yan et al., 2010), electrochemical deposition (Wu et al., 2010; Yin et al., 2010), and vapor deposition (Son et al., 2010). In-situ crystallization approach have been the most commonly used methods to synthesize composites of GO or rGO and semiconductor nanomaterials. For example, graphene–CdS composites were prepared by mixing GO and $Cd(CH_3COO)_2$ in DMSO, which was then heated in an autoclave at 180 ° C for 12 h (Cao et al., 2010). During the synthetic process, the hydrothermal process results in the simultaneous formation of CdS nanoparticles (NPs) and the reduction of GO to rGO in DMSO, which acts as both the solvent and the sulfur source. Time-resolved fluorescence spectroscopy data showed a picosecond ultrafast electron transfer process from CdS NPs to the graphene sheet, which demonstrates the potential optoelectronic application of this graphene–CdS hybrid material. The in-situ crystallization approach is also applicable to synthesis of many other types of semiconductor nanostructures on graphene-based templates such as MnO_2 nanoneedles (Chen et al., 2010), TiO_2 rods (Wang et al., 2009), and SnO_2 NPs (Wang et al., 2010).

2.4.3 Graphene-based Noble Metal Nanocomposite

The attractive properties of metal nanoparticles incorporated on graphene shows high electrocatalytically, excellent conductivity, and selectivity which makes metal nanostructures decorated on graphene an ideal choice to be used as an active material in electrochemical sensors. Furthermore, the absence of interfering oxidation and reduction peaks in graphene-metal nanocomposite in the sensors shows promising anti-interference effect. These properties of graphene and its derivatives have made them ideal templates for the synthesis of metal nanoparticles (NPs), such as Au (Huang et al., 2010; Liu et al., 2010; Xu et al., 2008; Zhou et al., 2009), Ag (Kamat, 2009; Lu et al.,

2009; Shen et al., 2010; Zhou et al., 2009), Pd (Hassan et al., 2009; Johnson et al., 2010; Mastalir et al., 2008; Scheuermann et al., 2009), Pt (Liu et al., 2010; Si & Samulski, 2008; Xu et al., 2008), Ni (Wang et al., 2010), and Cu (Hassan et al., 2009). The graphene–metal NP composites have been applied in a broad range of application areas, such as surface-enhanced Raman scattering (SERS) (Goncalves et al., 2009; Zhou et al., 2009), catalysis (Mastalir et al., 2008; Scheuermann et al., 2009), and electrochemical sensing. The graphene–metal NP composites can be prepared by chemical reduction (Guo et al., 2009; Kim et al., 2010; Muszynski et al., 2008; Xu et al., 2008), photochemical synthesis (Huang et al., 2010; Kosel & Kamat, 2010), microwave assisted synthesis (Hassan et al., 2009), electroless metallization (Zhou et al., 2009), and thermal evaporation (Zhou et al., 2009). The first graphene–Au NP composite was prepared by the reduction of $AuCl_4^-$ with $NaBH_4$ in rGO octadecylamine (ODA) solution.

In addition to spherical metal NPs obtained in most reported syntheses, Au nanorods have been successfully prepared on rGO films (Kim et al., 2010; WookáLee & WooáHan, 2010), which were immersed in growth solutions of cetyl trimethylammonium bromide (CTAB), $HAuCl_4$, and ascorbic acid. It was found that the growth of Au nanorods could be realized on both rGO and seed modified rGO films (WookáLee & WooáHan, 2010). The fabricated Au nanorods give significantly enhanced Raman signals of rGO—34 times higher at the rod tip (WookáLee & WooáHan, 2010), which is much higher than that of snowflake-shaped Au structures deposited on rGO (Jasuja & Berry, 2009).

2.4.4 Graphene-based Noble Metal/Protein Nanocomposite

The electrochemical protein sensors are based on the immobilization of redox proteins on an electrode. In most of the cases the electrode itself can replace physiological partners or natural electron acceptors, providing the driving force to

energize the reaction and a sensor to measure the response. For instance, in the case of glucose oxidase (GOx), which catalyses the reaction glucose^{+} O_2 glucolactone^{+} H_2O_2, with oxygen acting as its natural electron acceptor to regenerate the enzyme, the electrode can take the role of its natural partner oxygen (Cai & Chen, 2004; Patolsky et al., 2004). Therefore, the main purposes of preparing redox enzymatic sensors are to preserve the biomolecule activity when it is immobilized on the electrode and to assurance a good electrochemical communication between the redox active center and the electrode to facilitate the enzyme turnover (Gooding et al., 2003; Guiseppi-Elie et al., 2002; Katz & Willner, 2004; Wang, 2005). However, these goals are rather difficult to achieve since proteins, when adsorbed on electrode surfaces, undergo denaturation with the consequent loss of their electrochemical activity. Moreover, some enzymes contain the redox active center buried deep inside the protein and it is necessary to utilize mediators to accomplish an electrochemical response (Cai & Chen, 2004; Katz & Willner, 2004). Therefore, the nature and properties of the surface of the electrode are crucial in dictating how the electron exchange takes place. In another words, the disposition of the protein and its redox active center on the surface is important in electrochemical reactivity, which strongly depends on the electrode charge density, its hydrophilicity/hydrophobicity or the strength of the interaction (Pacios et al., 2011).

Beside that, the direct electron transfer has also been observed with many metalloproteinases such as cytochrome C, horseradish peroxidase, microperoxidase (MP-11), myoglobin, hemoglobin, catalase, azurin, etc, immobilized on different CNT modified electrodes (Esplandiu et al., 2009; Gooding et al., 2003; Kumar et al., 2011; Pacios et al., 2009; Zhang et al., 2003; Zhao et al., 2006). Among them, immobilization of Mb with nanostructured materials has been proved to be an effective method to realize its direct electrochemistry (Peng et al., 2011; Qiu et al., 2010; Zhao et al., 2008). It is due to their excellent properties such as high biocompatibility, good conductivity,

strong adsorptive ability and distinctive size related electronic. Myoglobin (Mb), a small water soluble protein involved in the binding and storage of oxygen in cells, has been the subject of numerous studies in redox protein sensors. This protein has a hemin core capable of redox activity and exhibits a catalytical response in presence of some analytes such as oxygen, H_2O_2 or NO (Li et al., 2006; Pacios et al., 2009; Zhang et al., 2003). The Mb functions physiologically in the storage of oxygen and in the enhancement of the rate of oxygen diffusion, and has catalytic activity for H_2O_2 similar to horseradish peroxidase (HRP) (Hildebrand et al., 1996).

The myoglobin/gold nanoparticles (AuNPs) has recently reported that emerged as building blocks for the immobilization of biomolecules and fabricating biosensors (Li et al., 2008; Zhang et al., 2006; Zhang & Oyama, 2005). It is an ideal model molecule for the electron transfer study of heme proteins and for biosensing and biocatalysts. During the past decades, numerous efforts were made for the exploration of direct electrochemistry of Mb by immobilizing it into various modified electrodes (Yue et al., 2011). Though several CNTs and graphene based modified electrodes were reported for the immobilization of Mb towards determination of H_2O_2 (Mani et al., 2014). Yue et al. (2011) fabricated the platform composed of SLGnP–heme protein (myoglobin) composite film for nitrite biosensor (Yue et al., 2011). Recently, reduced graphene oxide-multiwalled carbon nanotubes-platinum nanoparticles/myoglobin (RGO-MWCNT-Pt/Mb) has reported for the direct electrochemistry of myoglobin and its application towards determination of hydrogen peroxide (H_2O_2) and nitrite (NO_2^-) (Mani et al., 2014). The RGO-MWCNT-Pt nanocomposite has been prepared by simple solution method. The modification of myoglobin with three-dimensional reduced graphene oxide-gold composite modified electrode also showed excellent electrocatalytic reduction to trichloroacetic acid (Shi et al., 2016).

2.4.5 Tested Analytes

The electrochemical detection of nitrite can be divided into a number of categories. Fortunately, these can be broadly grouped within the distinctions of voltammetric and potentiometric systems. The voltammetric techniques have been employed from the beginning of the 1900s, whereby copper electrodes were used to reduce the nitrate ion (Davis et al., 2000; Shibata et al., 1995) electrochemically. The nitrite would appear to be rather more fortunate in that this ion can be oxidized or reduced at a glassy carbon electrode (Chamsi & Fogg, 1988; Newbery & de Haddad, 1985). Other techniques utilise the reduction of nitrite to NO, which can then be detected amperometrically at modified Au electrodes covered with a PTFE film (Kobayashi & Hikuma, 2000). The more sophisticated approaches to the electrochemical detection of nitrate and nitrite probably lie with the use of biological catalysts. Reshetilov et al. (2000) have proposed the use of a biosensor based on the oxidation of nitrite by bacteria based on the N. ulgaris strain (Reshetilov et al., 2000). An electrochemical variation/adaptation of the Griess assay has been attempted with the reduction of the diazonium salts resulting from the reaction of nitrous acid with substituted phenylene diamines providing the analytical signal. The iodine–iodide couple is a reversible electrochemical system on both gold and platinum electrodes in sulphuric acid media (Desideri et al., 1973), which can be exploited for indirect analysis of nitrite.

Jena and Raj developed a NADH biosensor based on the integrated assembly of dehydrogenase enzymes and gold nanoparticles (Jena & Raj, 2006). The NADH biosensors were stable, fast responding, and exhibited high sensitivity toward NADH (0.056 ± 0.001 nA nM^{-1}) with an amperometric detection limit of 5 nM. Li et al. (2011) synthesized graphene–Au nanorods hybrid nanosheets (GN–AuNRs) through electrostatic interaction (Li et al., 2011). Due to the synergistic effect between AuNRs and GN, the hybrid nanosheets exhibited excellent performance toward

dihydronicotinamide adenine dinucleotide (NADH) oxidation, with a low detection limit of 6 μM.

The detection of nitroaromatic compounds continues to generate enormous interest due to their relevance for national security and environmental monitoring. Electrochemical sensors are especially attractive owing to their simplicity, low cost, and portability compared to other detection strategies. The first electrochemical approach based on the direct oxidation of NO on a platinum electrode was reported by Shibuki (Shibuki, 1990), using a miniature Clark-type electrode. Malinski and Taha reported in 1992 on a very interesting application of an electropolymerized nickel porphyrin film electrode for in situ amperometric detection of NO in biological systems (Malinski & Taha, 1992). Pontié et al. (2000) have prepared electrochemical NO-sensors using two combinations of nickel tetrasulfonated phthalocyanine (NiTSPc), *o*-phenylenediamine (*o*PD) and Nafion layers to modify the surface of conventional carbon electrodes (3 mm diameter) (Pontié et al., 2000). Schoenfisch's group reported on the fabrication of a planar ultramicroelectrode NO sensor capable of measuring NO release from a surface with high spatial resolution and without any deleterious effects from analyte trapping (Oh et al., 2006). The sensor performance was characterized as having response times on the order of a few seconds and a detection limit of 5 nM, indicating suitability for biological measurements. Griveau et al. (2007) described an electrochemical sensor for measuring both exogenous and induced endogenous NO in a mouse tumor tissue (Griveau et al., 2007). Nickel hexacyanoferrate-modified platinum electrodes were fabricated by Krylov and Lisdat for use as NO sensors (Krylov & Lisdat, 2007). Lee and Kim (2007) reported the development of a dual planar amperometric microsensor capable of measuring both NO and carbon monoxide (Lee & Kim, 2007). The detection limits for NO and CO were 1 nM and less than 5 nM, respectively. Meyerhoff and coworkers showed successful examples of implementation of a controlled catalytic

process, to release NO from RSNO, within the sensing chemistry devoted to the electrochemical detection of NO (Cha et al., 2005; Hwang et al., 2008). As a result, the RSNO sensor had a limit of detection of less than 0.1 μM. One of the main directions of our research is now devoted to the detection of NO in plasma and blood. A large part of the continuous production of NO is converted into *S*-nitrosothiols (RSNO) by the interaction of NO with thiol-containing biomolecules such as albumin, thiols such as glutathione or free cysteine (so-called RSH) and with cysteine residues of plasma, cell-surface and intracellular proteins (Hughes, 2008). Recently reported on the design, microfabrication and use of a ring disk ultramicroelectrodes array (RD-UMEs) for direct detection of nitric oxide (NO) release from decomposition of S-nitrosoglutathione (GSNO) catalyzed by copper species (Kim et al., 2011).

2.4.6 Electrolyte

An electrolyte is crucial component in electrochemical sensor because it facilitates the cell reaction and carries the ionic charge across the electrodes efficiently. It must also form a stable reference potential with the reference electrode and be compatible with materials used within the sensor. If the electrolyte evaporates too quickly, the sensor's signal will deteriorate. Therefore, an electrolyte should efficiently regenerate itself. The choice of electrolyte is depended on the material used for working electrode and also the analytes need to be tested. By careful selection of the electrolyte and/or the sensing electrode, one can achieve the selectivity towards the target analyte, but the sensitivity may be reduced. The electrolyte used in an electrochemical sensor is liquid electrolyte. The liquid electrolyte exhibits dielectric constant organic solvent or uses low viscous ionic liquid as a solvent medium. The dielectric constant value, viscosity of the organic solvent and number of donor will greatly influence the performance of the electrolyte. The most common electrolyte use is phosphate buffered saline (PBS) as the supporting electrolyte. The PBS were prepared by blending standard solutions of sodium

phosphate monobasic (NaH_2PO_4) and disodium phosphate dehydrate ($Na_2HPO_4.2H_2O$) with distilled water (Gao et al., 2014; Yusoff et al., 2015).

2.4.7 Electrochemical Sensor Electrodes

The selection of the electrode material is very important for an electrochemical sensor. It is a catalyzed material which performs the half cell reaction over a long period of time. Generally, the electrode is made from a noble metal, such as platinum or gold, and catalyzed for an effective reaction with gas molecules. Depending on the design of the sensor, all three electrodes can be made of different materials to complete the cell reaction. A conventional electrochemical cell of three electrodes consists of a working electrode, on which there is oxidation and reduction reactions of the species involved, the counter electrode (or auxiliary electrode), which serves to complete the electric circuit of the electrochemical system, and the reference electrode, which provides a reference for the assessment of other measured parameters (Holler et al., 2007).

2.4.7.1 Reference Electrode

A sensor requiring an external driving voltage, it is important to have a stable and constant potential at the sensing electrode. In reality, the sensing electrode potential does not remain constant due to the continuous electrochemical reaction taking place on the surface of the electrode. It causes deterioration of the performance of the sensor over extended periods of time. To improve the performance of the sensor, a reference electrode is introduced. The reference electrode is placed within the electrolyte in close proximity to the sensing electrode. A fixed stable constant potential is applied to the sensing electrode. The reference electrode maintains the value of this fixed voltage at the sensing electrode. There is no current flow to or from the reference electrode. The analyte molecules react at the sensing electrode and the current flow between the sensing and the counter electrode is measured and is typically related directly to the

analyte concentration. The value of the voltage applied to the sensing electrode makes the sensor specific to the different target of analytes.

The group of Lewenstam introduced a conducting polymer with pH buffering ligands as a new reference electrode concept (Blaz et al., 2005). The systems appear to work quite well, especially at physiological pH. While the mechanism is not completely understood at this stage, the reference electrode appears to at least partly act as a self-buffering system. As the pH buffer partitions from the polymer film into the sample may maintain a local pH that is independent of the sample pH in a certain range. Maksymiuk and co-workers also used conducting polymers to construct reference electrodes (Kisiel et al., 2005). In one approach, conducting polymers were fabricated to exhibit no ion-exchange properties. In agreement with theoretical expectations, the resulting open circuit potentials were independent of electrolyte concentration, but dependent on the nature of the electrolyte. Ha et al. (2005) used polymeric junction membrane on the basis of cellulose acetate and polyurethane to solid state reference electrodes that can in principle be mass produced (Ha et al., 2005). Lowy and coworkers characterized a previously reported miniaturized reference electrode based on a silver sulfide inner reference element embedded into an acrylic copolymer matrix for use in biological and organic media (Ciobanu et al., 2004). A microtubular hydrogen electrode was proposed by Kunimatsu et al. (2005) as a miniaturized replacement of the traditional hydrogen electrode (Kunimatsu et al., 2005), but the electrode was found to only function in contact with acidic solutions.

Several types of reference electrodes are convenient to use for analytical electrochemistry. In the three reference electrode design, saturated calomel and silver-silver chloride are among the most common commercially available and convenient fabricated reference electrodes (Kissinger & Heineman, 1996). The saturated calomel electrode (SCE) is a reference electrode based on the reaction between elemental

mercury and mercury (I) chloride. The aqueous phase in contact with the mercury and the mercury (I) chloride (Hg_2Cl_2, "calomel") is a saturated solution of potassium chloride in water (Banus, 1941). The silver-silver chloride electrode consist a silver wire that is coated with a thin layer of silver chloride, either physically by dipping the wire in molten silver chloride, or chemically by electroplating the wire in concentrated hydrochloric acid.

2.4.7.2 Auxiliary Electrode (Counter Electrode)

The auxiliary electrode, often also called the counter electrode, is an electrode used in a three electrode electrochemical cell for voltammetric analysis or other reactions in which an electric current is expected to flow (Kissinger & Heineman, 1996). The auxiliary electrode is distinct from the reference electrode, which establishes the electrical potential against which other potentials may be measured, and the working electrode, at which the cell reaction takes place. In a three electrode cell is used to perform electroanalytical chemistry, the auxiliary electrode, along with the working electrode, provides circuit over which current is either applied or measured. Here, the potential of the auxiliary electrode is usually not measured and is adjusted so as to balance the reaction occurring at the working electrode. This configuration allows the potential of the working electrode to be measured against a known reference electrode without compromising the stability of that reference electrode by passing current over it.

Auxiliary electrodes are often fabricated from electrochemically inert materials such as gold, platinum, or carbon.

2.5 Applications of electrochemical sensors

The physical size, geometry, selection of various components, and the construction of an electrochemical sensor usually depends on its intended use. Electrochemical sensors require very little power to operate. In fact, their power consumption is the lowest among all sensor types available. For this reason, the sensors are widely used in portable instruments that contain multiple sensors. Indeed, significant advances have been made in several areas related to the design and application of electrochemical sensors. The synthesis of nanostructured labels including quantum dots, metal clusters, magnetic particles, and carbon nanotubes to improve sensor performance represents a burgeoning area of research. The further applications based on reduced graphene oxide modified electrodes were summarized in Table 2.1.

Table 2.1 Further applications of reduced graphene based modified electrodes.

Analytes	Electrode	Electrode construction and applications	Reference
Glucose oxidase	Chemically reduced graphene oxide (CR-GO)	The first graphene-based glucose biosensor with graphene/-polyethylenimine-functionalized ionic liquid nanocomposites modified electrode which exhibits wide linear glucose response (2 to 14 mM, R = 0.994), good reproducibility (relative standard deviation of the current response to 6 mM glucose at -0.5 V was 3.2% for 10 successive measurements), and high stability (response current +4.9% after 1 week).	(Shan et al., 2009)
	Graphene-chitosan	Exhibited excellent sensitivity (37.93 μA mM^{-1} cm^{-2}) and long-term stability for measuring glucose.	(Kang et al., 2009)
Hydrogen peroxide	Graphene (chemically reduced graphene oxides, CR-GO)	Such significantly enhanced performance on graphene-based electrodes for detecting H_2O_2 with superior electrocatalytic activity of graphene toward H_2O_2. The linear relationship of H_2O_2 at -0.2 V on CR-GO/GC electrode is 0.05 – 1500 μM.	(Zhou et al., 2009)
NAD^+/NADH -dependent dehydrogenas -es	Graphene (chemically reduced graphene oxides, CR-GO)	Shows a remarkable increase in electron transfer rate compared with graphite/ GC and GC electrodes. The peak potentials of NADH oxidation is shifted from 0.70 V on GC and graphite to 0.40 V on CR-GO.	(Tang et al., 2009)
	Methylene Green-graphene	The oxidation of NADH on MG-graphene electrode takes place ~ 0.14 V, which is much lower than that (+0.40 V) for pristine graphene.	(Liu et al., 2009)
Hydrogen peroxide and Oxygen gas	Graphene/Au NPs/chitosan	Exhibited the wide linear response to H_2O_2 ranging from 0.2 to 4.2 mM (R = 0.998) at -0.2 V, high sensitivity of 99.5 μA mM^{-1} cm^{-2} and good reproducibility.	(Shan et al., 2010)

Table 2.1 (Continued).

Dopamine (DA)	Multilayer graphene nanoflake films (MGNFs)	The MGNFs based electrode was synthesized through catalyst-free microwave plasma enhanced chemical vapor deposition. The MGNFs exhibited well resolved simultaneous discrimination of AA, DA, and UA, and the detection limit of DA is 0.17 µM.	(Shang et al., 2008)
DNA sensor	Chemically reduced graphene oxide	Able to efficiently separate all four DNA bases (i.e., guanine (G), adenine (A), thymine (T), and cytosine (C)) in both single-stranded DNA (ssDNA) and doublestranded DNA (ds-DNA), which are more difficult to oxidize than free bases.	(Zhou et al., 2009)
Heavy metal ions (Pb^{2+} and Cd^{2+})	Nafion-graphene composite	The stripping current signal is greatly enhanced on graphene electrodes. The linear range for the detection of Pb^{2+} and Cd^{2+} is wide (0.5 µg L^{-1} – 50 µg L^{-1} and 1.5 µg L^{-1} – 30 µg L^{-1} for Pb^{2+} and Cd^{2+}, respectively). The detection limits (S/N = 3) are 0.02 µg L^{-1} for both Cd^{2+} and Pb^{2+}.	(Li et al., 2009)
Paracetamol	Graphene-modified glassy carbon	A quasi-reversible redox process of paracetamol at the modified electrode was obtained, and the over-potential of paracetamol decreased significantly compared with that at the bare GCE with a detection limit of 3.2×10^{-8} M, a reproducibility of 5.2% relative standard deviation, and a satisfied recovery from 96.4% to 103.3%.	(Kang et al., 2010)

CHAPTER 3: MATERIALS AND METHODOLOGY

3.1 Materials

Materials and chemicals used in this thesis are summarized in Table 3.1.

Table 3.1 Materials and chemicals used in this thesis.

Materials/ Chemicals	**Formula**	**Purity (%)**	**Supplier**
Graphite flakes (3061)	-	99	Asbury Graphite Mill Inc.
Zinc acetate dehydrate	$Zn(CH_3COO)_2 \cdot 2H_2O$	99.9	Sigma Aldrich
Horse heart myoglobin	-	≥ 90	Sigma Aldrich
Hydrogen tetrachloroaurate (III) hydrate	$HAuCl_4.3H_2O$	99.9	Sigma Aldrich
Cetytrimethylammonium bromide	$CH_3(CH_2)_{15}N(Br)(CH_3)_3$	≥ 99	Sigma Aldrich
Potassium permanganate	$KMnO_4$	99.9	R&M Chemicals
Sodium hydroxide	NaOH	99.9	R&M Chemicals
N-(trimethoxysilylpropyl) ethylenediamine triacetic acid trisodium salt	$C_{14}H_{25}N_2Na_3O_9Si$	-	Gelest Inc.
Ammonia solution	$NH_3.H_2O$	25	Riedel-de Haën
Sulfuric acid	H_2SO_4	98	Systerm
Phosphoric acid	H_3PO_4	85	Systerm
Hydrochloric acid	HCl	30	Systerm
Hydrogen peroxide	H_2O_2	30	Systerm
Hydrazine hydrate	$NH_2NH_2 \cdot xH_2O$	50	Sigma Aldrich
Sodium dihydrogen phosphate	NaH_2PO_4		Systerm
Disodium hydrogen phosphate	Na_2HPO_4		Systerm
Sodium nitrite	$NaNO_2$		Merck
β-Nicotinamide adenine dinucleotide disodium salt hydrate	$C_{21}H_{27}N_7Na_2O_{14}P_2.xH_2O$	97	Sigma Aldrich

3.2 Synthesis method

3.2.1 Preparation of functionalized graphene oxide (FGO)

The functionalized graphene oxide was prepared as follows (Figure 3.1). Typically, 200 mg of dried GO (prepared by a simplified Hummers method (Huang et al., 2011)) was dispersed into 300 mL of ethanol by ultrasonication, and then a freshly prepared aqueous solution of 3% N-(trimethoxysilylpropyl) ethylenediamine triacetic acid sodium salt was added drop-wise into the ethanolic graphene oxide solution under vigorous stirring. The reaction flask was kept in an oil bath maintained at 60 °C for 18 h for the silylation process. Finally, the product was isolated by centrifugation; repeatedly washed with acetone, methanol, and water several times; and then dried at 80 °C for 12 h.

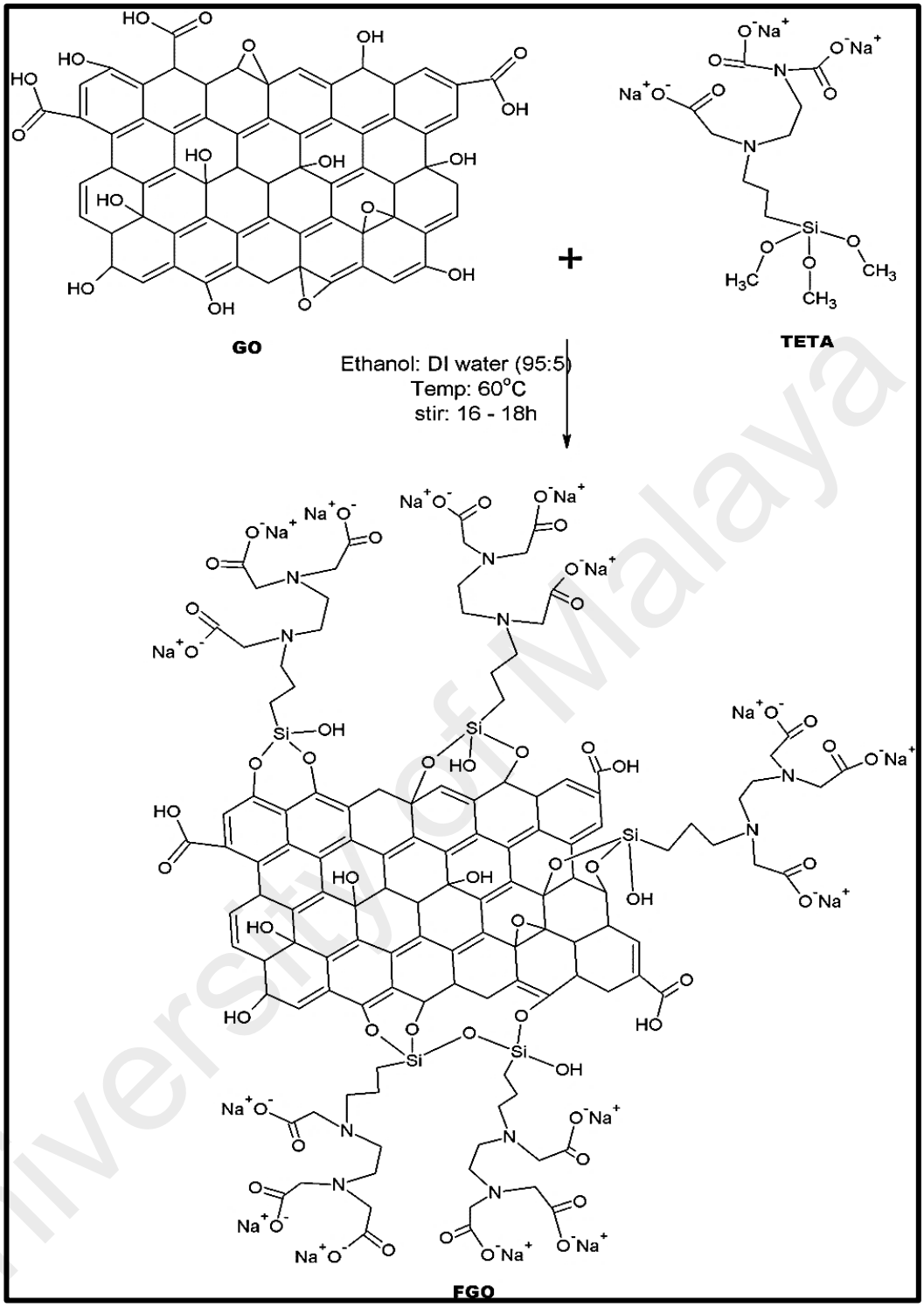

Figure 3.1: Schematic of preparation of functionalized graphene oxide (FGO).

3.2.2 Synthesis of flower-like zinc oxide/reduced functionalized graphene oxide (*f*-ZnO@rFGO) nanocomposite

The *f*-ZnO@rFGO nanocomposite was prepared (Figure 3.2) by mixing 2 mL of 0.1 M $Zn(CH_3COO)_2 \cdot 2H_2O$ into the functionalized graphene oxide (1 $mg \cdot mL^{-1}$) and sonicating the mixture for 30 min to obtain a homogeneous dispersion. The solution was continually stirred at 60 °C for 1 h to form the functionalized graphene oxide-zinc complex. Then, the solution was subjected to hydrothermal treatment at 180 °C for 24 h. The product was obtained by washing several times with ethanol and deionized water. The *f*-ZnO@rFGO was dried at 60 °C for 1 day. For comparison, reduced functionalized graphene oxide was prepared using the same conditions.

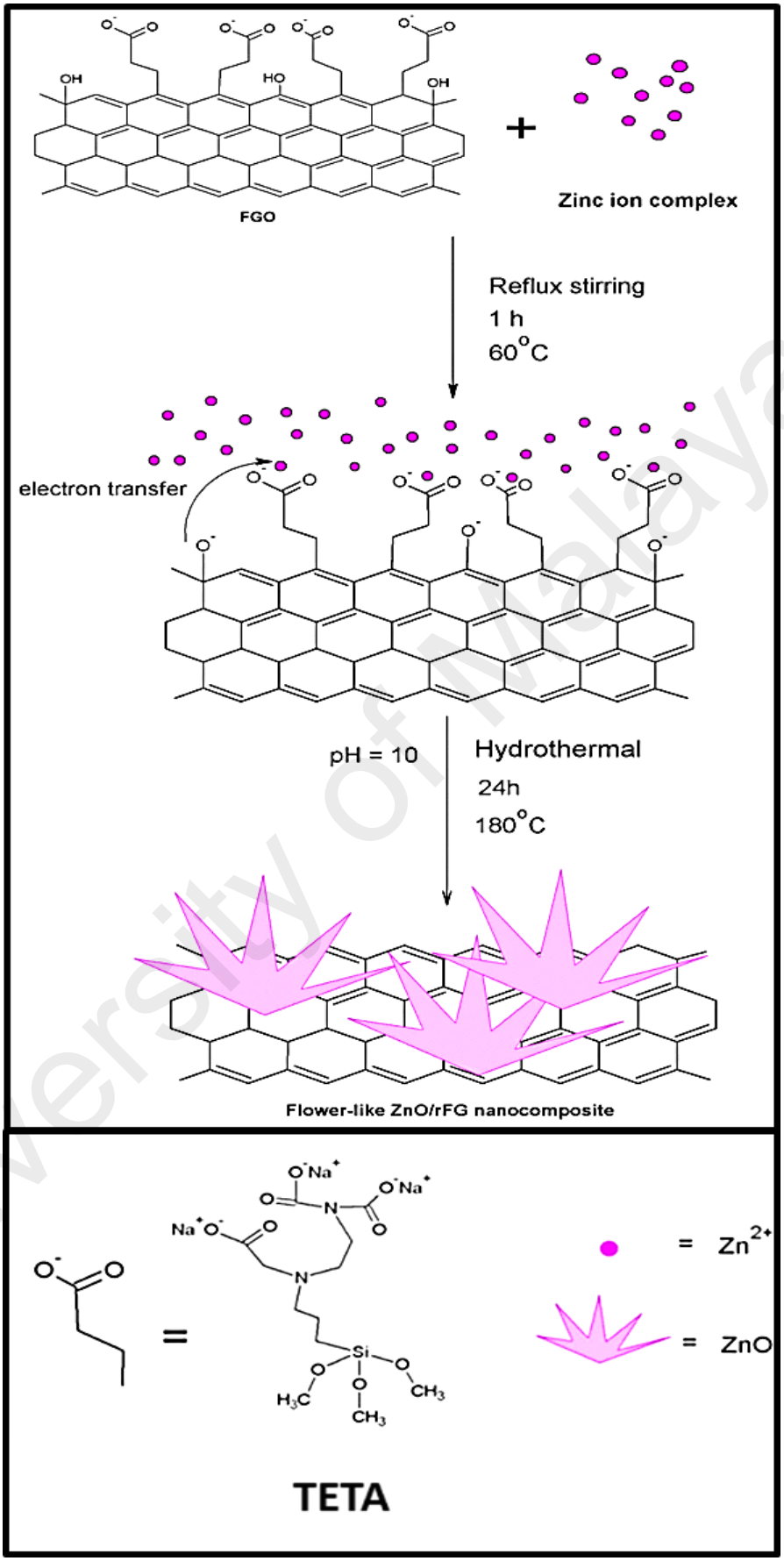

Figure 3.2: Schematic of preparation of nanoflower-like *f*-ZnO@rFGO nanocomposite.

3.2.3 Preparation of Graphene oxide (GO)

The GO was prepared by a simplified Hummers method (Huang et al., 2011). A 3 g of graphite flakes was added into a mixture of 360 mL of concentrated H_2SO_4 and 40 mL of H_3PO_4 under vigorous stirring. The ratio of the concentrated H_2SO_4 to H_3PO_4 is 9 to 1. Then, 18 g of $KMnO_4$ was slowly added and the reaction mixture was allowed to stir for three days at room temperature. After that the mixture was poured into 400 mL of ice cold-deionized water with 27 mL of 30 % H_2O_2. Then the stirring was continued for another 10 min until the mixture turned yellow and it mixture was washed with 1 M HCl and deionized water to remove metal ions and acid impurities. Finally the GO solution obtained. Figure 3.3 displays step of the synthesis process of GO via the simplified Hummers method.

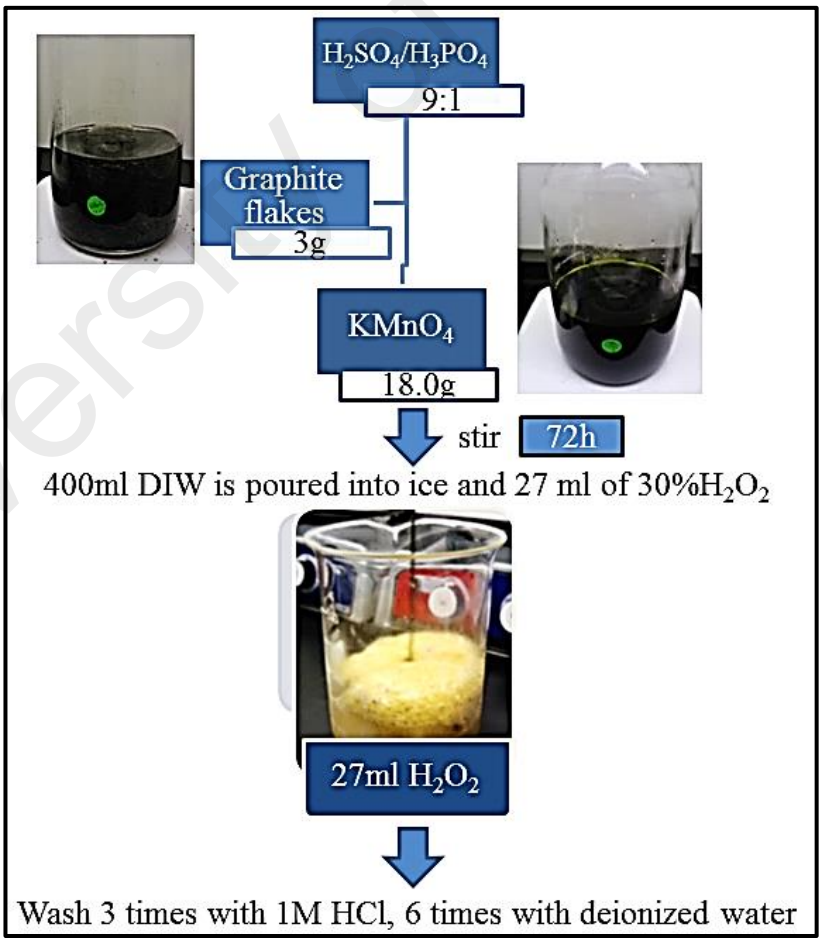

Figure 3.3: Step of the synthesis process of GO via the simplified Hummers method.

3.2.4 Preparation of gold nanorods (AuNRs)

The AuNRs was prepared by seed-mediated growth method that developed by El-Sayed et al. (Nikoobakht & El-Sayed, 2003) and Jana et al. (Jana et al., 2001). Initially, a seed solution of Au nanoparticles was prepared by reducing chloroauric acid with sodium borohydride in an aqueous cetyltrimethylammonium bromide (CTAB) solution. Then, the growth solution was prepared by reducing Au^{3+} ions into Au^{+} ions with a mild reducing agent (ascorbic acid) in an aqueous solution of CTAB and $AgNO_3$. Finally, certain amount of seed solution is added into the growth solution for the formation of AuNRs. The aspect ratio of AuNRs is controlled by varying the amount of $AgNO_3$. The advantage of using this seed-mediated growth method in the presence of Ag^{+} ions is the formation of a single-crystalline AuNR structure (Petrova et al., 2006).

3.2.5 Synthesis of reduced graphene oxide–gold (AuNR-RGO) nanorod

The AuNR-RGO nanorod was prepared as follows. Initially, the reduced graphene oxide was prepared using Wallace's method (Li et al., 2008). Briefly, 200 mL of preformed 1 mg/mL graphene oxide was sonicated for 10 min, and then 2 mL of hydrazine hydrate and 5 mL of ammonia solution were added under vigorous stirring for 30 h. The final product, RGO, was obtained after centrifuging three times with doubly distilled water at 12000 rpm (RCF = 14515.2 × g) for 30 min. Meanwhile, AuNR with an aspect ratio of 3.5 were separately prepared using a seed mediated-growth solution following the procedure of Nikoobakht and El-Sayed (Nikoobakht & El-Sayed, 2003). Then, 1.5 mL of the AuNR solution was mixed with 2 mL of RGO (0.5 $mg \cdot mL^{-1}$). The mixture was mildly sonicated for 30 min and kept for 24 h under stirring to incorporate the AuNRs on to the surface of RGO sheets. Figure 3.4 displays a pictorial illustration of the preparation of the AuNRs-RGO nanorod.

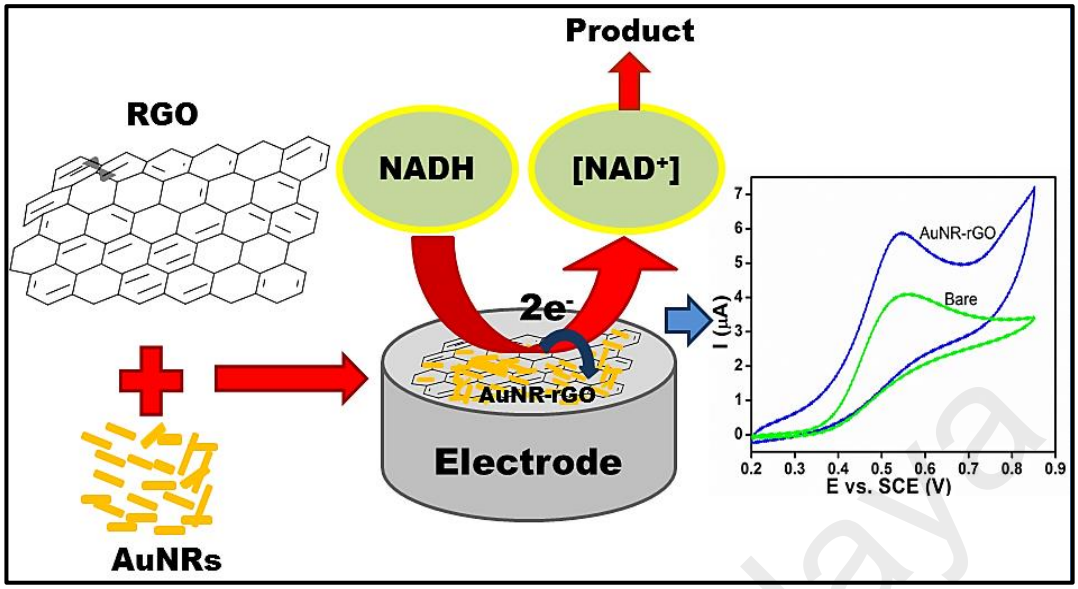

Figure 3.4: Schematic representation of preparation of AuNRs-RGO nanorod.

3.2.6 Synthesis of myoglobin-gold nanorods/reduced graphene oxide (Mb-AuNRs/RGO) nanohybrid

The Mb-AuNRs/RGO nanohybrid was prepared as follows. Initially, the reduced graphene oxide was prepared using Wallace's method (Li et al., 2008). Briefly, 200 mL of preformed 1 mg/mL graphene oxide was sonicated for 10 min, and then 2 mL of hydrazine hydrate and 5 mL of ammonia solution were added under vigorous stirring for 30 h. The final product, RGO, was obtained after centrifuging three times with doubly distilled water at 12000 rpm (RCF = 14515.2 × g) for 30 min. Meanwhile, AuNRs with an aspect ratio of 3.5 were separately prepared using a seed mediated-growth solution following the procedure of Nikoobakht and El-Sayed (Nikoobakht & El-Sayed, 2003). Then, 1.5 mL of the AuNR solution was mixed with 2 mL of myoglobin (2 mg/mL) and 2 mL of RGO (0.5 mg/mL). The mixture was mild sonicated for 30 min and kept for 24 h to complete the incorporate reaction. Figure 3.5 displays a pictorial illustration of the preparation of the Mb-AuNRs/RGO nanohybrid.

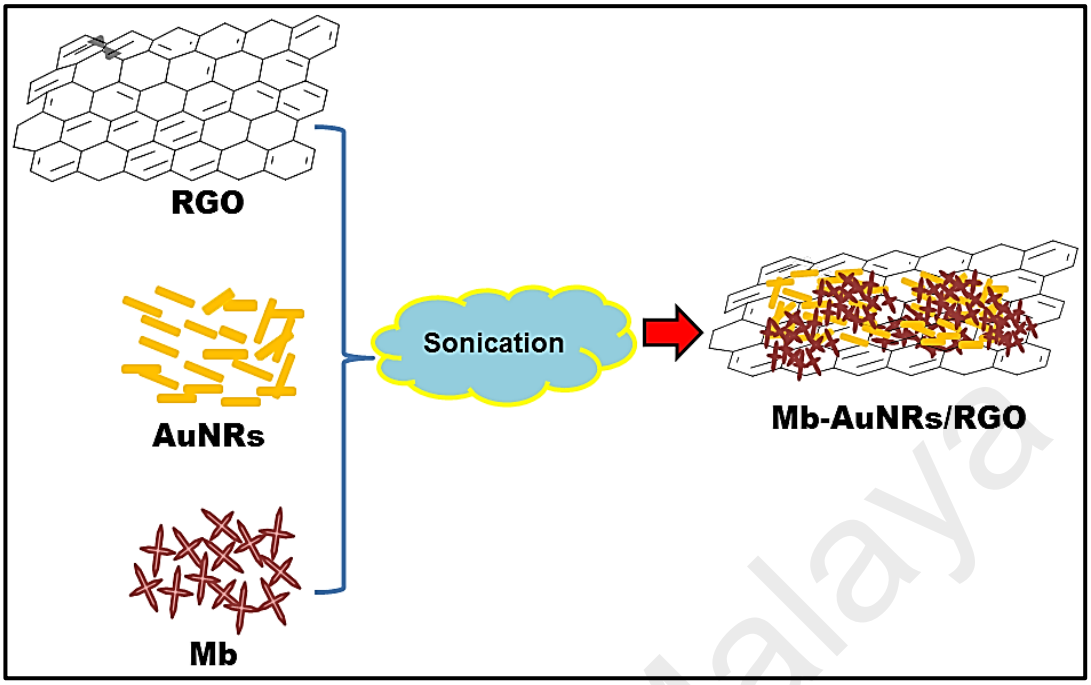

Figure 3.5: Schematic representation of preparation of Mb-AuNRs/RGO nanohybrid.

3.3 Characterization techniques

3.3.1 X-ray diffraction (XRD)

The crystalline phases of the nanorods were analyzed using a PANalytical EMPYREAN X-ray diffractometer with Kα radiation (λ = 1.5418 Å) at a scan rate of 0.03 degree s^{-1}, scanning from 5 - 80°. The atomic structure was analysed using the PANanalytical X'pert Highscore v 1.0 software. The wavelength attributed to Cu Kα is comparable to atomic distance in crystal and ideally suited for probing the structural arrangement of atoms in wide range of materials. Hence, the energetic x-rays not only penetrate deep into materials but also providing the information of their crystalline structures. The crystalline has noticeable sharp peak characteristic, while broad peak (look like a hump) is characteristic for amorphous structure. When x-rays, electrons and neutrons rays with the short wavelength close to interatomic distance are applied to crystals, thus diffraction phenomena occur on the lattice planes in the crystals. When the photons of incident x-rays collide with electrons, some photons are deflected away from

the incident x-rays direction. If the wavelength of scattered x-rays does not change by the collision, such process is known as an elastic scattering. The scattered x-rays are able to carry the information relating to electron distribution in crystals. The identification of unknown material has been performed with a thin film XRD. The thin film was prepared by drop casting method of few layer of sample solution. Thus, it can be the aggregation of fine grains with a single crystal structure and each of fine grain is randomly oriented. When x-rays is applied, the diffraction intensity is assumed to be the sum of x-rays deflected from all fine grains. Hence, the diffraction peak attributed to the Miller indices of the thin film is observed.

3.3.2 Fourier transform infrared spectroscopy (FT-IR)

The FT-IR is a sensitive technique particularly for identifying chemical bonds in a molecule by producing an infrared of absorption or emission spectrum. In this work, the spectrum was recorded on a Perkin-Elmer FTIR spectroscopy 1725x. In infrared spectroscopy is measured by how well a sample absorbs light at each specific frequency that is characteristic of their structure that matches the transition energy of the bond or group that vibrates. The energies are determined by the shape of the molecular potential energy surfaces, the masses of the atoms, and the associated vibronic coupling. When exposed to infrared radiation, sample molecules selectively absorb radiation of specific wavelengths which causes the change of dipole moment of sample molecules. Consequently, the vibrational energy levels of sample molecules transfer from ground state to excited state. The frequency of the absorption peak is determined by the vibrational energy gap. The number of absorption peaks is related to the number of vibrational freedom of the molecule. The intensity of absorption peaks is related to the change of dipole moment and the possibility of the transition of energy levels. Therefore, by analyzing the infrared spectrum, one can readily obtain the structure information of a molecule. Most molecules are infrared active except for several

homonuclear diatomic molecules such as O_2, N_2 and Cl_2 due to the zero dipole change in the vibration and its rotation.

3.3.3 Raman spectroscopy

Raman spectra are acquired by irradiating a sample with a powerful laser source of visible or near-infrared monochromatic radiation. During irradiation, the spectrum of the scattered radiation is measured at some angle (often 90 degree) with a suitable spectrometer. Raman provides the useful information about vibrational, rotational and other low frequency transition in the molecules. As the laser beam is considered as an oscillating electromagnetic wave with the electrical vector E, thus the interaction with the sample induces the electric dipole moment, $P = \alpha E$ which referred to deformed molecules. The deformation of the molecules causes vibrational of molecules with certain characteristic frequency υ_m. It relies on Raman scattering of monochromatic light from a laser beam in the visible, near to ultraviolet or near infrared region. The structures of samples were recorder on a Renishaw inVia Raman microscope with a laser excited at 514 nm. A sample is illuminated with a laser beam. Then the scattered light from illuminated spot is collected by a lens and is sent via a monochromator to obtain Raman spectra of the sample. Wavelengths are close to laser line due to elastic Rayleigh scattering that filtered out and the rest of the scattered light is dispersed onto a detector. The interaction of laser with molecular produced vibration or phonons in the system, thus results in shifting of laser phonon at higher or lower energy level. This shift in energy level gives the information about the vibrational, rotational and other low frequency of the system that being measured.

3.3.4 X-ray photoelectron spectroscopy (XPS)

X-ray photoelectron spectroscopy (XPS) is used to measure the elemental composition, chemical stoichiometry, chemical state and electronic state on the element that presence in the samples. X-ray is used as the light source for the excitement of the electrons that bond in the inner core-level orbital. The bonding energy of the photoelectrons will provide the information of material where the electron is escaped. The XPS spectra are obtained by irradiating a material with a beam of X-rays while simultaneously measuring the kinetic energy and number of electrons that escape from the top 1 to 10 nm of the material being analyzed. XPS requires ultra-high vacuum (UHV) conditions. In brief, XPS serve as a unique probe to impurities and its chemical formation on sample surfaces identifying the defects and contamination of products. In this work, the XPS was performed using synchrotron light at beamline no. 3.2 of the Siam Photon Laboratory, Synchrotron Light Research Institute, Thailand. The XPS data were obtained under the conditions of maximum photon energy of 600 eV and kinetic energy step of 0.1 eV.

3.3.5 Ultraviolet–visible spectroscopy

A UV-Visible spectroscopy is used to characterize the samples optically with known amount of light at specific wavelength passed through the samples. In order to measure the absorbance spectrum, the solution is put in the quartz container with the dimension of 1 x 1 x 4.5 cm^3. During measurement, the light beam from source will pass through the width of the container. The baseline measurement spectrum is taken using deionized water since the solutions involved were suspended in the deionized water. Thus all the solution spectra are referenced to deionized water. The optical properties of all the samples were studied using an Evolution 300 UV–visible spectrophotometer. The measurement was performed in the spectral region of 190 to 900 nm.

3.3.6 Photoluminescence (PL) spectroscopy

The photoluminescence (PL) spectroscopy is used to investigate the electronic structure, intrinsic and extrinsic of semiconducting or semi-insulating materials. The PL intensity gives a direct measure of the relative rates of radiative and nonradiative recombination. In this work, the recombination of electrons and holes is studied with a Renishaw fluorescence spectrophotometer and a 325-nm excitation line. First of all, an excited wavelength is selected by first monochromator then luminescence is observed through a second monochomator, which normally positioned at 90^{o} to the incident light in order to minimize the intensity of scattered light reaching the detector. When the light from the laser beam hits the sample, photoluminescence occurs and light is emitted from the sample at wavelengths dependent on the composition of the sample. This sample is oriented such that the reflected laser beam and the PL emission propagate in different directions. Then, the emitted light is directed into a fiber optic cable and then into a spectrometer. A filter may be placed in front of the fiber input to filter off any incident laser light. Inside the spectrometer, a diffraction grating diffracts different wavelengths in different directions towards an array of photo-detectors. The photo-detectors measured the intensity of each wavelength component. The digital information is then interpreted by the computer for displaying a PL spectrum. The spectrum indicates the relative intensities of the light of various wavelengths entering the detector. The whole process must be carried out in the dark.

3.3.7 Field emission scanning electron microscopy (FESEM)

A FESEM is used to visualize very small topographic details on the surface or entire or fractioned objects. The surface morphology of samples were recorded by using a FEI Nova NanoSEM 400 operated at 10.0 kV and a Hitachi SU8020 high-resolution instrument equipped with energy dispersive X-rays (EDX). The FESEM is used to visualize very small topographic details on the surface or entire or fractioned objects.

Researchers apply this technique to observe structures that may be as small as 1 nanometer (= billion of a millimeter). Electrons are liberated from a field emission source and accelerated in a high electrical field gradient. Within the high vacuum column these so-called primary electrons are focused and deflected by electronic lenses to produce a narrow scan beam that bombards the object. As a result secondary electrons are emitted from each spot on the object. The angle and velocity of these secondary electrons relates to the surface structure of the object. A detector catches the secondary electrons and produces an electronic signal. This signal is amplified and transformed to a video scan-image that can be seen on a monitor or to a digital image that can be saved and processed further.

3.3.8 High resolution transmission electron microscopy (HRTEM)

High resolution TEM is a tool that provides the images that show the structures at the atomic scale. That means it able to identify features on the size of 2Å (2.10^{-10} m). By using HRTEM, the spacing between lattice fringes can be measured. In this work, the atomic arrangement of nanocomposites was performed using a JOEL JEM 2100F operated at 100 kV. In order to obtain high resolution images containing lattice fringes, the interference of the unscattered and scattered beam is used. The electrons can be described as a wavefront by performing bright and dark strips know as lattice fringes which can appear in one or more directions. By using HRTEM, the spacing between lattice fringes can be measured. The lattice fringes was analysed by using iSolution lite software. If the specimen is very thin, this fringe can be interpreted as the projection of the tunnels between columns of atoms. While, the dark strips represent the atoms themselves.

3.4 Evaluation of Electrochemical Properties

All the electrochemical measurements including cyclic voltammogram (CV), linear sweep voltammogram (LSV), chronoamperogram (CV) and electrochemical impedance spectroscopy (EIS) were carried out using a VersaSTAT-3 electrochemical analyzer with a conventional three-electrode system under a nitrogen atmosphere at room temperature (27 °C). The *f*-ZnO@rFGO-modified GC electrode, platinum wire, and Ag/AgCl were used as the working, counter, and reference electrodes, respectively. The GCE-modified electrode was fabricated by drop casting 5 µL of the samples solution on a pretreated glassy carbon electrode in the oven for 5 min at 60 °C and drying at room temperature for 6 h. A 0.1 M phosphate buffer (pH = 7.2) was used as a supporting electrolyte. All the potentials are quoted against Ag/AgCl unless otherwise mentioned.

Meanwhile, the electrochemical measurements of Mb-AuNRs/RGO nanohybrid and AuNRs-RGO nanorod were performed using an Autolab electrochemical analyzer (PGSTAT204) with a conventional three-electrode system under a nitrogen atmosphere. The GCE-modified electrode was fabricated by drop casting 5 µL of the samples solution on a pretreated glassy carbon electrode in the oven for 5 min at 60 °C and drying at room temperature for 6 h. The sample was used as a working electrode, and a saturated calomel electrode (SCE) and platinum wire were used as the reference and counter electrodes, respectively. A 0.1 M phosphate buffer pH 2.5 and pH 7.2 were used as the supporting electrolyte for Mb-AuNRs/RGO nanohybrid and AuNRs-RGO nanorod, respectively. Nitrogen gas was bubbled into the electrolyte solution for 30 min before each experiment and the experiments were carried out under flowing N_2 gas. All the potentials given in this work were referred to the SCE, and all the experiments were carried out at room temperature.

CHAPTER 4: ELECTROCHEMICAL SENSING OF NITRITE USING A GLASSY CARBON ELECTRODE MODIFIED WITH REDUCED FUNCTIONALIZED GRAPHENE OXIDE DECORATED WITH FLOWER-LIKE ZINC

4.1 Introduction

Over the last few decades, nanostructured zinc oxide (ZnO) has received greater attention because of its excellent optical and electrical properties (Lee et al., 2003). The incorporation of ZnO nanostructures into graphene provides novel optical, electrical, and catalytic properties. Hence, it finds applications in photocatalysis, photoelectrochemical cells, electrocatalysis, and sensor devices (Zhang et al., 2005). Since the graphene sheets act as a support for the ZnO nanostructures, they promote electron transport by increasing the performance in the above-mentioned applications. Several synthetic methods have been adopted to prepare ZnO–graphene nanocomposites, including microwave-assisted reduction (Lu et al., 2011), an aqueous solution (Li et al., 2012), an electrochemical method (Yin et al., 2010), and hydrothermal treatment (Marlinda et al., 2012). Although various routes have been used to prepare ZnO–graphene, these preparation methods have some disadvantages, including the need for complex and high-temperature synthesis routes, less dispersion in solvents, and the poor dispersion of ZnO into the graphene. However, the adoption of a hydrothermal process is a simple and easy way to obtain a ZnO nanostructure (Akhavan, 2010) with reduced graphene oxide (RGO).

The hydrothermal method was selected because it is a simple method to fabricate a hybrid structure. ZnO nanoparticles are anchored on functionalized graphene sheets (FGS) using an intermediate to combine zinc ions with carbon materials. Water-soluble $Zn(CH_3COO)_2 \cdot 2H_2O$ and monodispersed GO were used as the precursors of the ZnO nanoparticles and FGO, respectively, and the transformations occurred during thermal

treatment. It is supposed that this method can be easily amplified at a low cost because (i) the raw materials are inexpensive, (ii) the fabrication process is simple, and (iii) the necessary pieces of equipment such as the magnetic reflux stirrer and calcining furnace are common.

Graphene oxide (GO) is a combination of two-dimensional oxidized graphene sheets with a large number of functional groups such as carboxylic acid, hydroxyl, and epoxide groups (Stankovich et al., 2006; Zhu et al., 2010). These functional groups make graphene oxide highly soluble in water. However, removing such groups during reduction results in agglomeration and precipitation (Stankovich et al., 2007). Therefore, to obtain water-dispersible graphene, several chemical modifications have been carried out. Wang et al. (2009) showed the maximum solubility of graphene oxide functionalized (FGO) with allylamine (Wang et al., 2009). Hou et al. (2010) also reported the modification of graphene oxide with a hydrophilic silane functional group, and the thus-prepared functional graphene oxide showed a good dispersion in water and was more stable in an aqueous solution than it precursor (Hou et al., 2010). Thus, this functionalized graphene oxide with a high hydrophilic-group content will be a major contributor to the fabrication of nanocomposite materials (Schniepp et al., 2006).

Moreover, graphene has a theoretical surface area of 2630 m^2g^{-1}, which is superior to that of graphite (10 m^2g^{-1}) and twice that of CNTs (1315 m^2g^{-1}). The electrical conductivity of graphene (64 mS cm^{-1}) is ~60-fold greater than that of SWCNTs. In addition, graphene has oxygen-containing groups at its edges or surface, and these provide convenient attachment sites, which make it more favorable for electrochemical applications (Chen et al., 2011).

Nitrite ions (NO_2^-) are well-known toxic inorganic pollutants and are present in food, soil, water, and physiological systems. High concentrations of nitrite ions can originate from caustic radioactive waste (Coleman et al., 1995). Excess nitrite ions are

detrimental to the human body, and a high concentration in drinking water is a serious health risk for infants. In the human body, nitrite can combine with hemoglobin in the blood to form methaemoglobin, which leads to a condition commonly known as "blue baby syndrome." Further, nitrite can also be converted into nitrosamine, which causes cancer and hypertension (Pandikumar et al., 2012). Hence, it is essential to monitor toxic nitrite ions in the environment.

To date, several analytical methods have been used for nitrite detection, including spectrophotometry, chemiluminescence and chromatography. However, these conventional analytical methods require a well-trained technician, expensive equipment, tedious detection procedures, and a long analysis period. In comparison to these traditional analytical methods, an electrochemical sensor platform offers a simple, rapid, selective, sensitive, inexpensive, reliable, and real-time analysis method for nitrite detection (Radhakrishnan et al., 2013; Veerapandian et al., 2012). Recently, various electrochemical nitrite sensors have been reported using graphene and its composite materials to modify electrodes. These have included Cu dendrites/rGO (Zhang et al., 2013), CR-GO (Mani et al., 2012), PEDOT/Graphene (Wang & Yun, 2012), graphene/polypyrrole/chitosan (Cui et al., 2011), Au/sulfonated graphene (Li et al., 2013), and CoNi/ErGO (Gholivand et al., 2014).

The use of expensive polymer and noble metals will hinder the commercialization of a sensor and increase its fabrication cost. Compared to polymers and noble metals, graphene and ZnO are cheap. In this study, we successfully used a one-step hydrothermal method to synthesize a flower-like zinc oxide/reduced functionalized graphene oxide (*f*-ZnO@rFGO) nanocomposite for the electrochemical detection of nitrite ions. The *f*-ZnO@rFGO nanocomposite was characterized using suitable techniques and then used for the fabrication of a modified electrode for an electrochemical sensor application.

4.2 Results and discussion

4.2.1 Optical studies of *f*-ZnO@rFGO nanocomposites

The flower-like ZnO showed an ultraviolet absorption below 390 nm, which is characteristic of ZnO semiconductor nanostructures due to the ZnO band gap of 3.12 eV (Figure 4.1 (a)) (Suresh et al., 2011). The functionalized graphene oxide had an absorbance at 230 nm (data not shown for brevity), which corresponded to the $\pi \longrightarrow \pi^*$ transition of aromatic C=C, along with another bump observed at 300 nm due to $\pi \longrightarrow \pi^*$ transition of carbonyl groups (Zhu et al., 2010). After the functionalized graphene oxide reduction to reduced functionalized graphene oxide, the absorbance at 264 nm (Figure 4.1 (b)) and bump at 300 nm disappeared, which were attributed to the complete removal of oxygen functional groups from the functionalized graphene oxide and the formation of a graphitic conjugation network on the resultant reduced functionalized graphene oxide. The *f*-ZnO@rFGO showed two characteristic absorption peaks at 264 and 367 nm. The former absorption was due to the reduced functionalized graphene oxide, and the latter was due to the presence of ZnO nanostructures, as seen in Figure 4.1 (c). Whereas Figure 4.1 (d) showed the characteristic absorption peak at 264 nm same as the rFGO Figure 4.1 (b).

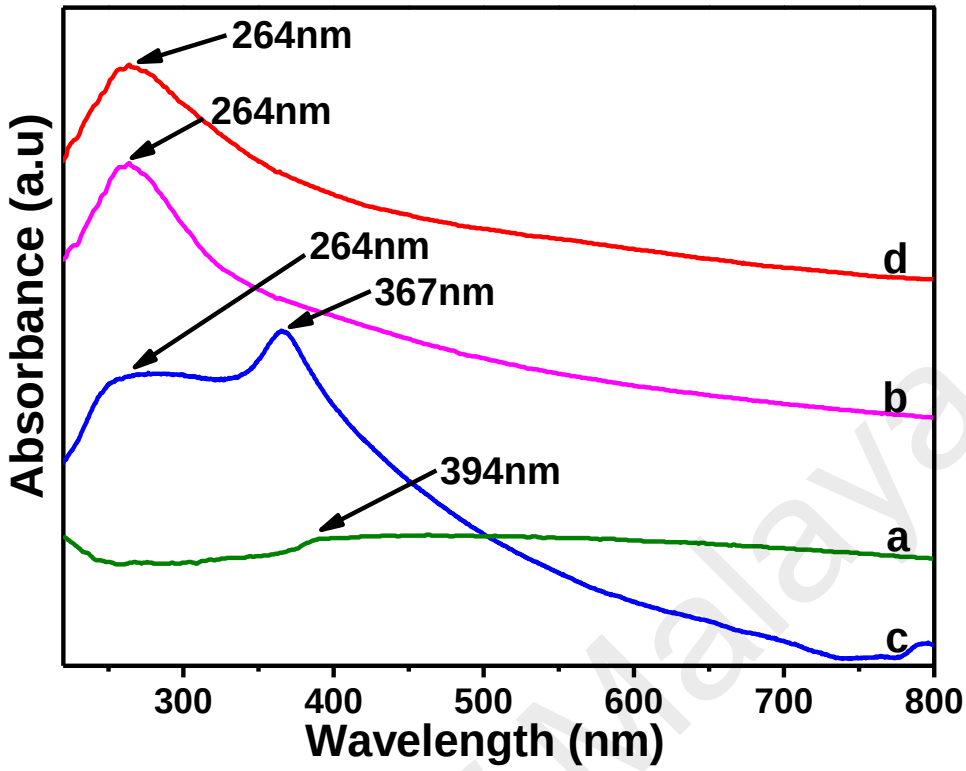

Figure 4.1: UV–vis absorption spectra of (a) ZnO, (b) rFGO, (c) *f*-ZnO@rFGO nanocomposite and (d) RGO, respectively.

The photoluminescence intensity of ZnO was significantly decreased after the incorporation into the rFGO (*f*-ZnO@rFGO) because the rapid electron transfer led to less recombination, as seen in Figure 4.2 (a and c). The reduced functionalized graphene oxide did not show any emission (Figure 4.2 (b) and inset). As comparison the reduced graphene oxide also exhibited no significant emission (Figure 4.2 (d). Both ZnO and *f*-ZnO@rFGO showed a weak emission at around 390 nm and a green emission band at around 550–650 nm. The presence of an ultraviolet emission and a sharp and intense emission in the visible region were related to ionized oxygen vacancies due to the good crystallization quality and high stoichiometric nature of the ZnO and *f*-ZnO@rFGO. The near-ultraviolet peak at 390 nm was attributed to the band-edge emission, while the broad visible bands were due to the deep-level defects in the ZnO crystal, such as the vacancies and interstitials of zinc and oxygen (Sheppard et al., 1939; Suresh et al., 2011).

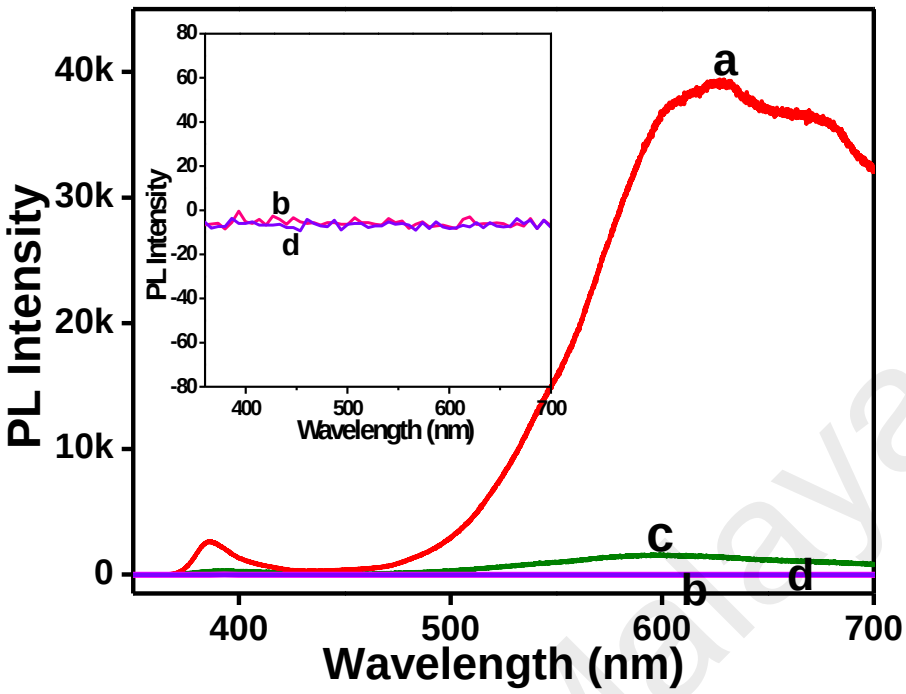

Figure 4.2: Photoluminescence spectra of (a) ZnO, (b) rFGO, (c) *f*-ZnO@rFGO nanocomposite and (d) RGO, respectively.

4.2.2 FT-IR Characterization

The functionalization of the GO was further confirmed by FTIR studies (Figure 4.3). The characteristic peaks of FGO and RGO in the spectrum appear at 3400 cm^{-1} (O–H stretching), 1595 cm^{-1} (O–H bending vibration), 1405 cm^{-1} (C–OH deformation) and around 1098 cm^{-1} (C–OH and C–O–C merged). The functionalization of the GO with TETA-silane showed the appearance of new methylene peaks at 2937–2806 cm^{-1}, along with the C–N stretching peak of the TETA-silane molecules at 1212 cm^{-1}. The successful formation of Si–O–C bonds between the GO and TETA was confirmed by the appearance of a peak at 710 cm^{-1}. The increased intensity of the broad peak at 3300 cm^{-1} in the FGO was due to the increased number of ionized carboxyl groups (Vijay Kumar et al., 2013). The decrease in broad peak at 3300 cm^{-1} was clearly seen in the RGO because of the removal of the carboxyl groups.

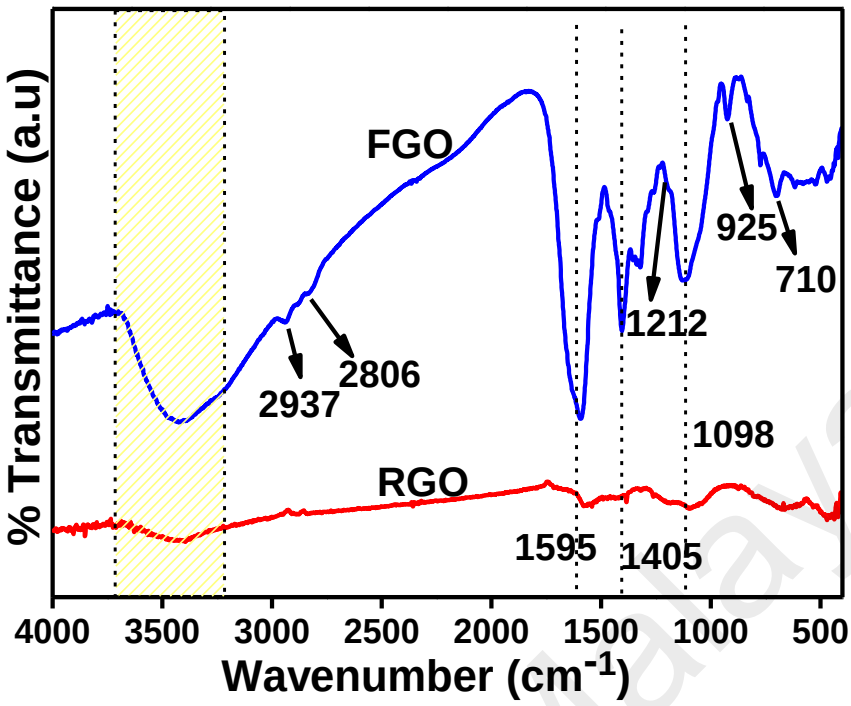

Figure 4.3: FT-IR spectra of FGO and RGO, respectively.

4.2.3 XRD analysis of *f*-ZnO@rFGO nanocomposites

All the diffraction peaks of the pure ZnO and nanocomposite matched the standard data for hexagonal-structured ZnO (JPCDS file no. 01-089-0510) (Figure 4.4 (a and c)). The appearance of a diffraction peak at 25.1° for the reduced functionalized graphene oxide was due to a complete reduction of the functionalized graphene oxide and exfoliation of the graphene layers (Hassan et al., 2009; Liu et al., 2011) (Figure 4.4 (b)). The observed weak diffraction peak at 25.1° was attributed to the removal of oxygen functional groups after the hydrothermal process (Radhakrishnan et al., 2014) and the decoration of flower-like ZnO on either side of the two dimensional thin rFGO nanosheets. The hump diffraction peak at 26° showed the reduction of RGO (Figure 4.4 (d)). In addition, we noted that the relative intensity of the nanocomposite was higher than the relative intensity of standard ZnO, which indicated that the prepared ZnO grew along the (002) crystal plane direction.

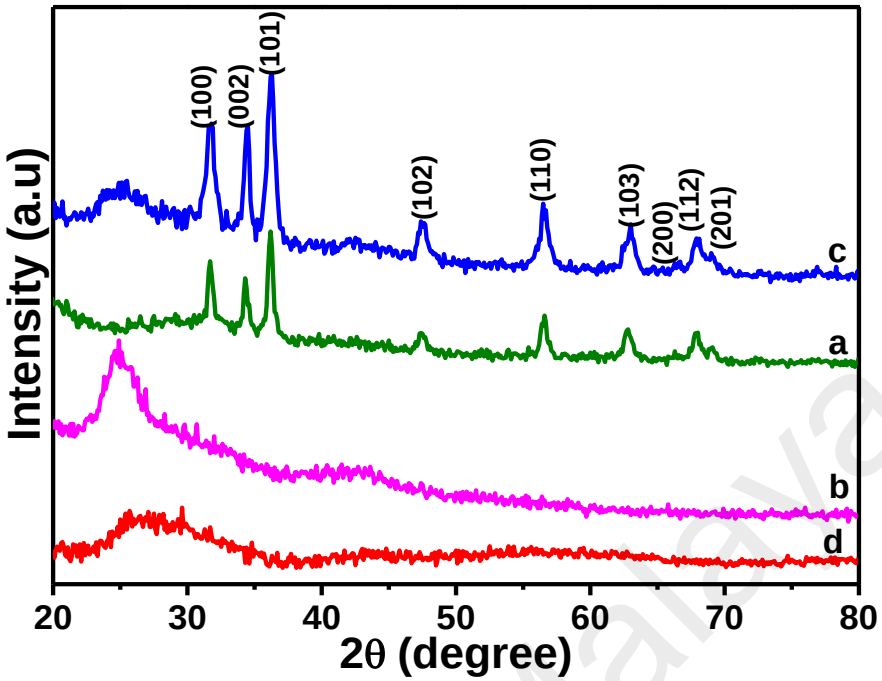

Figure 4.4: X-ray diffraction patterns of (a) ZnO, (b) rFGO, (c) *f*-ZnO@rFGO nanocomposite and (d) RGO, respectively.

4.2.4 Raman characterization of *f*-ZnO@rFGO nanocomposite

The Raman spectra of the functionalized graphene oxide and *f*-ZnO@rFGO were dominated by two intensity peaks at 1357 cm^{-1} and ~1600 cm^{-1} (Figure 4.5 (b and c)), whereas the ZnO did not show any peak in the displayed region (Figure 4.5 (a)). The observed former and latter peaks due to the D and G bands were related to the defects after the reaction process. The ratio of the intensities of the D and G bands (I_D/I_G) was related to the in-plane crystallite size of the graphene sheets with a few layers (Pimenta et al., 2007). According to the Raman spectra of the composite, the intensity ratio of the D peak to G peak of functionalized graphene oxide increased compared to reduced graphene oxide shown in (Figure 4.5 (d)). This indicated a decrease in the average size of the sp^2 domain upon the reduction of functionalized graphene oxide to reduced functionalized graphene oxide (Xiang et al., 2011; Zhou et al., 2011).

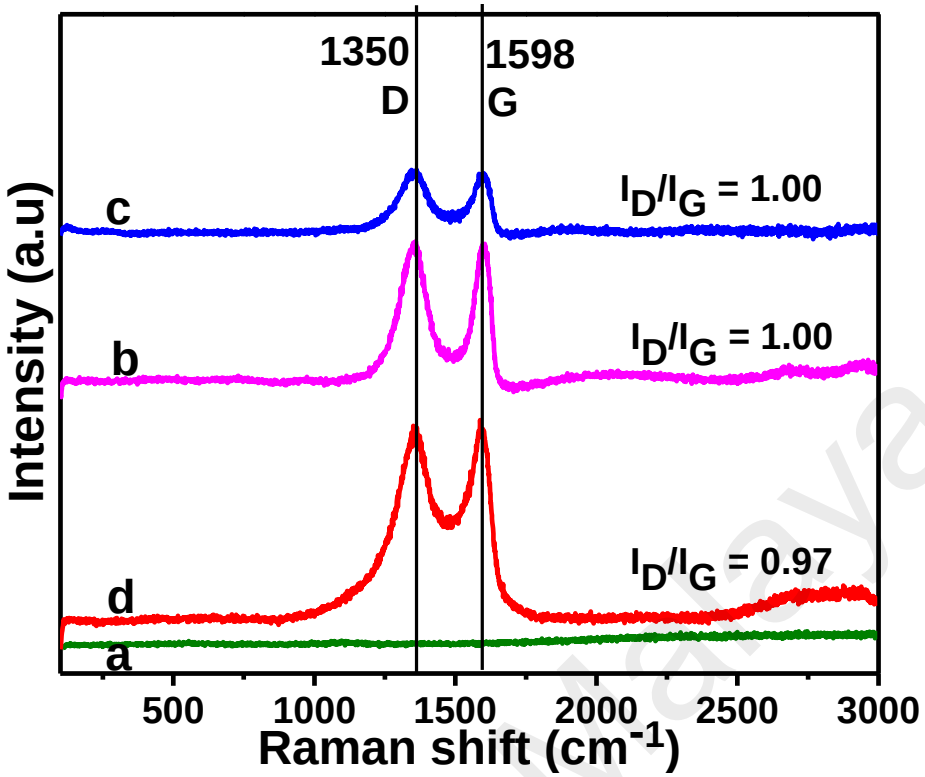

Figure 4.5: Raman spectra of (a) ZnO, (b) rFGO, (c) *f*-ZnO@rFGO nanocomposite and (d) RGO, respectively.

4.2.5 Morphological studies of *f*-ZnO@rFGO nanocomposite

The FESEM image of the pure ZnO shows a highly dense growth of ZnO with a star-anise-like architecture and a size of approximately 1 µm (Figure 4.6 (a)). The FESEM results for the flower-like ZnO@rFGO show a random distribution of ZnO particles decorated on both sides of the graphene sheets (Figure 4.6 (b)). At a higher magnification, the particles look flower-like, with an average size of 0.5 µm, which is smaller than that of pure ZnO (Figure 4.6 (c)). This proves that the shape and size of the ZnO particles are dependent on the presence of the functionalized graphene oxide support. The surface of the functionalized graphene oxide contained unreacted hydroxyl groups attached to the hexagonal basal plane and a large number of functionalized carboxylic groups from the N-(trimethoxysilylpropyl) ethylenediamine triacetic acid trisodium salt aqueous solution, which interacted with the zinc cations and formed a complex through electrostatic interaction. Under the hydrothermal condition, zinc ions

were anchored on the surface of the functionalized graphene oxide, forming flower-like nanostructures. Figure 4.6 (d) shows a TEM image of the *f*-ZnO@rFGO with a highly dense flower-like structure on both sides of the graphene sheets. An HRTEM analysis was performed on the synthesized *f*-ZnO@rFGO to determine its atomic arrangement in the nanometer domain (Figure 4.6 (e)). Figure 4.6 (f) shows lattice fringes with an interplanar distance of 0.281 nm, which can be assigned to the (100) plane of the hexagonal ZnO (Wu et al., 2010). The FESEM images clearly show that the flower-like ZnO grew on both sides of the reduced functionalized graphene oxide sheets (Figure 4.6 (c)). Figure 4.7 (a) shows a TEM image of FGO in the form of sheet layers. Even after a long period of sonication during the preparation of a TEM specimen, ZnO particles were still attached to the reduced functionalized graphene oxide sheets with a high density (Figure 4.7 (b and c)), which showed a strong interaction between the ZnO particles and reduced functionalized graphene oxide sheets. Further study by magnifying the image showed a flower-like petal with a length of 467.76 nm and a diameter of 126 nm (Figure 4.7 (c)).

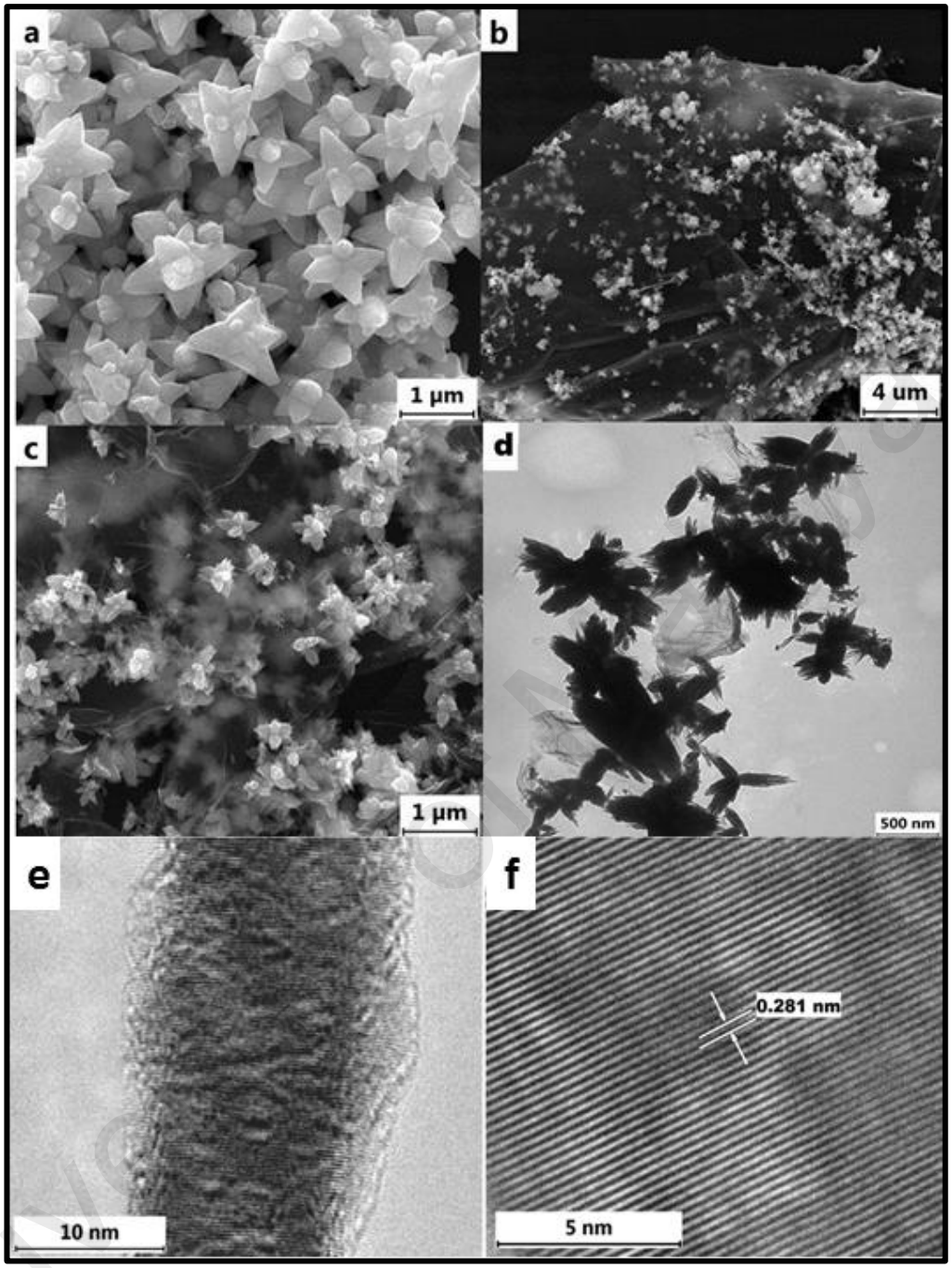

Figure 4.6: FESEM images of star-anise-like ZnO (a), flower-like *f*-ZnO@rFGO nanocomposite (b), nanocomposite at higher magnification (c), TEM image of flower-like *f*-ZnO@rFGO nanocomposite (d), HRTEM of flower-like *f*-ZnO@rFGO nanocomposite (e) and, lattice resolved TEM (f) image of flower-like *f*-ZnO@rFGO nanocomposite.

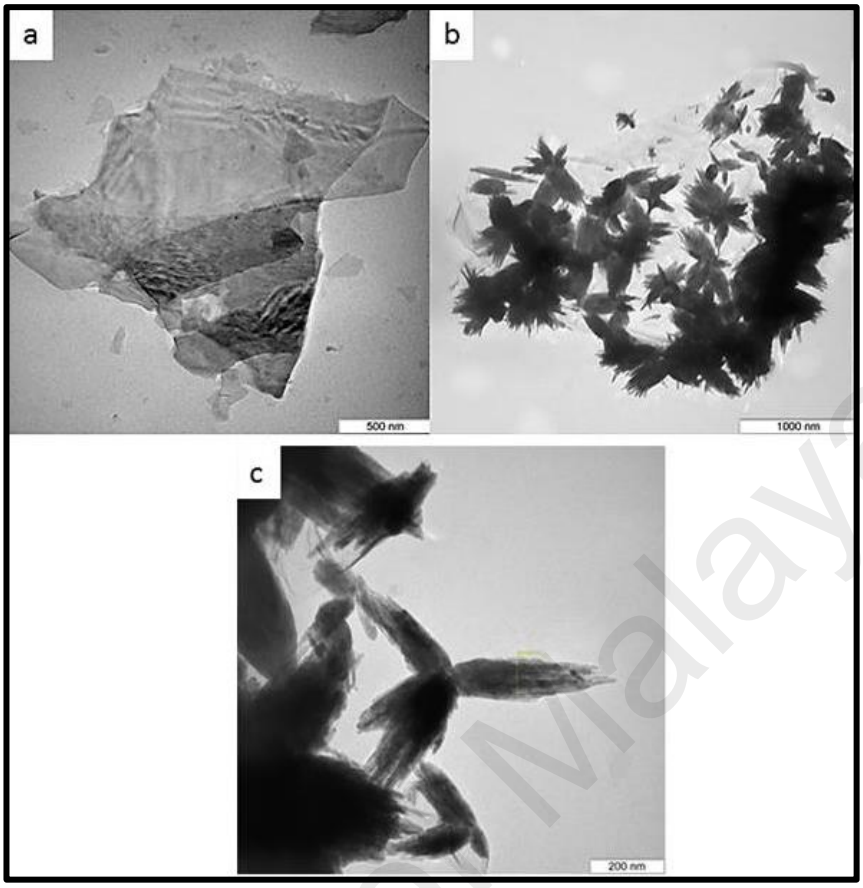

Figure 4.7: TEM images of FGO (a), and (b) lower and (c) higher magnifications of *f*-ZnO@rFGO nanocomposite.

4.2.6 Electrocatalytic activity of *f*-ZnO@rFGO modified electrode

The electrocatalytic oxidation of nitrite was studied by recording cyclic voltammograms for the bare GCE, ZnO, FGO, rFGO, and *f*-ZnO@rFGO nanocomposite in the presence of nitrite in order to find a sensor electrode for the electrochemical detection of nitrite. In our work, phosphate buffer with pH 7.2 was chosen for the electrocatalysis and sensor studies because of the instability of nitrite anions in an acidic medium (pH < 6.0 and pH = 2.5) (decomposition of NO_2^- into NO_3^- and NO) (Brylev et al., 2007; Pandikumar & Ramaraj, 2011). In a basic medium (pH > 7), the oxidation of nitrite became more difficult because of the lack of protons (Sun et al., 1999).

The cyclic voltammetric characteristics were recorded in a 0.1 M phosphate buffer (pH 7.2) solution containing 1 mM of nitrite at a scan rate of 50 $mV \cdot s^{-1}$. The schematic

mechanism of the electrocatalytic oxidation and the experimental results are shown in Figure 4.8. During the electrochemical oxidation of NO_2^-, the NO_2^- was oxidize to NO_3^- by transferring two electrons by following the second-order homogeneous disproportionation process (Guidelli et al., 1972; Li et al., 2013). This NO_3^- was the only oxidation product, which is more favorable for the electrochemical sensing of nitrite**.** The overall reaction is given in the following equation 4.1.

$$\boldsymbol{NO_2^- + H_2O - 2e^- \rightarrow NO_3^- + 2H^+} \qquad (4.1)$$

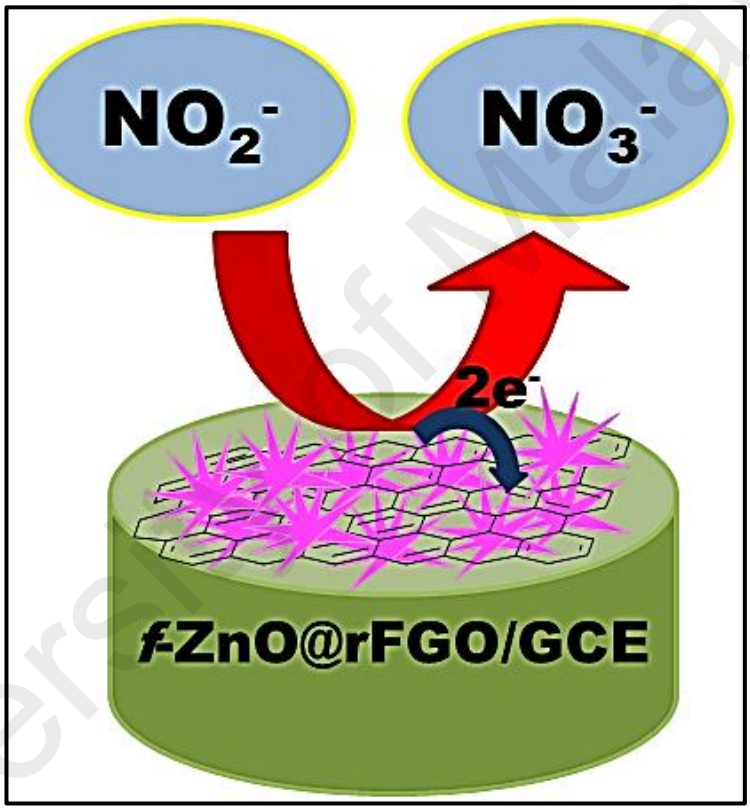

Figure 4.8: The schematic mechanism for the electrochemical sensing of nitrite with *f*-ZnO@rFGO nanocomposite.

As can be seen from Figure 4.9, the *f*-ZnO@rFGO-modified electrode showed a remarkable electrocatalytic response toward the oxidation of nitrite, with a higher current than the other modified electrodes. The nitrite oxidation potential of the *f*-ZnO@rFGO-modified electrode was significantly shifted toward a negative value with an increase in the peak current signal compared to the other modified electrodes. This increased peak current and decreased oxidation potential of nitrite for the *f*-ZnO@rFGO-modified electrode contributed to the following two factors: (i) the *f*-ZnO@rFGO composite restricted the reduced functionalized graphene oxide sheet aggregation by the introduction of flower-like ZnO on both sides of the reduced graphene oxide sheets and hence increased the surface area of the *f*-ZnO@rFGO nanocomposite compared to that of the reduced functionalized graphene oxide sheet. (ii) The ZnO flower-like structures in the *f*-ZnO@rFGO nanocomposite were well dispersed. Thus, electrochemical sites were accessible and highly active.

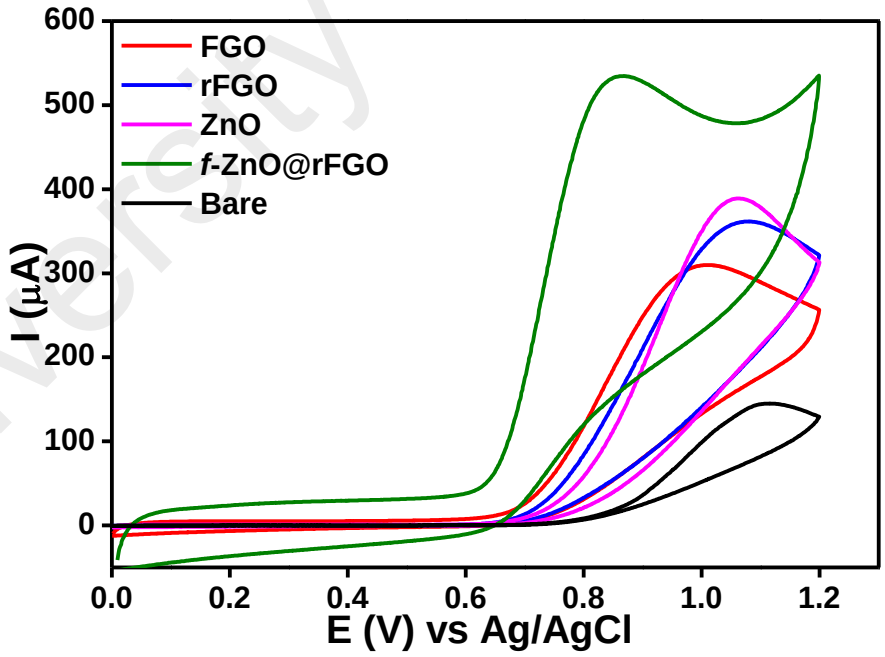

Figure 4.9: The CV plots of bare GC and various modified electrode in 0.1 M phosphate buffer (pH 7.2) with 1 mM concentration of nitrite at scan rate of 50 $mV \cdot s^{-1}$.

The *f*-ZnO@rFGO showed a higher electrocatalytic oxidation peak current than the ZnO-rGO due to the presence of functionalized RGO (rFGO). Thus, it could pre-concentrate the nitrite ions on the electrode surface (Figure 4.10). The data indicated that the *f*-ZnO@rFGO-modified electrode had a good catalytic activity toward nitrite sensing compared to those of the bare GC, ZnO, FGO, and rFGO.

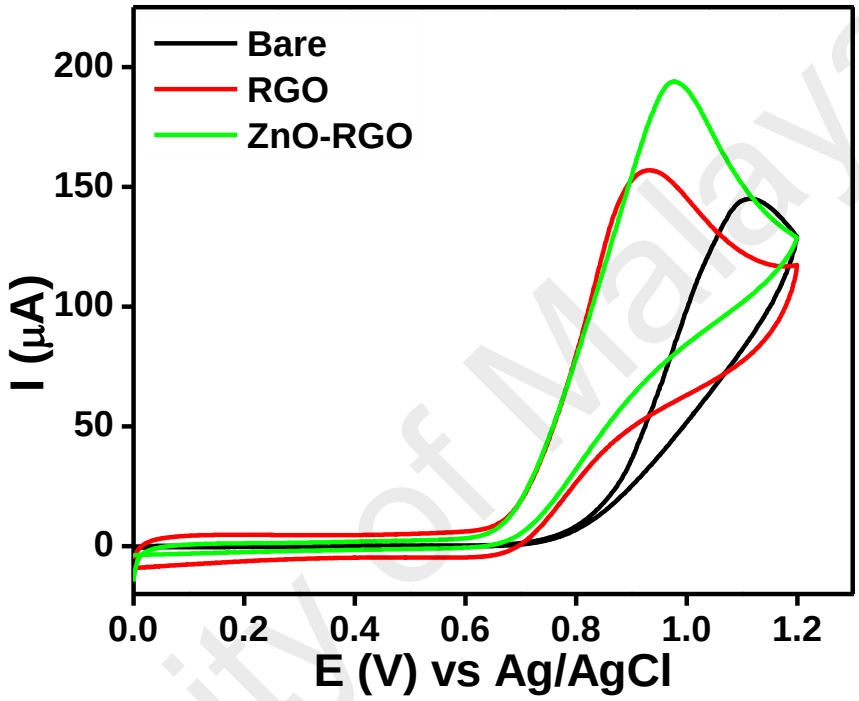

Figure 4.10: The CV plots of bare GC, RGO and ZnO-RGO modified electrode in 0.1 M phosphate buffer (pH 7.2) with 1 mM concentration of nitrite at scan rate of 50 $mV \cdot s^{-1}$.

4.2.7 Electrochemical detection of nitrite at *f*-ZnO@rFGO modified electrode

Figure 4.11 shows a linear sweep voltammogram obtained for the *f*-ZnO@rFGO-modified electrode in the presence of nitrite at a concentration range of 0.1–3 mM in 0.1 M phosphate buffer (pH 7.2) with a scan rate of 50 $mV \cdot s^{-1}$. It can be seen that the oxidation peak current was increased when the nitrite concentration was increase to 3 mM. The LSV curves show a well-defined and stable anodic oxidation peak current for nitrite. These results demonstrated that the *f*-ZnO@rFGO-modified electrode provided a good electrocatalytic activity toward nitrite sensing.

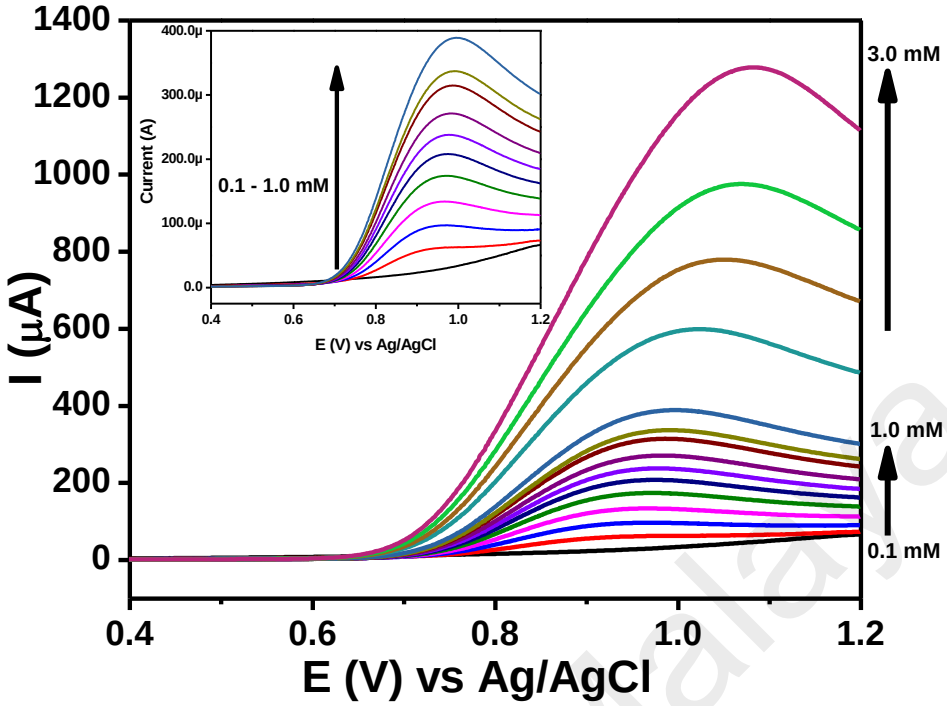

Figure 4.11: LSV obtained for *f*-ZnO@rFGO modified electrode in presence of nitrite at concentration range of 0.1–3 mM in 0.1 M pH 7.2 phosphate buffer at scan rate of 50 $mV{\cdot}s^{-1}$. Magnification of LSV for *f*-ZnO@rFGO modified electrode in presence of nitrite at concentration range of 0.1–1 mM (Inset).

Further, the observed calibration plot for the peak current against the nitrite concentration is shown in Figure 4.12. The calibration plot in Figure 4.12 shows the linear relation between the peak current and the nitrite concentration in the range of 0.1–3 mM. The calibration plot has a correlation coefficient (R) of 0.9987 with the following regression equation: $I\ (\mu A) = 0.3809(mM) + 0.1613 \mu A$. The limit of detection was calculated to be 33 µM (signal-to-noise ratio (S/N) = 3) by substituting the blank standard deviation (σ = 4.0849µ) and sensitivity (m = 0.3809 μA/mM) in the $\frac{3\sigma}{m}$ criterion.

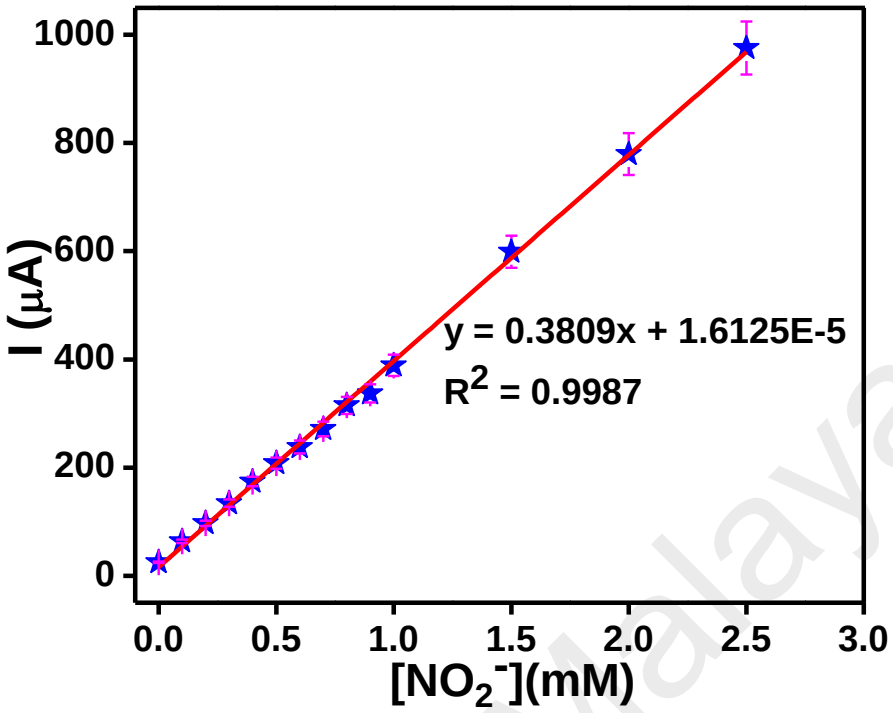

Figure 4.12: The linear correlation plot obtained for *f*-ZnO@rFGO modified electrode in presence of nitrite at concentration range of 0.1–3 mM in 0.1 M pH 7.2 phosphate buffer at scan rate of 50 $mV{\cdot}s^{-1}$.

Figure 4.13 shows the chronoamperometric curve for successive additions of nitrite at regular intervals to homogeneously stirred 0.1 M phosphate buffer (pH 7.2) with an applied potential of 0.9 V. Each addition of nitrite at 60 s intervals produced a drastic current response, and the steady-state value was reached within 5 s. Such a fast response implies that the GC/*f*-ZnO@rFGO efficiently promoted the oxidation of nitrite, which is desirable for the real-time analysis of samples. The current response was proportional to the nitrite concentration in the concentration range of 10 µM to 5.0 mM, and two different segments corresponding to different linear ranges were observed.

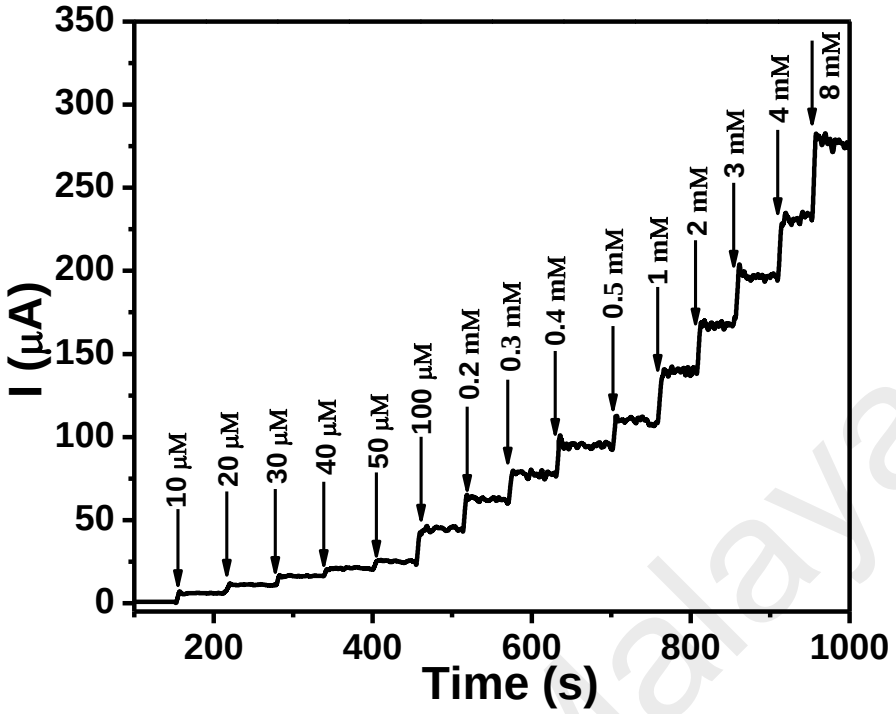

Figure 4.13: Amperometric *i–t* curve for determination of nitrite of *f*-ZnO@rFGO electrode in 0.1 M phosphate buffer (pH 7.2), where additions of nitrite were performed at regular intervals of 60 s at applied potential of 0.9 V.

These observed linear segments represented the kinetic limitation of the *f*-ZnO@rFGO nanocomposite, which was due to the decrease in current sensitivity at a higher concentration of analyte. The first linear segment ($y = 0.2145x + 1.1731E\text{-}5$) with a correlation coefficient of 0.9636 corresponded to the lower range, while the second linear segment ($y = 0.0355x + 9.7364E\text{-}5$) with a correlation coefficient of 0.9885 corresponded to the higher range of the nitrite concentration (Figure 4.14). The detection limit (LOD) for the linear calibration of the lower range was 41 μM (S/N = 3).

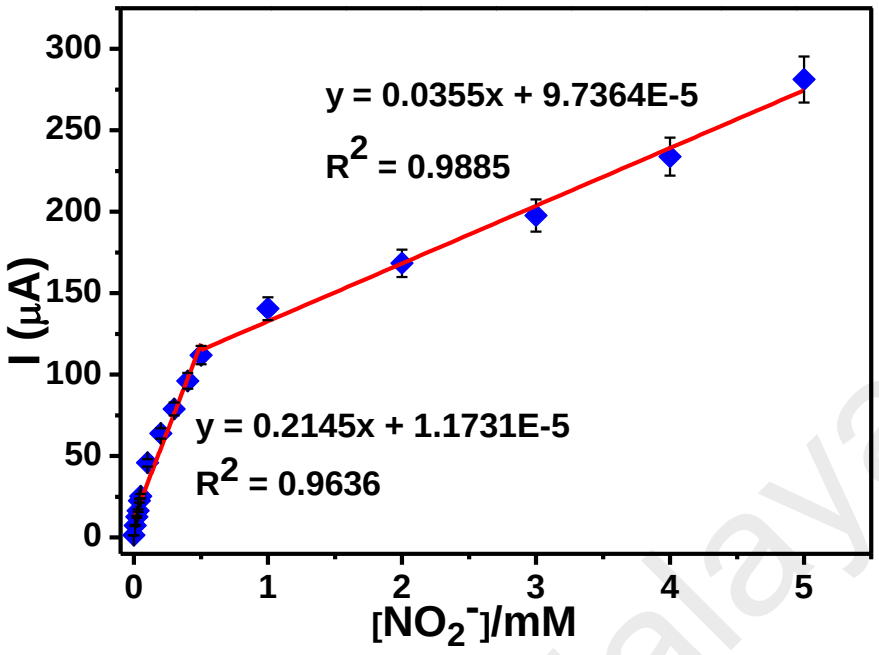

Figure 4.14: The linear correlation plot obtained for *f*-ZnO@rFGO modified electrode in presence of nitrite at concentration range of 10 µM to 5 mM in 0.1 M pH 7.2 phosphate buffer at scan rate of 50 $mV{\cdot}s^{-1}$.

The present nitrite detection results were compared with previous reports, as summarized in Table 4.1.

Table 4.1: Analytical parameters reported for some modified electrodes towards nitrite detection.

Modified electrode	Linear range	Detection limit	Reference
PEDOT/Graphene modified electrode	0.5-240 µM	0.15 µM	(Wang & Yun, 2012)
Graphene nanoplatelet-protein composite film	50 µM-2.5 mM	10 mM	(Cui et al., 2011)
NP-Fe_2O_3-CoO composite	0.2-16.2 mM	0.1 µM	(Wang et al., 2014)
GR/PPy/CS nanocomposite modified GCE	0.5-722 µM	0.1 µM	(Ye et al., 2011)
HAC modified GCE	1-127 µM	0.07 µM	(Madhu et al., 2014)
CR-GO modified GCE	8.9-167 µM	1.0 µM	(Mani et al., 2012)
PEDOT/GR modified GCE CoNi/ErGO	0.3-600 µM 0.1-330 µM	0.1 µM 0.05 µM	(Nie et al., 2013; Gholivand et al., 2014)
CoOx/MWCNTs/GCE	0.5-250 µM	0.3 µM	(Meng et al., 2011)
Nano-Au/P_3MT modified GCE	10-1000 µM	2.3 µM	(Huang et al., 2008)
GCE/*f*-ZnO@rFGO	10 µM-8 mM	33 µM	This Work

Foot note: PEDOT = poly(3,4-ethylenedioxythiophene); SPCEs = screen-printed carbon electrodes; MWCNTs = multi-wall carbon nanotubes; NP-Fe_2O_3-CoO = nanoporous Fe_2O_3–CoO composite ; GCE = glassy carbon electrode; GR/PPy/CS = graphene/polypyrrole/chitosan; HAC = heteratom-enriched activated carbon; CR-GO = chemically reduced graphene oxide; PEDOT/GR = poly(3,4-ethylenedioxythiophene)/graphene nanocomposite; IL–SWCNT = ionic liquid single-walled carbon nanotube; Hb/Au/GACS = hemoglobin graphene with biocompatible chitosan; nano-Au/P_3MT = gold nanoparticles on poly(3-methylthiophene).

As illustrated in Table 4.1, the results indicated that the present sensor showed a wider linear range and lower detection limit than some other modified electrodes. Furthermore, this detection could be carried out in a neutral medium, which is greatly preferable for applications involving the biochemical detection of nitrite. However, the *f*-ZnO@rFGO-modified electrode showed a higher limit of detection than the other modified electrodes listed in Table 4.1. Nevertheless, the present study is more

promising because of the low cost fabrication, facile synthetic method, and long-term stability.

The selective determination of nitrite in the presence of interfering compounds using the *f*-ZnO@rFGO-modified electrode was tested using various common ions such as Cu^{2+}, K^{+}, Na^{+}, Cl^{-}, NO_3^{-}, and SO_4^{-}, and also in the presence of electroactive compounds such as uric acid, glucose, ascorbic acid, dopamine, and hydrogen peroxide. No changes in the chronoamperometry current response (Figure 4.15 (A and B)) were observed for nitrite when the interfering species were introduced. As a result, it can be concluded that the present *f*-ZnO@rFGO-modified electrode is highly selective toward the determination of nitrite even in the presence of these potential interferences.

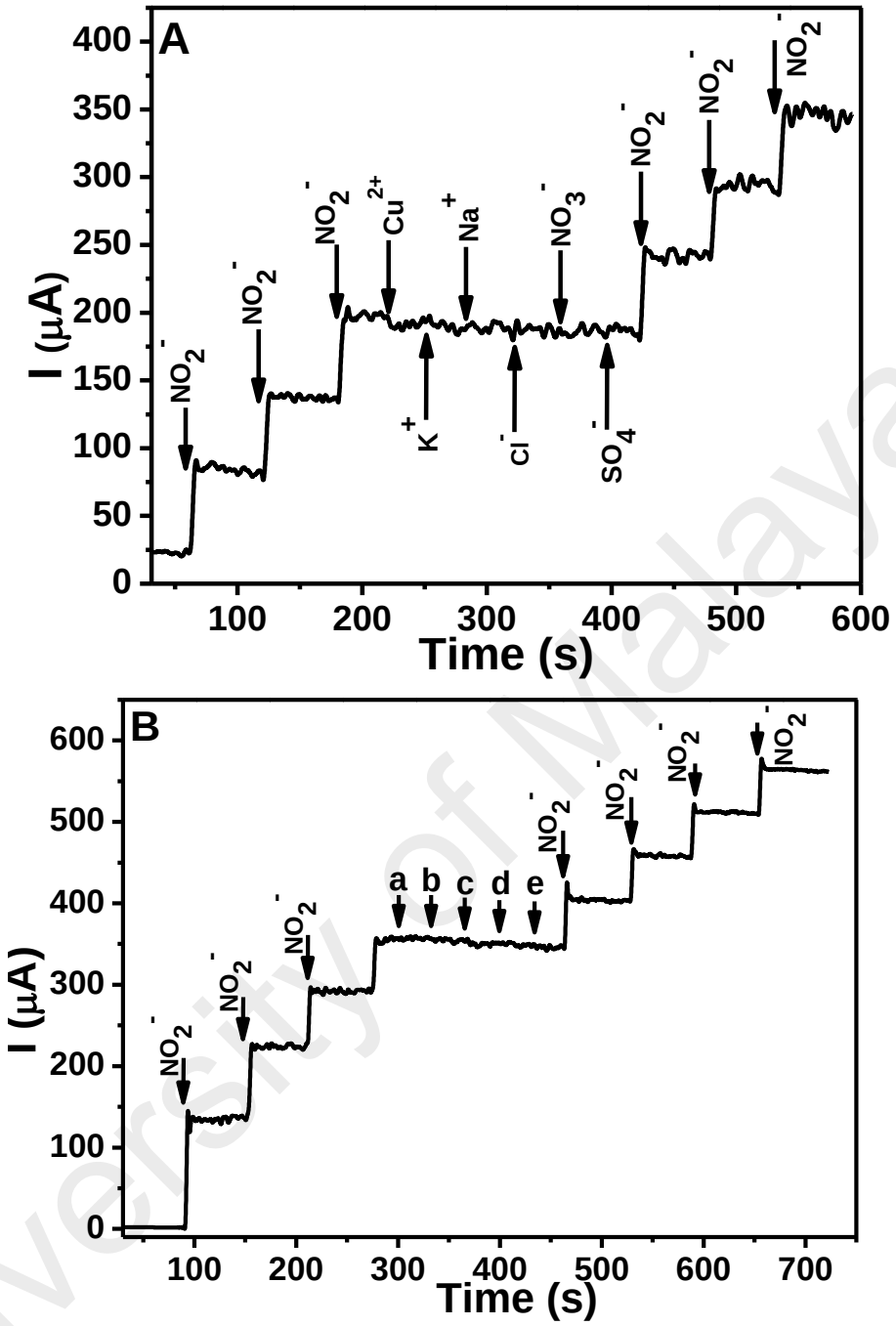

Figure 4.15: The amperometric *i–t* curve for determination of nitrite in the presence of each metal ion interferences (A), and in the presence of each electroactive compound (B): uric acid (a), glucose (b), ascorbic acid (c), dopamine (d) and hydrogen peroxide (e), added one by one to same solution at GC/*f*-ZnO@rFGO electrode in 0.1 M phosphate buffer (pH 7.2) with E_{app} = 0.9 V.

The stability of the signal was studied using the amperometric *i–t* curve for 1 mM nitrite with *f*-ZnO@rFGO-modified electrode in a 0.1 M phosphate buffer (Figure 4.16). Over a period of time, the detected current signal very slowly decreased due to the oxidation of nitrite, but there were no significant changes at a fixed potential of 0.9 V.

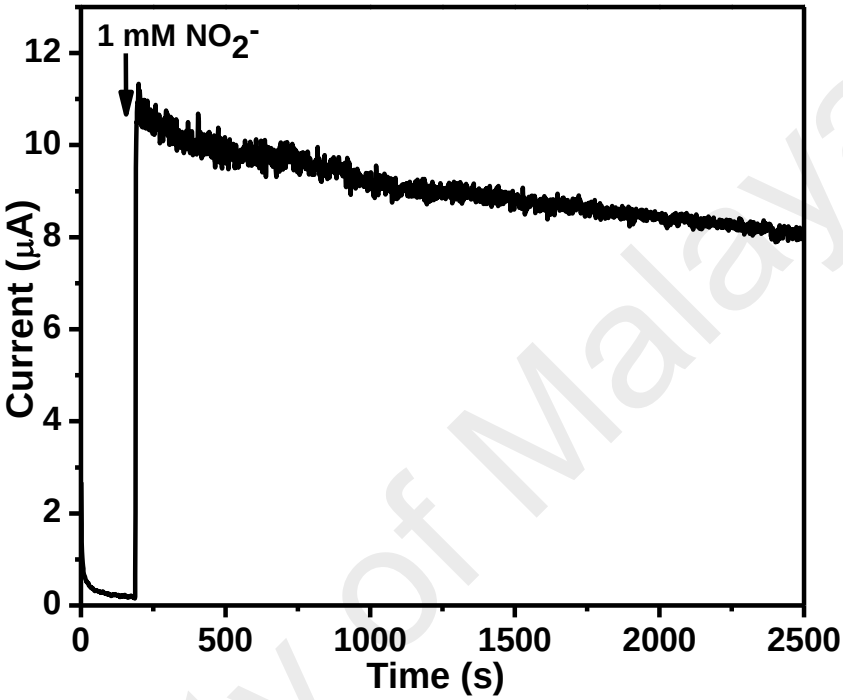

Figure 4.16: The amperometric *i–t* curve obtained for the 1 mM of nitrite with *f*-ZnO@rFGO modified electrode in 0.1 M phosphate buffer (pH 7.2) at applied potential of 0.9 V.

Further, to investigate the possible use of the fabricated electrode, experiments were conducted using various water samples (river, lake, sea and tap water) to determine the amperometric concentration of nitrite by using the standard addition method. The river water was collected from Taman Rimba Bukit Kerinchi, and the lake water was from Banting Lake. The sea water was collected from Port Dickson beach, whereas the tap water was from the University of Malaya. The obtained results are summarized in Table 4.2. The flower-like *f*-ZnO@rFGO-modified electrode exhibited recoveries in the range of 84% –108%. This reveals that the proposed method outlined in this work for nitrite sensing holds promise for the direct analysis of environmental samples.

Table 4.2: Determination of nitrite in various real samples by using chronoamperometric method with the *f*-ZnO@rFGO modified electrode.

Real samples	Analyte	Added (μM)	Found (μM)	Recovery (%)
River water	NO_2^-	50	42	84
Lake water	NO_2^-	50	43	86
Sea water	NO_2^-	50	54	108
Tap water	NO_2^-	50	54	108

4.3 Conclusion

A flower-like *f*-ZnO@rFGO nanocomposite was successfully synthesized using a simple hydrothermal route and characterized using suitable analytical techniques. The *f*-ZnO@rFGO modified electrode was used for the electrochemical detection of nitrite. The *f*-ZnO@rFGO modified electrode exhibited an excellent electrocatalytic activity toward the oxidation of nitrite with a higher current, and also significantly reduced the over potential by up to ~200 mV compared to the other controlled electrodes because of the synergistic catalytic effect between the ZnO and rFGO. The sensor electrode showed a linear oxidation current in the concentration range of 10 μM–8 mM for the nitrite, and the detection limit was found to be 33 μM. The excellent electrocatalytic activity, low detection limit, high sensitivity, and rapid response time demonstrated by this newly prepared *f*-ZnO@rFGO nanocomposite could make it a potential candidate for practical applications.

CHAPTER 5: CHRONOAMPEROMETRY DETERMINATION OF DIHYDRONICOTINAMIDE ADENINE DINUCLEOTIDE USING A GLASSY CARBON ELECTRODE MODIFIED WITH GOLD NANORODS AND REDUCED GRAPHENE OXIDE

5.1 Introduction

Dihydronicotinamide adenine dinucleotide (NADH) is an important coenzyme involved in metabolic processes, and is commonly found in every cell of living organisms (Tang et al., 2009). It alternates between the oxidized state (NAD+) and the reduced state (NADH) for the production of ATP, and serves as a hydrogen and electron carrier in cellular respiration, photosynthesis, etc. (Huang et al., 2005). More than 300 enzymes have been identified as NADH-dependent dehydrogenases, and are responsible for maintaining cellular growth, differentiation, and energy metabolism (Álvarez-González et al., 2000; Gorton & Domí, 2002; Tang et al., 2005). As the coenzyme for quinone reductases in microbes, NADH also plays an important role in the metabolism of quinone compounds. Therefore, methods for analyzing NADH have been given tremendous attention as an effective approach to investigate the metabolism and degradation processes in the microbial treatment of contaminants. Sensors for NADH-dependent dehydrogenase can undoubtedly play a significant role in numerous application fields such as pollution control, clinical biology, the food industry, and other bioprocess monitoring fields (Rao et al., 1999; Tang et al., 2009). Because the nicotinamide ring of NADH undergoes a two-electron oxidation to produce NAD+, a considerable amount of the analytical research conducted in previous decades has been concerned with the electrochemistry of the NAD+/NADH redox couple in attempts to electrochemically monitor the NADH concentration through its reoxidation to NAD+ (Álvarez-González et al., 2000).

Nanostructured materials such as nanorods, nanotubes, and nanoparticles exhibit interesting physical properties (excellent biochemical stability, good mechanical strength, and a wide electrical conductivity range) which can be utilized in the electrochemical detection of NADH. Their electrical conductivity depends on the size and morphology of the materials (Valentini et al., 2004; Wang et al., 2003; Zhang et al., 2007).

Gold nanorods (AuNRs) are one of the nanostructures with unique optical properties, which depend on their shape anisometry (Chen et al., 2013; Huang et al., 2009; Pérez-Juste et al., 2005). The unique properties of AuNRs find potential applications in imaging, therapy, and sensing (Chen et al., 2013). Graphene is another attractive material that is given much attention because of its useful properties, including a large surface area, high electrical conductivity, wide electrochemical detection window, and chemical inertness (Chen, 2010; Wen et al., 2012). Most of the chemically synthesized graphene materials contain oxygen as a principal element and are called reduced graphene oxide (rGO) (Tabrizi & Zand, 2014). Combining AuNRs and graphene has shown a synergistic effect in several electrocatalysis and sensor applications (Bai et al., 2014; Zhang et al., 2013).

In this work, we report the detection of NADH based on a gold nanorod-reduced graphene oxide nanocomposite (AuNR-RGO), which was synthesized using a simple seed-mediated growth solution process. The AuNR-RGO-modified electrode showed good electrocatalytic activity toward the NADH oxidation. The AuNR-RGO exhibited an excellent amperometric response to NADH, showing great promise for the fabrication of biosensors for practical applications.

5.2 Results and discussion

5.2.1 Morphological studies of AuNR-RGO nanorod

Figure 5.1 shows a typical field emission scanning electron microscopy (FESEM) image of the synthesized AuNR-RGO nanorod. The FESEM image shows that the RGO sheets decorated with Au nanorods had an ultra-thin wrinkled morphology, and the corresponding histogram provides the average lengths and widths of 50 nanorods. The image shows that the nanorods were 44 ± 3 nm in length and 12 ± 2 nm in width. Each of the nanorods had an aspect ratio of 3.5 and a smooth surface.

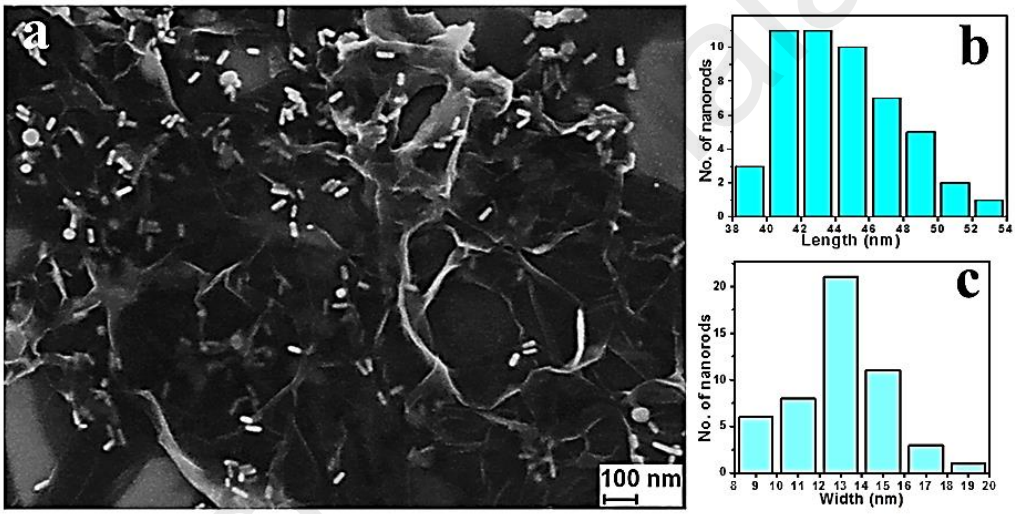

Figure 5.1: (a) FESEM image of AuNR-rGO and histogram obtained for (b) length and (c) width of the AuNR.

5.2.2 Electrochemical behaviors of modified electrode

Cyclic voltammograms were recorded for the bare glassy carbon electrode (GCE) and gold nanorod-reduced graphene oxide/glassy carbon electrode (AuNR-RGO/GCE) using 3 mM of $Fe(CN)_6^{3-}/Fe(CN)_6^{4-}$ in 0.1 M KCl (Figure 5.2). The voltammograms showed two nearly symmetric anodic and cathodic peaks related to the redox system of the $Fe(CN)_6^{3-}/Fe(CN)_6^{4-}$ solution. The cyclic voltammogram of the AuNR-RGO/GCE showed the characteristic oxidation peak at 0.27 V, and its corresponding reduction peak was observed at 0.07 V. Among the investigated electrodes, the AuNR-RGO/GCE

showed a higher current and lower peak-to-peak separation, which indicated the enhanced electrocatalytic activity of the AuNR-RGO/GCE.

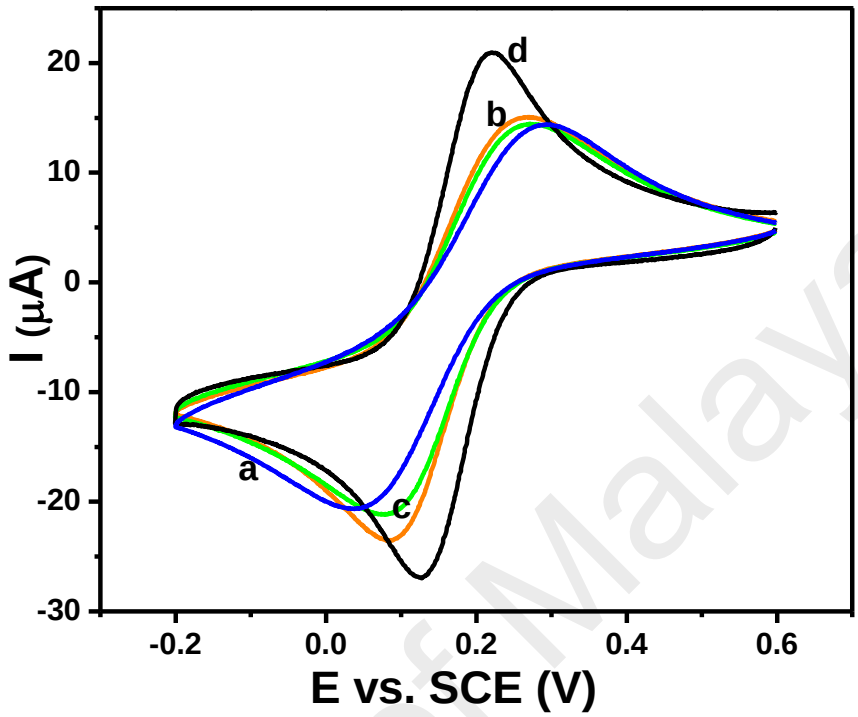

Figure 5.2: Redox analyte of bare GC (a), AuNR/GCE (b), RGO/GCE (c), and AuNR-RGO/GCE (d) in presence of 3 mM of $Fe(CN)_6^{3-}/Fe(CN)_6^{4-}$ in 0.1 M KCl.

In order to understand the observed characteristics of the sensor architectures in more detail, electrochemical impedance spectroscopy (EIS) measurements were carried out to elucidate the electron transfer properties of the samples. The electrochemical impedance spectra were obtained for the bare GCE, RGO/GCE, AuNR/GCE, and AuNR-RGO/GCE in the presence of 3 mM of $Fe(CN)_6^{3-}/Fe(CN)_6^{4-}$ in 0.1 M KCl. The open circuit potential was chosen as the electrode potential, and frequency range was 0.1 Hz–100 kHz. Figure 5.3 shows the Nyquist plots of the electrochemical impedance spectra recorded at the corresponding open circuit potentials of modified electrodes. The first intercept of the semicircle at the real axis in the high frequency region represents the resistance of the electrolyte; the contact resistance between the electrolyte, current collector, and active material; and the intrinsic resistance of the active material itself (Ju et al., 2008). The electron transfer resistance (R_{ct}) can be estimated from the diameter of

the semicircle. The charge transfer resistance is the resistance between the electrode and the aqueous electrolyte, i.e., the electrode/electrolyte interface. The key benefit of Nyquist plot is the convenience of observing the effects of the ohmic resistance of an electrode material. The linear slope in the lower frequency region relates to the capacitive behavior and the ionic diffusion of an electrode. A steeper slope that is nearly perpendicular to the real axis (*Z*') indicates good capacitive behavior and ionic diffusion, all of which are ideal characteristics of a good electrode for supercapacitor applications (Yen et al., 2015). The Nyquist plot shows a semicircle at higher frequencies corresponding to the electron transfer-limited process and a linear portion at lower frequencies corresponding to the diffusion-limited process (Suni, 2008). The Nyquist plot for the AuNR-RGO/GCE (Figure 5.3 (d)) showed a semicircle with an electron transfer resistance (R_{ct}) of 15 kΩ at higher frequency as to RGO/GCE and AuNR/GCE-modified electrodes as shown in Figure 5.3 (a) and Figure 5.3 (c) respectively. The GC electrode surface coated with AuNR-RGO had a greatly decreased electron transfer resistance as a result of the highly conductive nature of the carbon and metallic Au, which increased the electron transfer process. Where as, the RGO/GCE-modified electrode shows a steeper slope in lower frequency region indicates good capacitive behavior (Figure 5.3 (b)) (Yen et al., 2015).

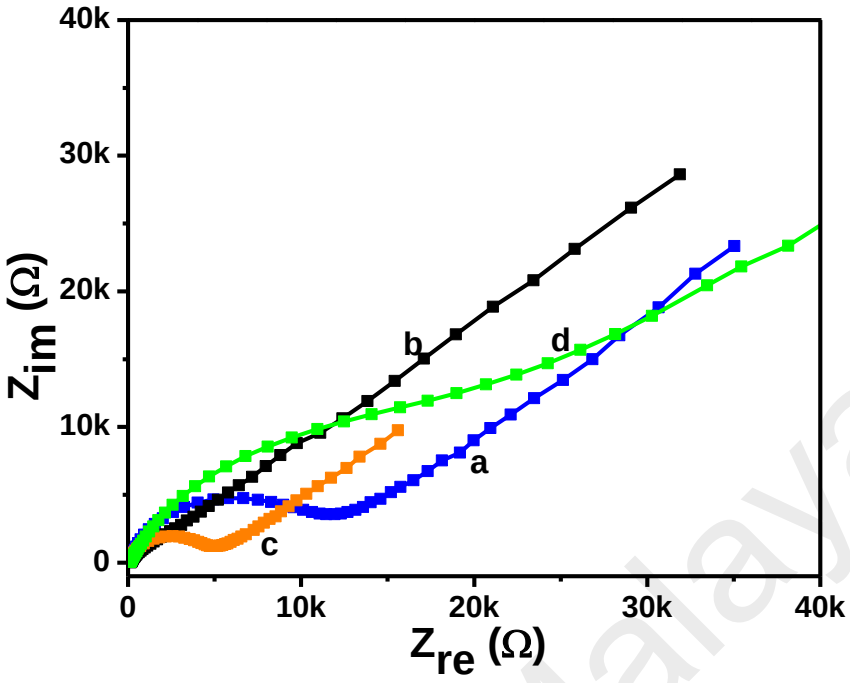

Figure 5.3: Nyquist plot of bare GCE (a), RGO/GCE (b), AuNR/GCE (c) and AuNR-RGO/GCE (d) in presence of 3 mM of $Fe(CN)_6^{3-}/Fe(CN)_6^{4-}$ in 0.1 M KCl.

Figure 5.4 shows the Bode phase plots obtained for the bare GCE, RGO/GCE, AuNR/GCE, and AuNR-RGO/GCE. It is known from the literature (Jeevagan & John, 2013; Lakshminarayanan & Sur, 2003; Wu et al., 2010) that if the phase angle of the modified electrode is greater than or equal to 90°, it will have an insulating behavior and act as an ideal capacitor indicating the insulating nature of the modified electrode. If the phase angle is lower than 90°, the electron transfer will be easy because of pinholes or defects in the electrode surface. It can be seen that the modified electrodes showed phase angles of less than 90°, which indicates that the electron transfer reaction was easy at the electrode-electrolyte interface.

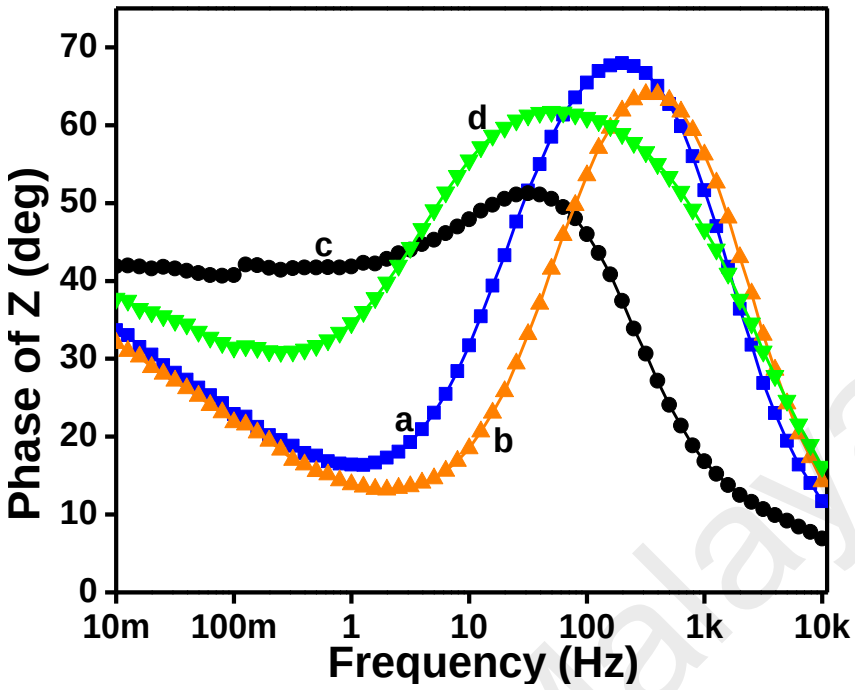

Figure 5.4: Bode plot of bare GC (a), AuNR/GCE (b), RGO/GCE (c), and AuNR-RGO/GCE (d) in presence of 3 mM of $Fe(CN)_6^{3-}/Fe(CN)_6^{4-}$ in 0.1 M KCl.

5.2.3 Electrocatalytic oxidation of NADH at AuNR-RGO-modified electrode

The electrocatalytic oxidation of NADH was investigated at the AuNR-RGO/GCE, RGO/GCE, AuNR/GCE, and bare GC electrode in 0.1 M phosphate buffer (pH 7.2) to obtain an electrode for a sensor. The electrocatalytic oxidation results for NADH at the bare GCE, RGO/GCE, and AuNR-RGO/GCE are shown in Figure 5.5. In the presence of NADH, the electrocatalytic oxidation showed a higher catalytic current at the AuNR-RGO/GCE (Figure 5.5 (d)) compared to the bare GC electrode (Figure 5.5 (a)). The bare GC and AuNR-RGO/GCE showed oxidation peaks for the NADH at 0.57 and 0.54 V, respectively, with a positive shift in the oxidation potential of 30 mV.

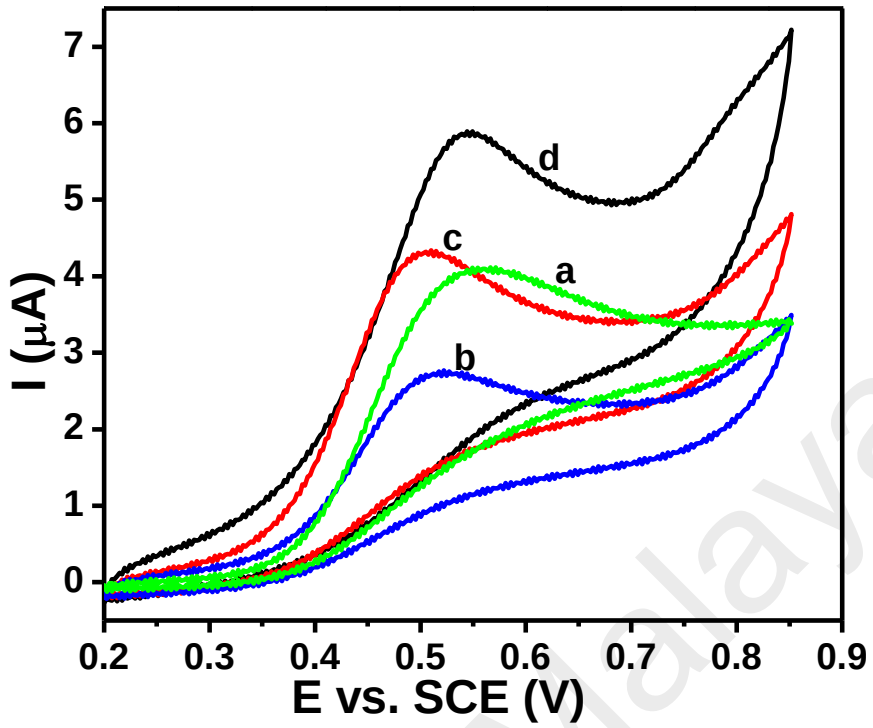

Figure 5.5: Cyclic voltammograms recorded at bare GCE (a), RGO/GCE (b), AuNR/GCE (c), and AuNR-RGO/GCE (d) in presence of 1 mM NADH in 0.1 M phosphate buffer (pH 7.2) at scan rate of 50 mV s^{-1}.

The influence of the scan rate on the electrocatalytic performance of AuNR-RGO/GCE toward NADH oxidation was studied by varying the scan rate in the range of 25–500 $mV{\cdot}s^{-1}$ in a 0.1 M phosphate buffer (pH 7.2) containing 1 mM of NADH, and the corresponding results are shown in Figure 5.6. It can be seen that when the scan rate was increased, the current response also increased. The linear relation obtained between the peak current and square root of the scan rate shown in Figure 5.7 inferred that the NADH oxidation at the AuNR-RGO modified electrode was a diffusion controlled process.

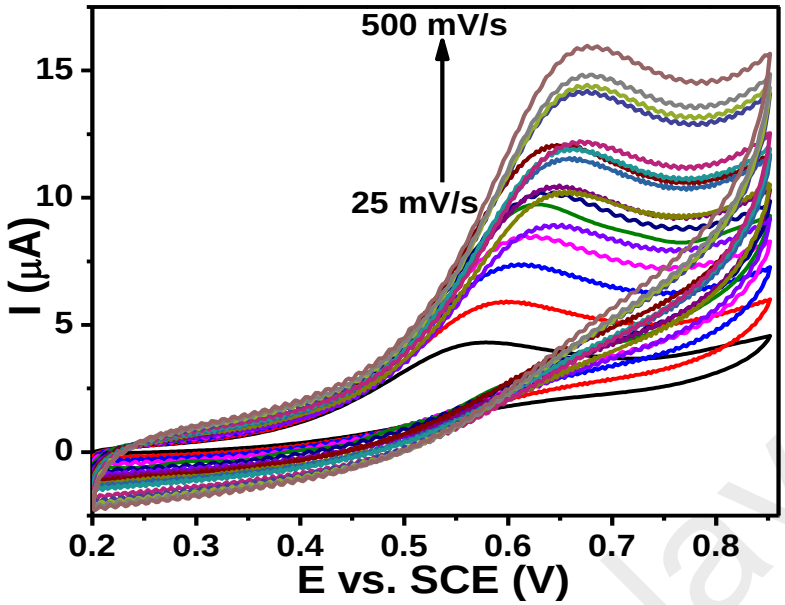

Figure 5.6: Cyclic voltammograms obtained for the AuNR-RGO/GCE in a 0.1 M phosphate buffer (pH 7.2) containing 1 mM of NADH at different scan rate ranges of 25 to 500 $mV \cdot s^{-1}$.

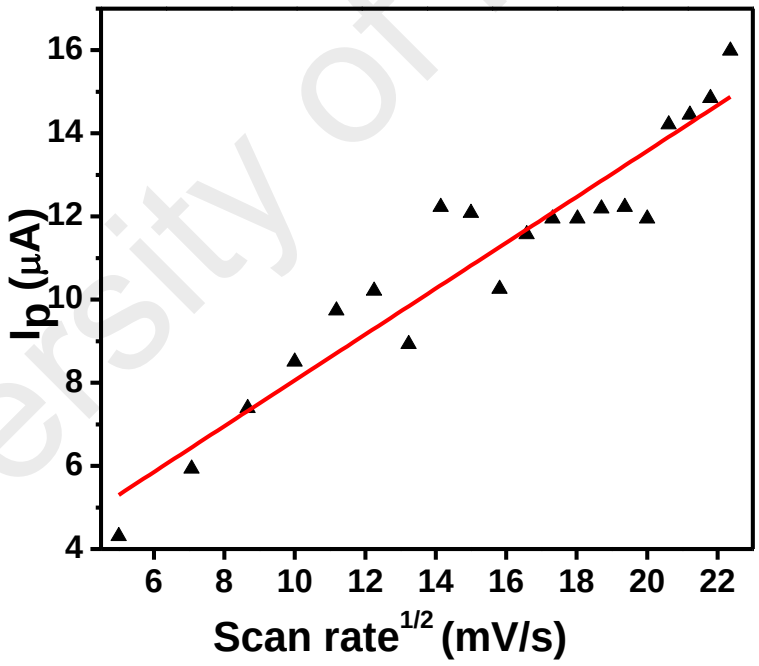

Figure 5.7: Plot obtained for anodic peak current *vs* square root of scan rate.

5.2.4 Amperometric response of NADH at sensor

The AuNR-RGO/GCE-based NADH sensor was further investigated using chronoamperometry at pH 7.2. The amperometric *i–t* responses for the detection of NADH at the AuNR-RGO/GCE were recorded at an applied potential of 0.54 V with repetitive additions of 1 µM NADH to the homogeneously stirred solution in 0.1 M phosphate buffer shown in Figure 5.8. The typical amperometric response for the detection of NADH and the corresponding calibration plot obtained at the AuNR-RGO/GCE with each addition of 1 µM NADH is shown in Figure 5.9. A linear relationship with a correlation coefficient of 0.9996 for the regression equation $y = 0.0098x + 7.0587E\text{-}10$ was obtained for the NADH concentration in the range of 1–31 µM (Figure 5.9), with a sensitivity of 0.0098 µA/µM. The response time was found to be 3 s, which indicated the presence of a fast electron transfer process at the modified electrode contributed by the conducting AuNR and RGO. The limit of detection (LOD) for NADH could be estimated using the standard deviation of the y-intercepts (SD) and the slope of the regression lines (S) (LOD = 3(SD/S) (Christian, 2004). The LOD was estimated to be 0.22 µM (S/N = 3) for the NADH at the AuNR-RGO/GCE. The amperometric experiment showed that the AuNR-RGO/GCE was a good sensor for the detection of NADH. The AuNR-RGO/GCE also responded very rapidly to changes in the NADH concentration, producing steady-state signals within 8–10 s. The analytical performance of the present AuNR-RGO/GCE-based NADH sensor was compared with those of some reported NADH sensors, and the results are summarized in Table 5.1. Compared to other NADH sensors, the present AuNR-RGO/GCE-based NADH sensor showed good sensing performance in terms of the limit of detection.

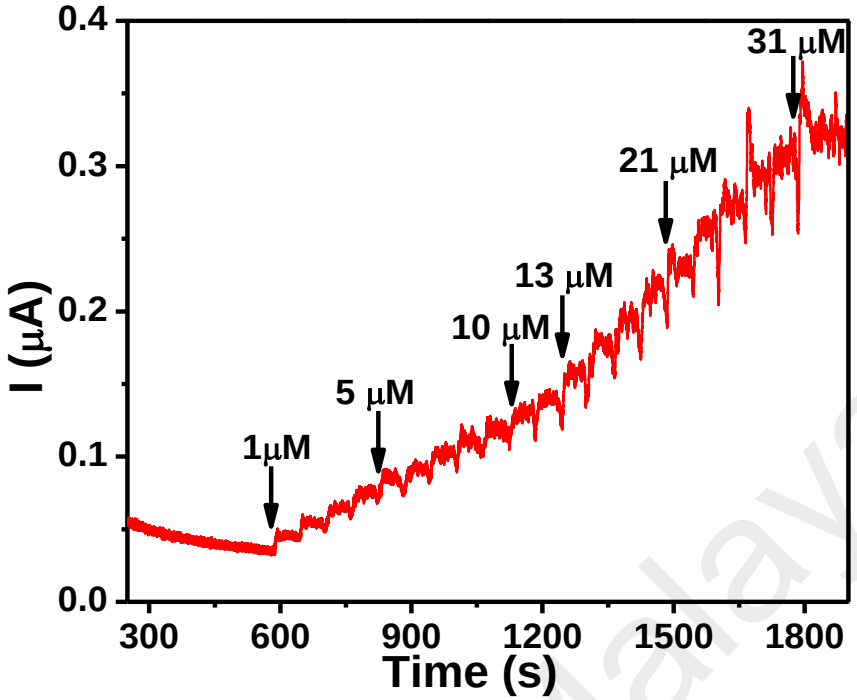

Figure 5.8: Amperometric *i–t* curve obtained for NADH at AuNR-RGO/GCE with 1 μM additions of NADH to homogeneously stirred solution in 0.1 M PBS recorded at applied potential of 0.54 V.

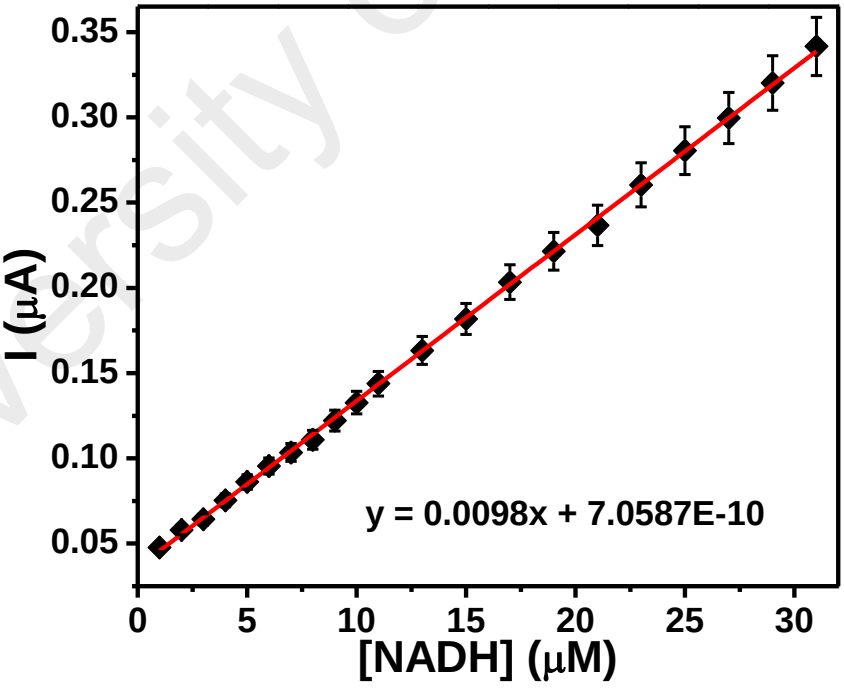

Figure 5.9: Calibration plot obtained at the AuNR-RGO/GCE with each addition of 1 μM NADH.

Table 5.1: Comparison of analytical parameters of some sensor electrodes for NADH determination.

Electrode materials[a]	Detection method	Linear range	Detection limit (M)	Ref.
Nafion/Graphene/-AuNPs/GCE	CA	36 nM to 20 μM	0.018×10^{-6}	(Wang et al., 2015)
Graphene–Au NRs	CA	20 to 160 μM	6×10^{-6}	(Li et al., 2013)
Au–TPDT silicate NRs	CA	1 to 13 μM	0.38×10^{-6}	(Jayabal & Ramaraj, 2015)
AuNR-RGO/GCE	CA	1 to 31 μM	0.22×10^{-6}	This work

[a]AuNPs = Gold nanoparticles; TPDT = N^1-[3-(trimethoxysilyl)propyl]diethylenetriamine; NRs = Nanorods; AuNR/RGO/GCE = Gold nanorod/reduced graphene oxide/glassy carbon electrode.

5.2.5 Stability and reproducibility of AuNR-RGO/GCE

Operational stability and reproducibility are vital parameters for electrochemical sensors. The operational stability of the AuNR-RGO/GCE was investigated by measuring the electrode response with 1 mM NADH (n = 50) for 50 continuous cycles. After 50 cycles, it continued to show a stable oxidation behavior, and the response to NADH retained 68% of its initial current, indicating its good stability. The repeated cyclic voltammetric responses of the sensor for 1 mM NADH (n = 5) were the same, with a relative standard deviation (RSD) of 0.36%. The RSD of the cyclic voltammetric response was 2.51% for the NADH determination at the same concentration using different batch sensors (n = 5). Both indicated that the sensor had a good reproducibility for the determination of NADH.

5.2.6 Interference study

The amperometric *i–t* curve for the AuNR-RGO/GCE was recorded in the presence of electroactive compounds such as glucose, hydrogen peroxide, uric acid, ascorbate, and dopamine to study the selectivity of the modified electrode. Figure 5.10 shows the amperometric *i–t* curve obtained for NADH at the AuNR-RGO/GCE during successive 10 µM additions of each electroactive compound to a uniformly stirred solution of 0.1 M PBS (pH 7.2) at an applied potential of 0.54 V. The results showed that an amperometric sensor using the AuNR-RGO/GCE for the NADH detection could be fabricated without incorporating other interference analytes.

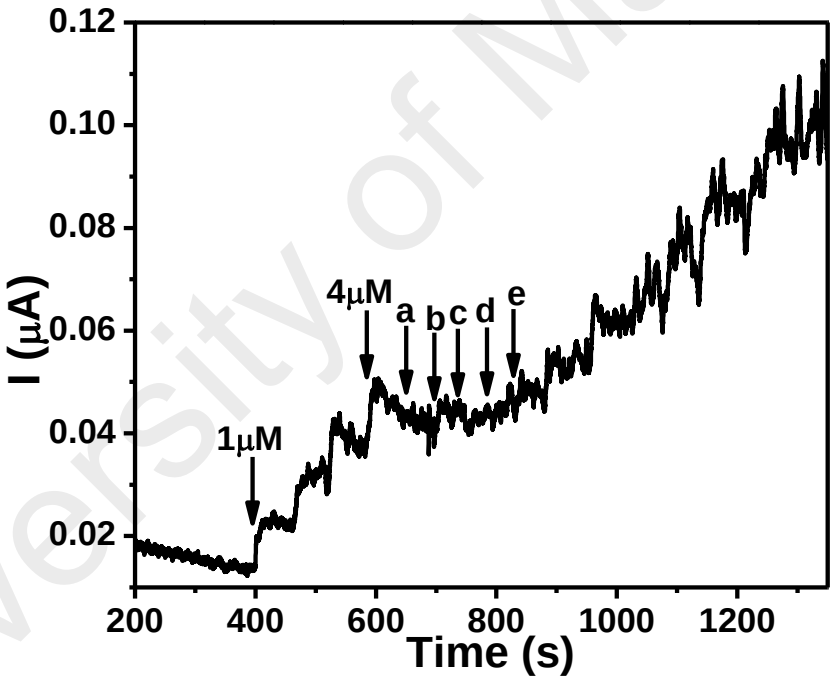

Figure 5.10: Amperometric *i–t* curve obtained at AuNR-RGO/GCE with additions of 1 µM NADH and 10 µM of interferents such as glucose (a), H_2O_2 (b), UA (c), AA (d), and DA (e).

5.3 Conclusion

An AuNR-RGO nanocomposite was successfully synthesized and characterized. The preparation of this AuNR-RGO nanocomposite was simple, and it was stable for more than a month at room temperature. The cyclic voltammetric studies of the AuNR-RGO/GCE revealed good electrical communication between the AuNR-RGO and the electrode carbon surface, which enabled the fabrication of a simple amperometric sensor for NADH detection. The AuNR-RGO/GCE showed an enhanced electrocatalytic activity toward the detection of NADH due to the synergistic effect of the RGO and AuNRs. The LOD for the NADH was determined to be 0.22 μM at the AuNR-RGO/GCE. The amperometric sensor for NADH prepared using the AuNR-RGO/GCE showed good selectivity in the presence of physiological interferents, along with a linear range, good stability, and reproducibility.

CHAPTER 6: VOLTAMMETRIC DETERMINATION OF NITRIC OXIDE USING A GLASSY CARBON ELECTRODE MODIFIED WITH A NANOHYBRID CONSISTING OF MYOGLOBIN, GOLD NANORODS, AND REDUCED GRAPHENE OXIDE

6.1 Introduction

Nitric oxide (NO) has been shown to be involved in regulating neuronal excitability, synaptic transmission, neuronal networks functioning, learning, and memory mechanisms (Brown et al., 2009; Ignarro et al., 1987; Thangavel & Ramaraj, 2008). An excess or a deficiency of NO results in various pathological conditions such as tumor angiogenesis (Thejass & Kuttan, 2007), atherosclerosis (Napoli & Ignarro, 2001), parkinson's disease (Kavya et al., 2006), and diabetes (Traub & Bibber, 1995). Therefore, the accurate measurement of NO is very important to unravel the action of this key compound. Because NO levels may become useful markers of inflammation and disease pathogenesis, the development of reliable and sensitive analytical techniques is of interest for the quantitation of NO production. Several analytical techniques are used for the detection of NO, including spectroscopic (Pourreza et al., 2012), chemiluminescence (Vishnuvardhan et al., 2008), chromatographic (Ferreira & Silva, 2008), capillary electrophoresis (Wang et al., 2012), and electrochemical methods (Radhakrishnan et al., 2014). However, those methods often have complicated operating procedures, and are time consumption, high cost, and occupy larger space. Hence, there is an urgent need to develop a cost-effective, easy-to-perform, rapid-response detection method for NO. In this respect, an electrochemical sensor has recently been adopted for the detection of NO, and it has several advantages over conventional detection methods, including a rapid response, robustness, high sensitivity and selectivity, low cost, miniaturization, and the potential for real-time monitoring (Dang et al., 2015). Several materials have been used as electrode modifiers for the electrochemical detection of

NO, including polymers, carbon nanotubes, graphene, metal oxide, and metal nanoparticles. Among these, metal nanoparticles possess high electrocatalytic activity, especially gold (Au) nanoparticles (Yusoff et al., 2015).

Recently, anisotropic gold nanostructures such as nanorods, nanoprisms, and nanopods have gained much attention because of their tunable optical and electronic properties (El-Sayed, 2001). These unique properties depend on the particle size and shape, and the structure of the local microenvironment (El-Sayed, 2001; Lin et al., 2012). In particular, gold nanorods (AuNRs) have been widely studied because of their unique properties and are finding potential applications in imaging, therapy, and biosensors (Alkilany et al., 2012; Chen et al., 2013; Huang et al., 2009; Jayabal et al., 2015; Pérez-Juste et al., 2005; Wang et al., 2006). AuNRs show two absorption peaks corresponding to their transverse (~ 520 nm) and longitudinal (≥ 600 nm) plasmonic modes of absorption (Jeevagan et al., 2013).

Graphene is another class of attractive material. It consists of a two-dimensional (2D) sheet of monolayer carbon atoms, and has recently attracted great attention because of its unique optical, catalytic, mechanical, thermal, and electronic properties (Shi et al., 2008). Molecular sensing can be achieved with this material, because graphene is electronically a very good low-noise material (Choi et al., 2010). The combination of graphene and gold nanostructures has made substantial progress in electrochemical biosensors (Artiles et al., 2011; Pandikumar et al., 2014).

Myoglobin (Mb), a small size of heme protein with a molar mass of approximately 17,500, plays an important role in protein electrochemistry (Fei et al., 2012). It is an ideal model molecule to study the electron transfer reactions of heme proteins, biosensing, and electrocatalysis (Hamachi et al., 1991; Zhang et al., 2008). However, Mb usually exhibits slow electron transfer at conventional electrodes, because the electroactive prosthetic groups are deeply buried in large three-dimensional protein

shells and the occurrence of denaturation adsorption of proteins on electrode surface (Zhang et al., 2007). More efforts have been made to enable the direct electron transfer of heme proteins (e.g. Mb) by modifying the electrodes using mediators, promoters, or other functional materials (Li & Hu, 2003).

In the present work, a nanohybrid consisting of myoglobin and gold nanorods that incorporated reduced graphene oxide (Mb-AuNRs/RGO) was prepared and used for detection of NO. The Mb-AuNRs/RGO/GCE showed an enhanced electrocatalytic activity toward the oxidation of NO, along with two different linear responses in the ranges of 10 -100 μM and 100 -1000 μM, with limit of detection (LOD) values of 5.5 and 26.6 μM, respectively. Moreover, this sensor electrode was more selective toward NO in the presence of other common interferents. The selectivity and sensitivity demonstrated by this Mb-AuNRs/RGO/GCE make it a promising candidate for the construction of a sensor for the detection of NO in practical applications.

6.2 Results and discussions

6.2.1 Absorption studies of Mb-AuNRs/RGO nanohybrid

The formations of AuNRs, reduced graphene oxide, and the Mb-AuNRs/RGO nanohybrid were investigated by recording the optical absorption spectra, which are shown in Figure 6.1. The optical absorption spectra obtained for the AuNRs showed the transverse LSPR band at 515 nm and the longitudinal LSPR band at 745 nm. The RGO displayed a peak at 264 nm, which confirmed that it was a completely reduced form of graphene oxide. The Mb-AuNRs/RGO nanohybrid showed the transverse LSPR band at 508 nm and the longitudinal LSPR band at 724 nm. The blue shift in the Mb-AuNRs/RGO compared to the AuNRs was due to the change in the local refractive index and medium surrounding the AuNRs. The decrements of intensity of the transverse and longitudinal LSPR bands were clearly observed for the Mb-AuNRs/RGO. The longitudinal LSPR band for the AuNRs is much higher than that of

the Mb-AuNRs/RGO because of the RGO and Mb medium surrounding the AuNRs. This was supported by the appearance of high-intensity RGO and Mb peaks at 264 nm and 410 nm, respectively.

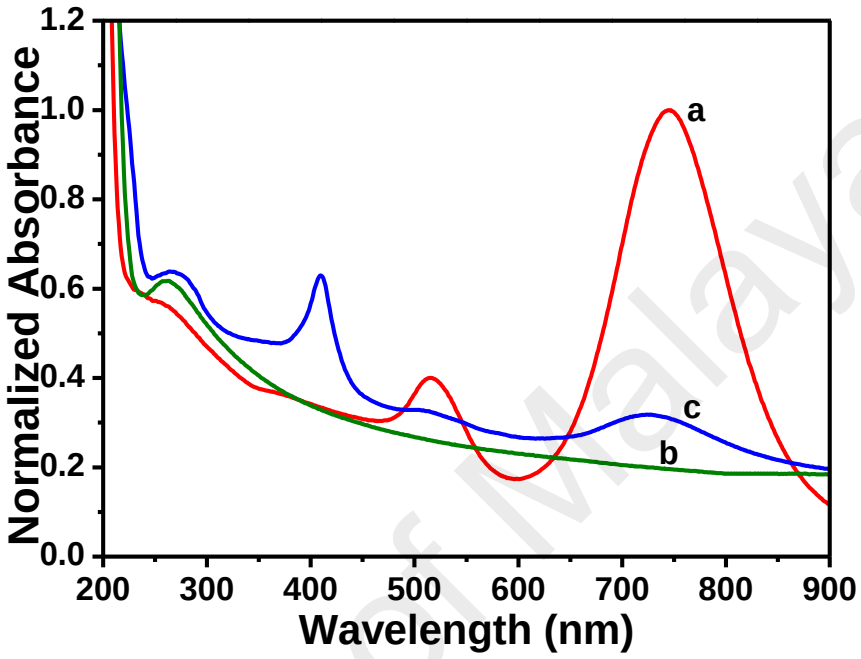

Figure 6.1: Absorption spectra of AuNRs (a), RGO (b), and Mb-AuNRs/RGO (c).

6.2.2 X-ray diffraction studies of Mb-AuNRs/RGO nanohybrid

The crystalline properties of the Mb-AuNRs/RGO nanohybrid were investigated by recording the X-ray diffraction pattern, and are shown in Figure 6.2. The XRD peaks of the pure AuNRs and Mb-AuNRs/RGO nanohybrid show four peaks at 2θ values of 38.3°, 44.6°, 64.7°, and 77.5° corresponding to the (111), (200), (220), and (311) planes, respectively, due to the gold (JPCDS file no.: 00-001-1172) (Figure 6.2 (a and d)). The appearance of a diffraction peak at 25.1° for the RGO was due to a complete reduction of the graphene oxide and exfoliation of the graphene layers (Hassan et al., 2009; Liu et al., 2011) (Figure 6.2 (c)). The observed weak diffraction peak at 25.1° was attributed to the removal of oxygen functional groups after the reduction process using hydrazine. In contrast, the pure myoglobin displays no characteristic diffraction peaks.

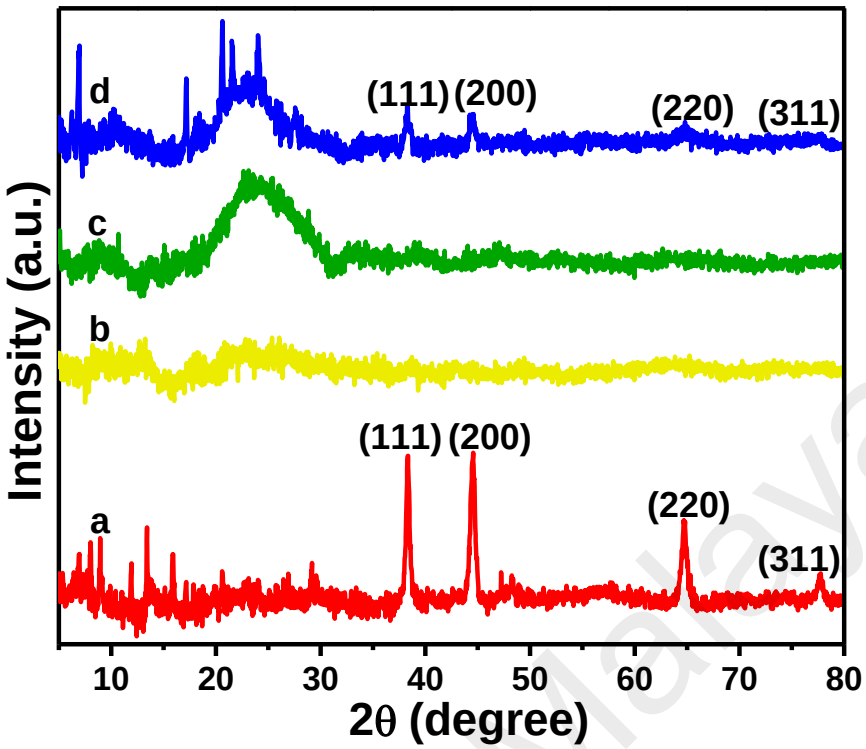

Figure 6.2: X-ray diffraction patterns obtained for AuNRs (a), Mb (b), RGO (c), and Mb-AuNRs/RGO (d).

6.2.3 X-Ray photoelectron spectroscopy studies of Mb-AuNRs/RGO nanohybrid

Further, the Mb-AuNRs/RGO was characterized by XPS. Figure 6.3 shows the XPS results obtained for the Mb-AuNRs/RGO, which clearly confirm the presence of AuNRs on the RGO surface. The XPS of Au4f shows two peaks at 85.75 eV for $4f_{7/2}$ and 89.36 eV for $4f_{5/2}$ (Figure 6.3).

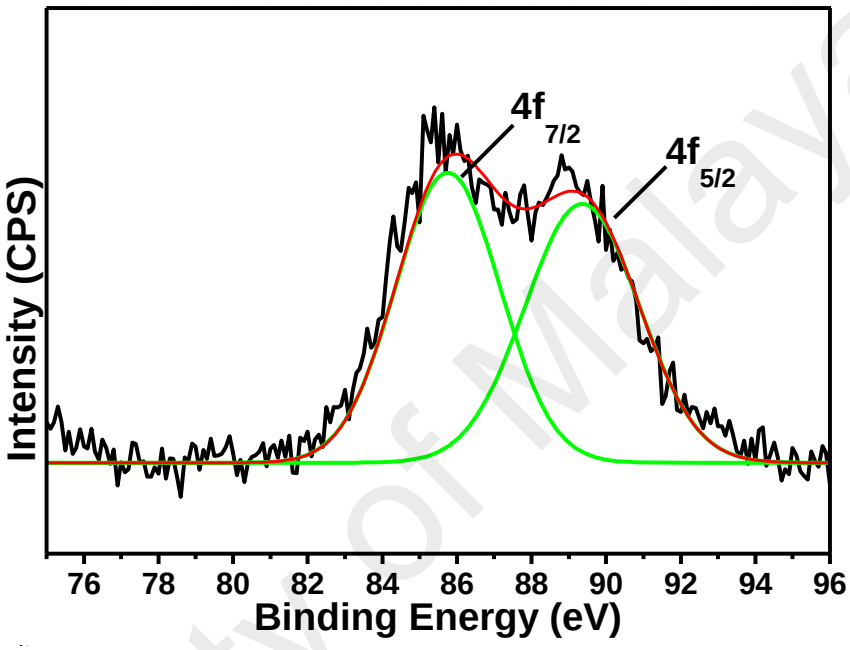

Figure 6.3: XPS results of Mb-AuNRs/RGO spectrum for Au4f.

The C_{1s} spectrum shows binding energy values at 284.71 eV and 287.63 eV for RGO (Figure 6.4), which clearly show a considerable degree of oxidation components corresponding to the non-oxygenated ring C and carboxylate carbon C=O, respectively. The non-oxygenated C-C is prominent because of the interaction with hydrazine during the reduction treatment. The small peak at 287.63 eV indicates that the C=O of the carboxylate group still appeared in the RGO.

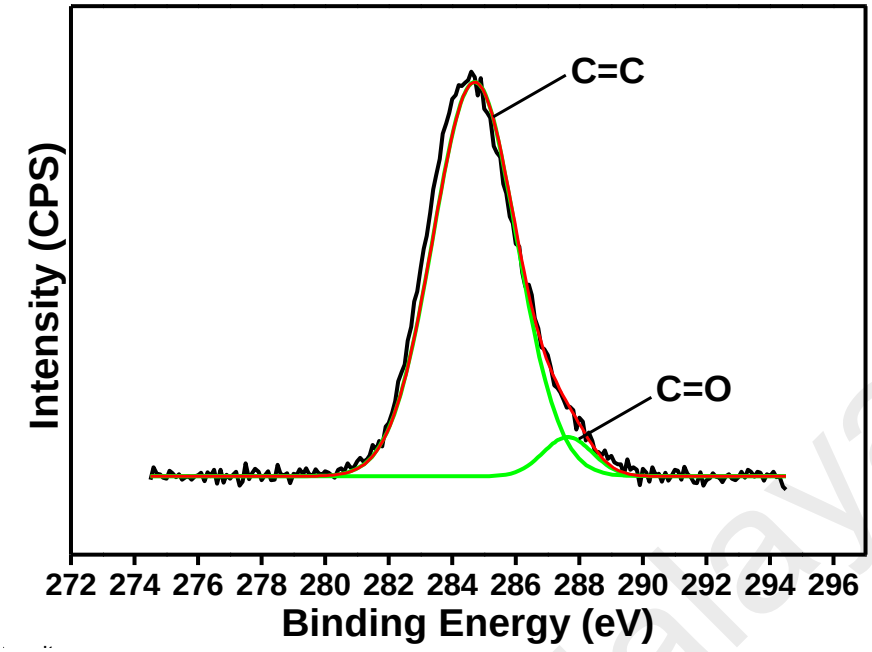

Figure 6.4: XPS results of Mb-AuNRs/RGO spectrum for C1s.

6.2.4 Morphological studies of Mb-AuNRs/RGO nanohybrid

The morphologies of the as-prepared AuNRs, AuNRs/RGO, and Mb-AuNRs/RGO nanohybrid were characterized by means of FESEM. At higher magnification (Figure 6.5 (a)), the FESEM images confirmed the formation of gold nanorods with an average length of 41 nm, a breadth of 12 nm, and an aspect ratio of ~3.4. Figure 6.5 (b and c) showed the FESEM images of the AuNRs in the presence of RGO and Mb with RGO. The images display the distribution of AuNRs on both sides of the RGO's surface. The nanorods have an average length of 38 nm and a breadth of 11 nm, with an aspect ratio of ~3.5. Figure 6.5 (c) displays highly dense AuNRs on the surface of RGO due to the presence of Mb after the hybridization process.

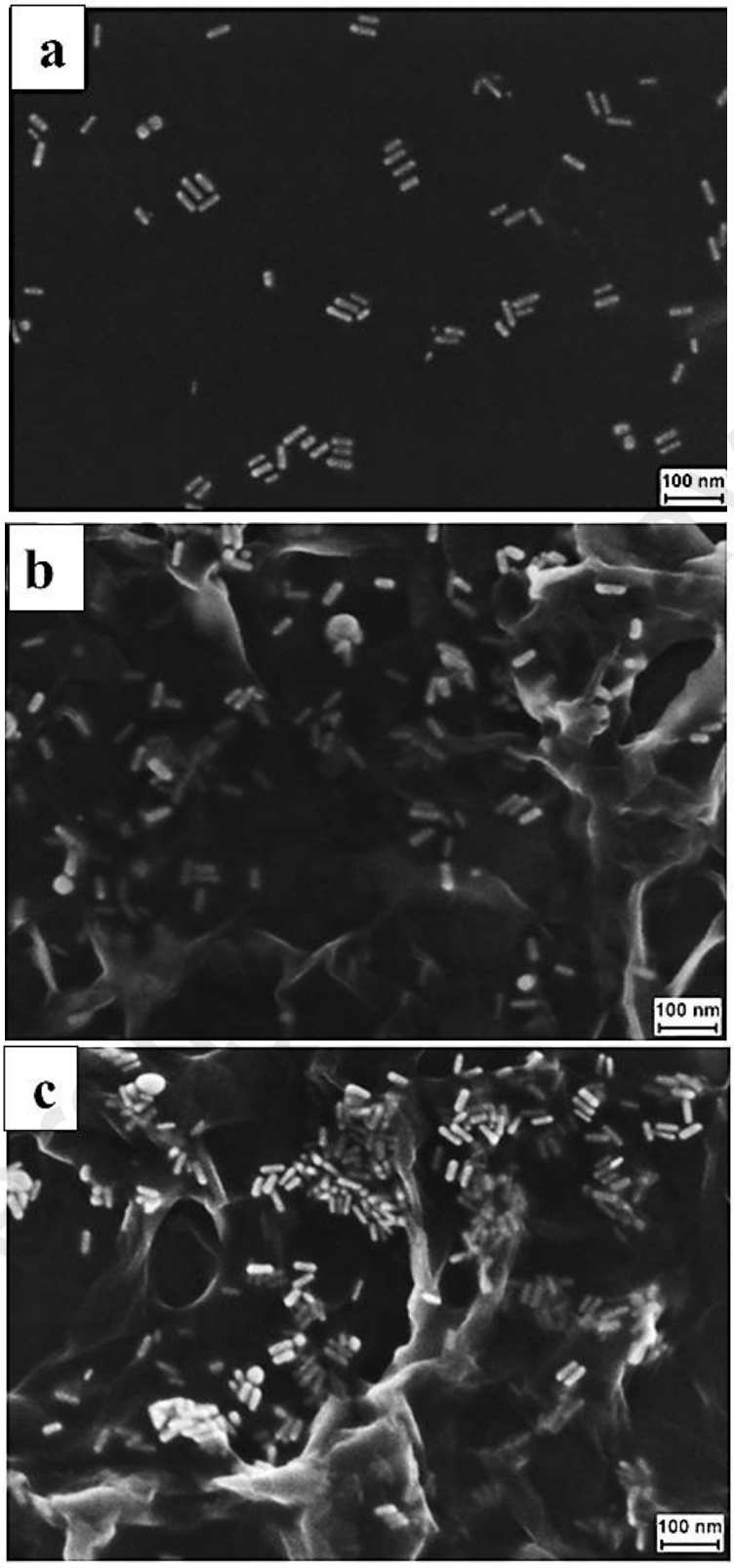

Figure 6.5: FESEM images of AuNRs (a), AuNRs/RGO (b), and Mb-AuNRs/RGO (c) samples.

An energy dispersive X-ray analysis (EDX) was also conducted based on the FESEM image of the Mb-AuNRs/RGO nanohybrid. Figure 6.6 shows the EDX of the selected surface area of the Mb-AuNRs/RGO nanohybrid, which confirmed the presence of elements such as Au (7.95%), O (11.78%), C (27.24%), and Si (53.03%). Si shows the highest percentage because of the substrate used to coat the sample.

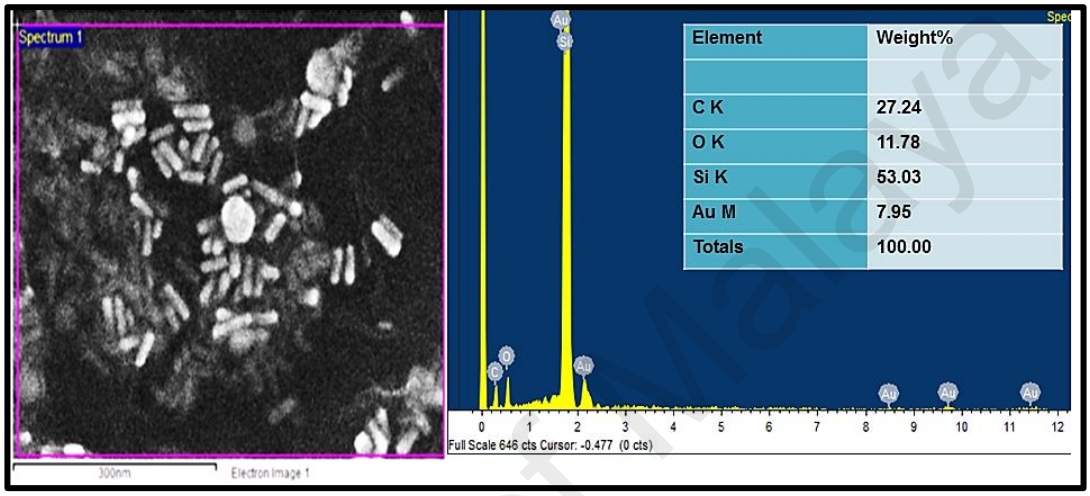

Figure 6.6: EDX analysis of Mb-AuNRs/RGO nanohybrid.

6.2.5 Electrocatalytic activity of Mb-AuNRs/RGO nanohybrid-modified electrode toward nitric oxide (NO)

The fabricated Mb-AuNRs/RGO nanohybrid-modified electrode was investigated in relation to electrocatalysis and the sensing of nitric oxide. An in-situ generated nitric oxide was used for the electrocatalysis and sensor. It is well known that sodium nitrite ($NaNO_2$) serves as a source of NO and in an acidic solution (pH < 4), it will undergo a disproportionation reaction (Equation 6.1) and thus produce NO (Beltramo & Koper, 2003; Cotton, 1988).

$$3HONO \rightarrow 2NO + NO_3^- + H_2O \qquad (6.1)$$

In our work, $NaNO_2$ was used as a precursor to produce NO in solution during the electrochemical study (Brylev et al., 2007; Pandikumar & Ramaraj, 2011). The addition

of a known amount of $NaNO_2$ into the bulk electrolyte solution at pH 2.5 generated a series of concentrations of NO.

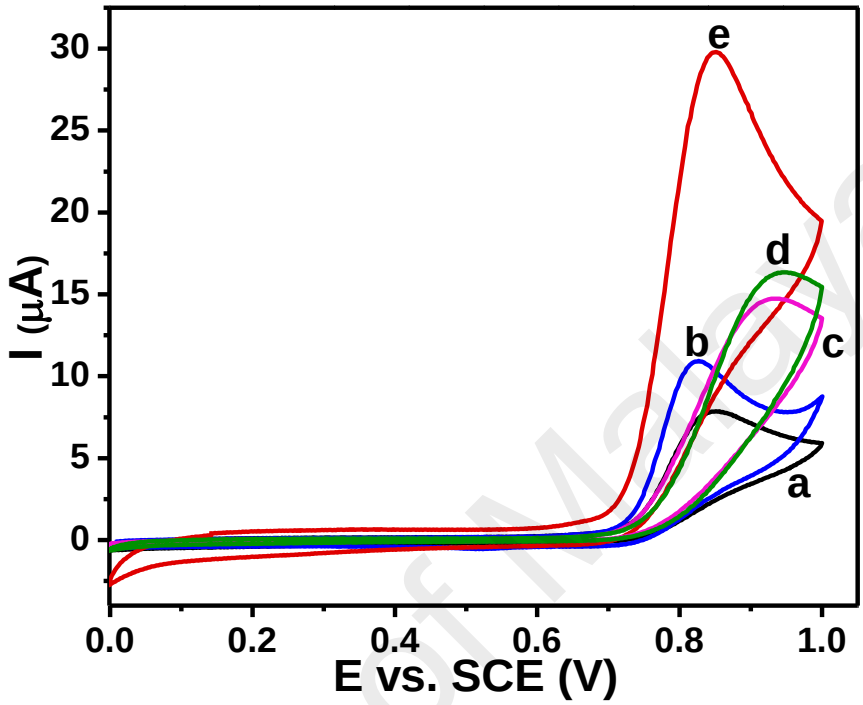

Figure 6.7: Cyclic voltammograms obtained for bare GCE (a), AuNRs/GCE (b), RGO/GCE (c), Mb/GC (d), and Mb-AuNRs/RGO/GCE (e) in 0.1 M phosphate buffer (pH 2.5) with1 mM NO_2^- at scan rate of 50 $mV.s^{-1}$.

As can be seen from Figure 6.7 the Mb-AuNRs/RGO nanohybrid-modified electrode showed a remarkably enhanced electrocatalytic response toward the oxidation of NO, with a higher current than the other investigated modified electrodes. The oxidation potential of NO for the Mb-AuNRs/RGO/GCE was significantly shifted toward a lower potential value with an increase in the anodic peak current compared to AuNRs/GCE-, RGO/GCE-, and Mb/GCE-modified electrodes. The bare GCE electrode showed less intense oxidation peaks for NO at 0.85 V compared to Mb-AuNRs/RGO/GCE. A higher catalytic current was obviously displayed by the Mb-AuNRs/RGO/GCE as a result of the synergistic electrocatalytic effect aroused by the combination of RGO, Mb, and AuNRs present in the Mb-AuNRs/RGO nanohybrid, and was also attributed to the AuNRs providing a larger surface area with specific interaction toward the substrate.

Thus, it resulted in improved electron-transfer kinetics and enhanced oxidation of NO (Jayabal et al., 2014). Figure 6.8 shows a schematic representation of the electrocatalytic oxidation of NO at the Mb-AuNRs/RGO nanohybrid-modified electrode.

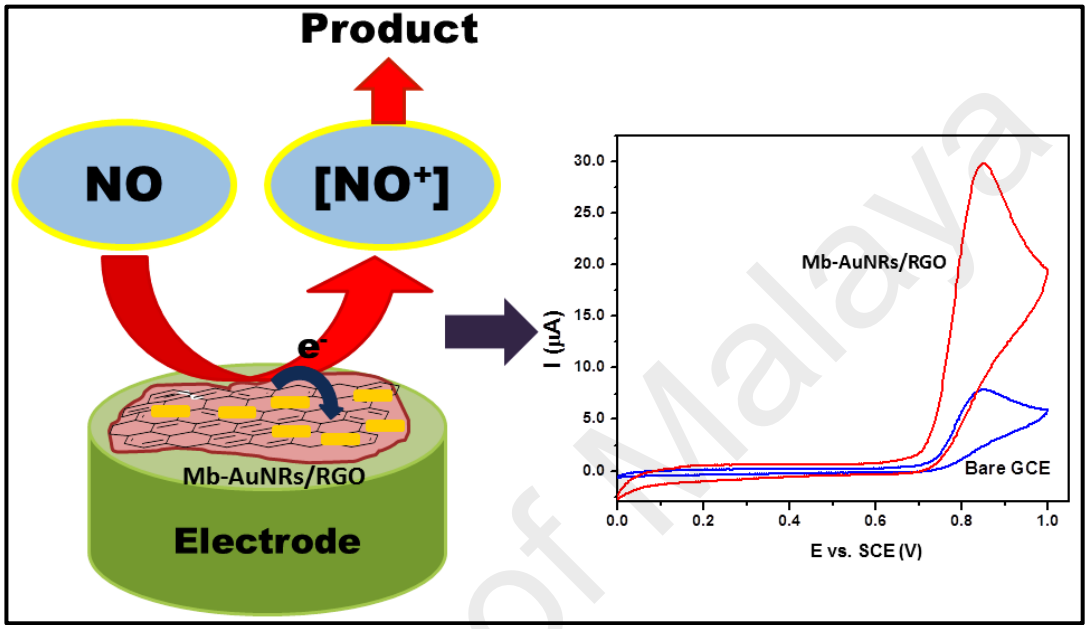

Figure 6.8: Schematic illustration of electrocatalytic oxidation of NO at Mb-AuNRs/RGO nanohybrid-modified electrode.

Figure 6.9 shows the cyclic voltammetric characteristics that were recorded in a 0.1 M phosphate buffer (pH 2.5) solution containing 1 mM of nitric oxide at different scan rates in the range of 0.25 -200 $mV{\cdot}s^{-1}$. The influence of scan rate on the electrocatalytic performance of Mb-AuNRs/RGO toward NO oxidation studied by varying the scan rate in the range of 25 -200 $mV{\cdot}s^{-1}$ in a 0.1 M phosphate buffer (pH 2.5) containing 1 mM of NO. It can be seen that while increase the scan rate the current response also increased. By plotting peak current (I_p) against square root of scan rates of CV plots at different scan rate (Figure 6.10), inferred that the nitrite oxidation at the Mb-AuNR/RGO-modified electrode is controlled by the diffusion process.

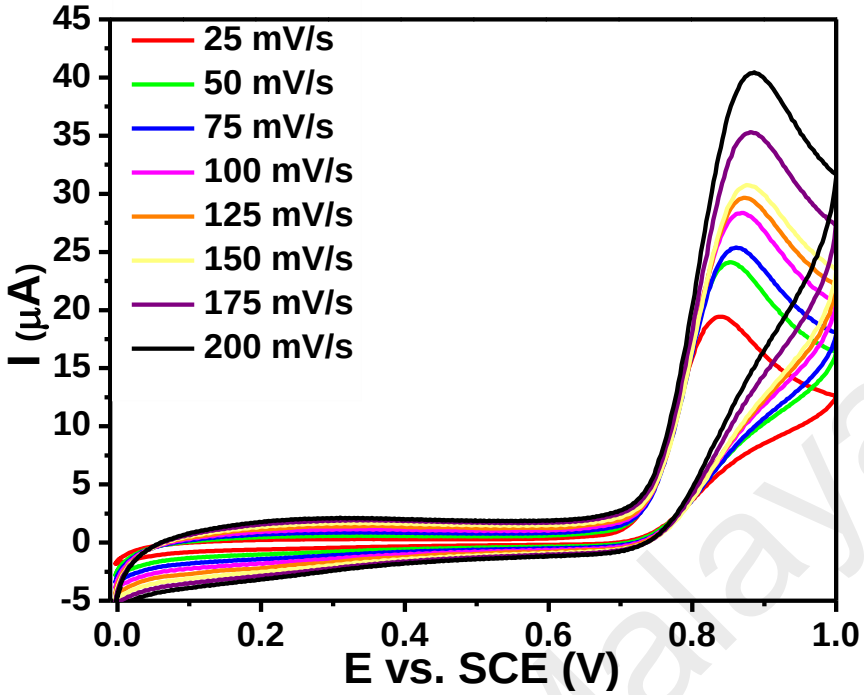

Figure 6.9: CV obtained in 0.1 M phosphate buffer (pH 2.5) solution containing 1 mM of nitric oxide at different scan rates in range of 0.25 -200 $mV{\cdot}s^{-1}$.

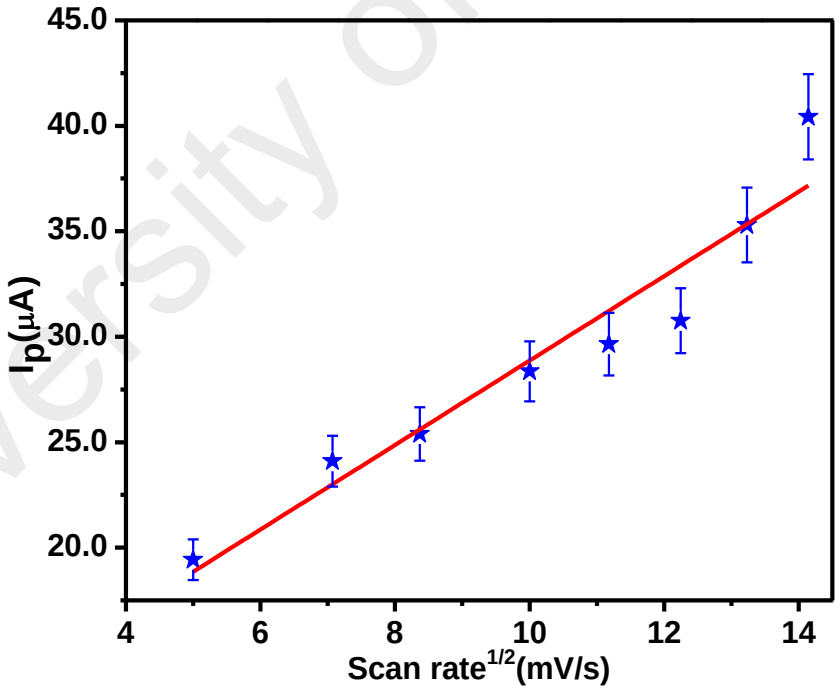

Figure 6.10: The plot obtained for anodic peak current *vs* square root of scan rate for Mb-AuNR/RGO/GCE in a 0.1 M phosphate buffer (pH 2.5) containing 1 mM of NO different scan rate at range of 25 to 200 $mV{\cdot}s^{-1}$.

6.2.6 Electrochemical detection of nitric oxide at Mb-AuNRs/RGO/GCE-modified electrode

Figure 6.11 shows a linear sweep voltammogram obtained for the Mb-AuNRs/RGO/GCE-modified electrode in the presence of NO_2^- at a concentration range of 10 µM–1 mM in the 0.1 M phosphate buffer (pH 2.5) with a scan rate of 50 $mV{\cdot}s^{-1}$. The Mb-AuNRs/RGO/GCE showed an anodic oxidation peak of ~0.85 V as a result of the NO oxidation. It can be seen that the oxidation peak current was increased when the NO_2^- concentration was increased up to 1 mM. The LSV curves show a well-defined and stable anodic oxidation peak current for the detection of NO. These results demonstrated that the Mb-AuNRs/RGO/GCE provided a good electrocatalytic activity toward nitric oxide sensing. Further, the observed calibration curve for the peak current against the NO_2^- concentration is shown in Figure 6.12.

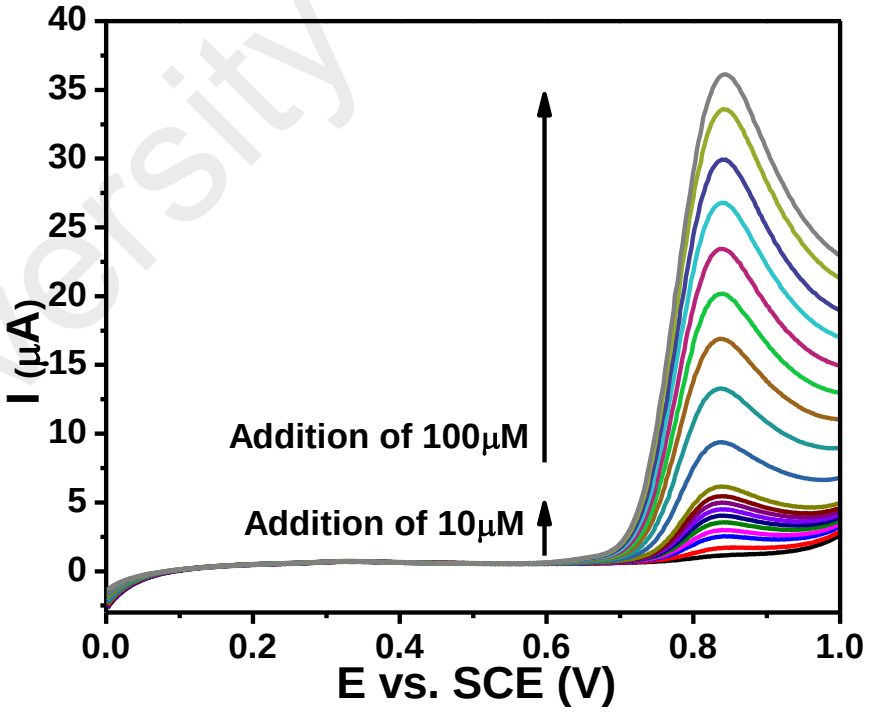

Figure 6.11: LSV obtained for Mb-AuNRs/RGO/GCE in presence of NO at concentration range of 10 µM – 1 mM in 0.1 M phosphate buffer at pH 2.5 and scan rate of 50 $mV.s^{-1}$.

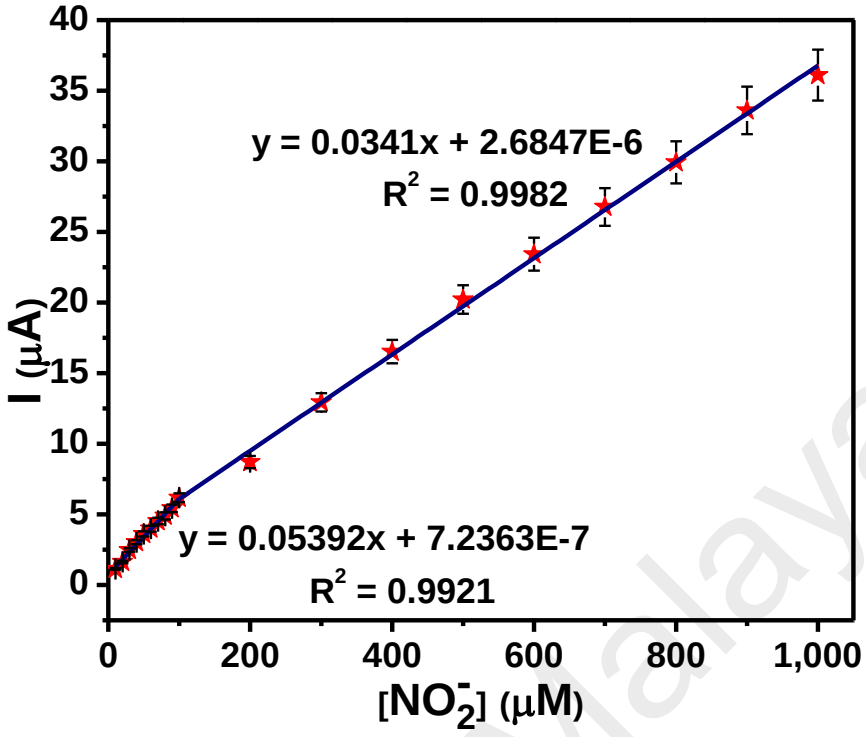

Figure 6.12: The calibration plot of the peak current against the NO_2^- concentration obtained for Mb-AuNRs/RGO/GCE.

Figure 6.12 shows the calibration curves for the plot of the current against the NO_2^- concentration. The measured peak currents were found in two linear ranges with increasing concentrations: 10 -100 μM and 100 -1000 μM. The first linear segment in the range of 10 -100 μM had a sensitivity of 0.0539 μA/μM (R^2 = 0.9921), with a linear regression equation of y = 0.05392x + 7.2363E-7. The limit of detection (LOD) was calculated based on the relationship LoD = $\frac{3\sigma}{m}$ (Christian, 2004), where σ is the relative standard deviation of the intercept of y-coordinates from the line of best fit, and m is the slope of the same line. The LOD value of 5.5 μM was obtained for the first linear segment. The second linear segment in the range of 100 -1000 μM showed a sensitivity of 0.0341 μA/μM (R^2 = 0.9982), with a linear regression equation of y = 0.0341x + 2.6847E-6 and the LOD was found to be 26.6 μM. The obtained LOD of 5.5 μM for the detection of NO using the Mb-AuNRs/RGO/GCE was comparable to the values of

other reported electrochemical sensors. The present nitric oxide detection results were compared with previous reports, as summarized in Table 6.1.

Table 6.1: Analytical parameters reported for some modified electrodes towards nitric oxide detection.

Electrode materials	Fabrication method	Detection method	Linear range (M)	Detection limit (M)	Ref.
PEI/[(PSS/PAH)$_2$/PSS/AuNP]^3	Infiltration, layer by layer	CV	0.05×10^{-3}–0.5×10^{-3}	0.010×10^{-3}	(Yu et al., 2003)
Hemoglobin –DNA/PG	Deposition	DPV	0.1×10^{-3}–1×10^{-3}	1.8×10^{-5}	(Fan et al., 2000)
GC/G-Nf	Hydro-thermal	SWV	0.05×10^{-3}–0.45×10^{-3}	11.61×10^{-6}	(Yusoff et al., 2015)
GC/Hb–CPB/PAM	Layer by layer	CV	9.8–100 mM	9.3×10^{-6}	(He & Zhu, 2006)
Mb-AuNRs/RGO/GCE	Sonication	LSV	1×10^{-5}–1×10^{-3}	5.5×10^{-6}	This work

Foot note: PEI/[(PSS/PAH)$_2$/PSS/AuNP]^3 = poly-(ethylenimine)/[(poly(sodium 4-styrenesulfonate)/poly(allylamine hydrochloride))$_2$/poly(sodium 4-styrenesulfonate)/ gold nanoparticles]^3; PG = pyrolytic graphite; G = graphene; Nf = Nafion; Hb–CPB = hemoglobin–cetylpyridinium bromide; PAM = polyacrylamide.

6.2.7 Selectivity of Mb-AuNRs/RGO/GCE

In order to prove the selectivity of the Mb-AuNRs/RGO/GCE toward NO, LSV curves were recorded in the presence of common interfering compounds such as $NaNO_3$, NaF, KCl, NH_4Cl, and Na_2CO_3, and also in the presence of electroactive compounds such as ascorbic, dopamine, glucose, and uric acid. No significant oxidation current was observed at 0.85 V in the LSV curves (Figure 6.13). An obvious change occurred upon the injection of 0.1 mM of NO, and an enhancement in the oxidation peak current was observed. As a result, it can be concluded that the present Mb-AuNRs/RGO/GCE is highly selective toward the determination of NO even in the presence of these potential interferences.

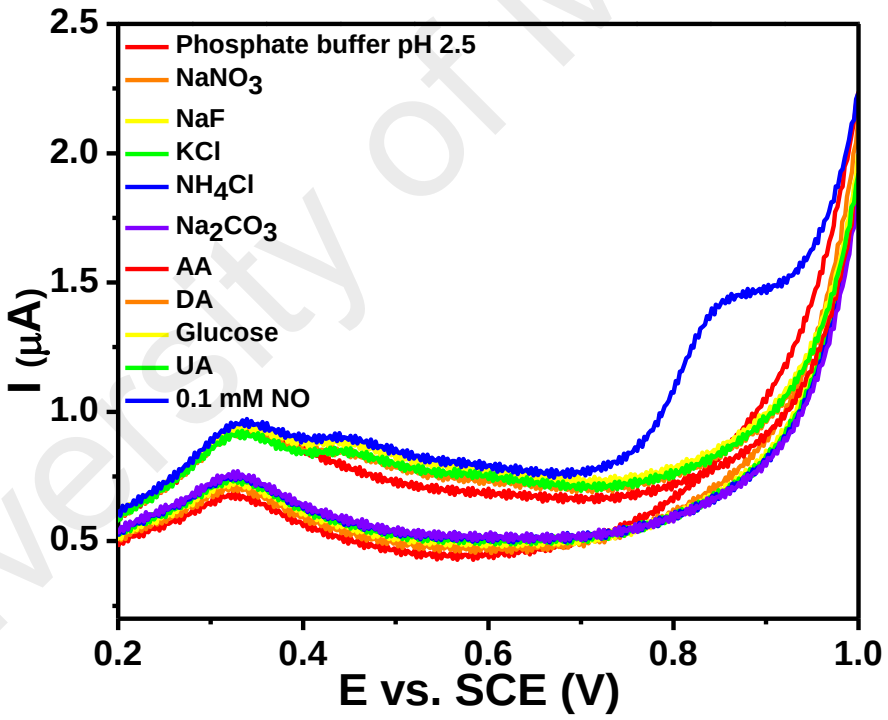

Figure 6.13: Linear sweep voltammograms obtained for Mb-AuNRs/RGO/GCE in 0.1 M phosphate buffer (pH 2.5) in presence of various analytes at scan rate of 50 $mV.s^{-1}$.

6.3 Conclusion

In conclusion, nanohybrid composed of myoglobin-gold nanorods that incorporated reduced graphene oxide (Mb-AuNRs/RGO) was prepared and used for the construction of an electrochemical sensor for the selective and sensitive detection of NO. The Mb-AuNRs/RGO/GCE showed an enhanced electrocatalytic response toward the oxidation of NO compared to those of the other investigated electrodes. The presence of gold nanostructures greatly improved the electrical communication and electrocatalytic properties. The Mb-AuNRs/RGO/GCE showed two different linear responses in the ranges of 10 -100 μM and 100 -1000 μM, with limit of detection (LOD) values of 5.5 and 26.6 μM, respectively, via LSV techniques. Moreover, this fabricated sensor electrode possessed good selectivity toward NO in the presence of high concentrations of common interferents and other electroactive compounds. The excellent selectivity and sensitivity toward NO indicates that this Mb-AuNRs/RGO/GCE could be a potential sensor electrode for practical applications.

CHAPTER 7: CONCLUSION AND FUTURE WORK RECOMMENDATIONS

7.1 Conclusion

The aim of this research was to developed metal and metal oxide graphene based nanocomposites, which harness the unique physical and electrochemical benefits toward the electrochemical sensors. The synthesis and modification of the graphene based with metal oxide (zinc oxide) and noble metal (Au) element, and electrochemical characterizations were presented in this work. This work is divided into three parts and summarized in the following.

Firstly, it was demonstrated that the nanocomposite consisting of flower-like zinc oxide (ZnO) and reduced functionalized graphene oxide (rFGO) was prepared via a hydrothermal route, and characterized by spectrophotometry, photoluminescence, Raman spectroscopy, X-ray diffraction, scanning electron microscopy, and transmission electron microscopy. The nanocomposite was deposited on the surface of a glassy carbon electrode and studied using impedance spectroscopy. It exhibited excellent electrocatalytic activity toward the oxidation of nitrite. At a working potential of 0.9 V (*vs.* Ag/AgCl), it displayed a higher current and lower over potential (reduced by up to ~200 mV) than controlled electrodes. This was attributed to the synergistic catalytic effects of the ZnO and rFGO. The oxidation current was linearly related to the concentration of nitrite in the 10 μM to 8 mM range, and the detection limit was 33 μM. Its excellent electrocatalytic activity, wide linear range, low detection limit, high sensitivity, and rapid response time make this nanocomposite-based electrode a potential candidate for practical applications.

Reduced graphene oxide–gold nanorods was the second nanocomposite explored in this work. The facile synthetic method for the preparation of reduced graphene oxide–gold nanorods in an aqueous medium and its application to the electrochemical sensing of dihydronicotinamide adenine dinucleotide (NADH) were reported. The gold

nanorods (AuNRs) had an average length of 44 ± 3 nm and a width of 12 ± 2 nm. The electrochemical characteristics of the gold nanorod-reduced graphene oxide/glassy carbon electrode (AuNR-RGO/GCE) were studied using cyclic voltammetry, and the NADH sensing was studied using chronoamperometry. The AuNR-RGO/GCE showed excellent electrocatalytic activity toward the oxidation of NADH due to the synergistic catalytic effect of the AuNR-RGO. The amperometric current increased linearly when the NADH concentration was increased in the range of 1–31 μM, and the lowest detection limit (LOD) was estimated to be 0.22 μM (S/N = 3). The AuNR-RGO/GCE was simple to prepare and showed a rapid amperometric response toward NADH detection.

The third part of this work featured modification of reduced graphene oxide–gold nanorods with myoglobin was presented. The myoglobin-modified gold nanorods incorporating reduced graphene oxide (RGO) were fabricated and deposited on a glassy carbon electrode (GCE) to obtain a sensor for nitric oxide (NO). The Mb-AuNR/RGO nanohybrid showed a transverse localized surface plasmon resonance (LSPR) band with a peak at 508 nm, and a longitudinal LSPR band at 724 nm. The AuNRs have an average length of 38 ± 3 nm and a width of 11 ± 1 nm. The GCE modified with the nanohybrid is shown to be a viable sensor for the determination of NO by linear sweep voltammetry. Its electrocatalytic response toward the oxidation of NO is distinctly enhanced compared to other electrodes. The sensor, best operated at a working voltage of 0.85 V (vs. SCE), showed two linear response ranges (from 10 to100 μM, and from 100 to 1000 μM), with a detection limit of 5.5 μM. Furthermore, it exhibits excellent selectivity for NO over common interferents such as $NaNO_3$, and also over electroactive species such as ascorbate, dopamine, glucose, and uric acid. These properties make it a promising tool for the detection of NO in situations such as capillary and pulmonary hypertension and embolism, and during vasodilation.

The systematic strategically combining graphene based with metal oxide/metal materials for electrochemical sensors are summarized in Table 7.1.

Table 7.1: Summary of the electrochemical sensor performance and the optimization techniques carried in this research work.

Electrode materials	Analyte detection	Detection method	Linear range	Detection limit (M)
f-ZnO@rFGO /GCE	nitrite	CA	10 µM-8 mM	33×10^{-6}
AuNR-RGO/GCE	NADH	CA	1 to 31 µM	0.22×10^{-6}
Mb-AuNR/RGO/GCE	NO	LSV	10 µM to 1 mM	5.5×10^{-6}

Foot note: GCE = glassy carbon electrode; *f*-ZnO@rFGO = zinc oxide-reduced functionalized graphene oxide; AuNR/RGO = Gold nanorod/reduced graphene oxide; Mb = myoglobin.

7.2 Summary of contributions

The novelty and important findings acquired in this work can be summarized as follows;

1) One-step method for the hydrothermal synthesis of a unique flower-like zinc oxide/reduced functionalized graphene oxide (*f*-ZnO@rFGO) nanocomposite for the electrochemical detection of nitrite ions.

2) Reliable test in real sample analysis revealed the proposed method outlined in this work for nitrite sensing holds promise for the direct analysis of environmental samples.

3) The immobilization of Mb with gold nanorods and RGO will amplify the detection signal, improve the electron transducer, and reduce the detection limit in electrochemical sensors for analytical purposes.

4) The modified electrodes highly selective toward the determination of a selected analyte even in the presence of various potential interference species.

7.3 Future work recommendations

Based on the understanding acquired in these studies, the suggestions are worth investigating in the future for electrochemical sensor development:

1) Further efforts should be made focusing on the development of functional nanoparticles that are soluble and long-term stable in different buffered saline solutions, and amenable to limited non-specific binding to fabricate NO analysis systems with better sensitivities and selectivity;
2) Miniaturization of the nanoparticles ensembles with the ultimate goal of using a single functionalized nanoparticle, such as nanotube or nanowire, for the witnessed and in vivo sensing of NO;
3) Extending application of semiconductor nanoparticles or quantum dots (QDs) nanocrystals for developing ultra-sensitive, multiplexed NO sensor;
4) Combination of different analytical techniques, such as electrochemistry, spectroscopy and chromatography, based on different type of nanoparticles or their functionalized particles;
5) Extending of application to practicality of the modified electrodes to real sample analysis in human urine, blood serum, and pharmaceutical injections.

REFERENCES

Akhavan, O. (2010). Graphene nanomesh by ZnO nanorod photocatalysts. *ACS Nano, 4*(7), 4174-4180.

Alkilany, A. M., Thompson, L. B., Boulos, S. P., Sisco, P. N., & Murphy, C. J. (2012). Gold nanorods: Their potential for photothermal therapeutics and drug delivery, tempered by the complexity of their biological interactions. *Advanced Drug Delivery Reviews, 64*(2), 190-199.

Allen, M. J., Tung, V. C., & Kaner, R. B. (2009). Honeycomb carbon: A review of graphene. *Chemical Reviews, 110*(1), 132-145.

Álvarez-González, M. I., Saidman, S. B., Lobo-Castañón, M. J., Miranda-Ordieres, A. J., & Tuñón-Blanco, P. (2000). Electrocatalytic detection of NADH and glycerol by NAD+-modified carbon electrodes. *Analytical Chemistry, 72*(3), 520-527.

Artiles, M. S., Rout, C. S., & Fisher, T. S. (2011). Graphene-based hybrid materials and devices for biosensing. *Advanced Drug Delivery Reviews, 63*(14), 1352-1360.

Astrup, P., & Severinghaus, J. W. (1986). *The history of blood gases, acids, and bases*: Munksgaard.

Bai, W., Huang, H., Li, Y., Zhang, H., Liang, B., Guo, R., et al. (2014). Direct preparation of well-dispersed graphene/gold nanorod composites and their application in electrochemical sensors for determination of ractopamine. *Electrochimica Acta, 117*, 322-328.

Banus, M. G. (1941). A design for a saturated calomel electrode. *Science, 93*(2425), 601-602.

Beltramo, G., & Koper, M. (2003). Nitric oxide reduction and oxidation on stepped Pt [n (111)×(111)] electrodes. *Langmuir, 19*(21), 8907-8915.

Blaz, T., Migdalski, J., & Lewenstam, A. (2005). Junction-less reference electrode for potentiometric measurements obtained by buffering pH in a conducting polymer matrix. *Analyst, 130*(5), 637-643.

Brown, F. O., Finnerty, N. J., & Lowry, J. P. (2009). Nitric oxide monitoring in brain extracellular fluid: characterisation of Nafion®-modified Pt electrodes in vitro and in vivo. *Analyst, 134*(10), 2012-2020.

Brownson, D. A., & Banks, C. E. (2010). Graphene electrochemistry: An overview of potential applications. *Analyst, 135*(11), 2768-2778.

Brownson, D. A., Foster, C. W., & Banks, C. E. (2012). The electrochemical performance of graphene modified electrodes: An analytical perspective. *Analyst, 137*(8), 1815-1823.

Brylev, O., Sarrazin, M., Roué, L., & Bélanger, D. (2007). Nitrate and nitrite electrocatalytic reduction on Rh-modified pyrolytic graphite electrodes. *Microchimica Acta, 52*(21), 6237-6247.

Cai, C., & Chen, J. (2004). Direct electron transfer of glucose oxidase promoted by carbon nanotubes. *Analytical Biochemistry, 332*(1), 75-83.

Cao, A., Liu, Z., Chu, S., Wu, M., Ye, Z., Cai, Z., et al. (2010). A facile one-step method to produce graphene–CdS quantum dot nanocomposites as promising optoelectronic materials. *Advanced Materials, 22*(1), 103-106.

Céspedes, F., Martinez-Fabregas, E., & Alegret, S. (1996). New materials for electrochemical sensing I. Rigid conducting composites. *TrAC Trends in Analytical Chemistry, 15*(7), 296-304.

Cha, W., Lee, Y., Oh, B. K., & Meyerhoff, M. E. (2005). Direct detection of S-nitrosothiols using planar amperometric nitric oxide sensor modified with polymeric films containing catalytic copper species. *Analytical Chemistry, 77*(11), 3516-3524.

Chamsi, A. Y., & Fogg, A. G. (1988). Oxidative flow injection amperometric determination of nitrite at an electrochemically pre-treated glassy carbon electrode. *Analyst, 113*(11), 1723-1727.

Chatterjee, S., & Chen, A. (2012). Voltammetric detection of the α-dicarbonyl compound: Methylglyoxal as a flavoring agent in wine and beer. *Analytica Chimica Acta, 751*, 66-70.

Chen, A. R., Emma I Compton, Richard G. (2009). Abrasive stripping voltammetry in room temperature ionic liquids. *Electroanalysis, 21*(1), 29-35.

Chen, D., Tang, L., & Li, J. (2010). Graphene-based materials in electrochemistry. *Chemical Society Reviews, 39*(8), 3157-3180.

Chen, H., Shao, L., Li, Q., & Wang, J. (2013). Gold nanorods and their plasmonic properties. *Chemical Society Reviews, 42*(7), 2679-2724.

Chen, S., Zhu, J., Wu, X., Han, Q., & Wang, X. (2010). Graphene oxide−MnO_2 nanocomposites for supercapacitors. *ACS Nano, 4*(5), 2822-2830.

Chen, S. Q., & Wang, Y. (2010). Microwave-assisted synthesis of a Co_3O_4–graphene sheet-on-sheet nanocomposite as a superior anode material for Li-ion batteries. *Journal of Materials Chemistry, 20*(43), 9735-9739.

Chen, X.-m., Wu, G.-h., Jiang, Y.-q., Wang, Y.-r., & Chen, X. (2011). Graphene and graphene-based nanomaterials: the promising materials for bright future of electroanalytical chemistry. *Analyst, 136*(22), 4631-4640.

Choi, W., Lahiri, I., Seelaboyina, R., & Kang, Y. S. (2010). Synthesis of graphene and its applications. *Critical Reviews in Solid State and Materials Sciences, 35*(1).

Christian, G. D. (2004). *Analytical* Chemistry. New York: Wiley.

Ciobanu, M., Wilburn, J. P., & Lowy, D. A. (2004). Miniaturized reference electrodes. II use in corrosive, biological, and organic media. *Electroanalysis, 16*(16), 1351-1358.

Clark, L. (1956). Monitor and control of blood and tissue oxygen tensions: Transactions of the American Society for Artificial Internal Organs, v. 2.

Clark, L., & Lyons, C. (1962). Electrode systems for continuous monitoring in cardiovascular surgery. *Annals of the New York Academy of Sciences, 102*(1), 29-45.

Coleman, D. H., White, R. E., & Hobbs, D. T. (1995). A parallel-plate electrochemical reactor model for the destruction of nitrate and nitrite in alkaline waste solutions. *Journal of the Electrochemical Society, 142*(4), 1152-1161.

Cotton, F. A. W., G. (1988). *Advanced Inorganic Chemistry* (5th ed.). New York: Wiley.

Cremer, M. (1906). *Über die Ursache der elektromotorischen Eigenschaften der Gewebe, zugleich ein Beitrag zur Lehre von den polyphasischen Elektrolytketten*: R. Oldenbourg.

Cui, L., Meng, X., Xu, M., Shang, K., Ai, S., & Liu, Y. (2011). Electro-oxidation nitrite based on copper calcined layered double hydroxide and gold nanoparticles modified glassy carbon electrode. *Electrochimica Acta, 56*(27), 9769-9774.

Dang, X., Hu, H., Wang, S., & Hu, S. (2015). Nanomaterials-based electrochemical sensors for nitric oxide. *Microchimica Acta, 182*(3-4), 455-467.

Davis, J., Moorcroft, M. J., Wilkins, S. J., Compton, R. G., & Cardosi, M. F. (2000). Electrochemical detection of nitrate and nitrite at a copper modified electrode. *Analyst, 125*(4), 737-742.

Desideri, P., Lepri, L., Heimler, D., & Bard, A. (1973). *Encyclopedia of Electrochemistry of the Elements*. New York: Dekker.

Du, J., Lai, X., Yang, N., Zhai, J., Kisailus, D., Su, F., et al. (2010). Hierarchically ordered macro−mesoporous TiO_2−graphene composite films: improved mass transfer, reduced charge recombination, and their enhanced photocatalytic activities. *ACS Nano, 5*(1), 590-596.

Eggins, B. R. (2008). *Chemical Sensors and Biosensors* (Vol. 28): John Wiley & Sons.

El-Sayed, M. A. (2001). Some interesting properties of metals confined in time and nanometer space of different shapes. *Accounts of Chemical Research, 34*(4), 257-264.

Esplandiu, M., Pacios, M., Cyganek, L., Bartroli, J., & Del Valle, M. (2009). Enhancing the electrochemical response of myoglobin with carbon nanotube electrodes. *Nanotechnology, 20*(35), 355502.

Fan, C., Li, G., Zhu, J., & Zhu, D. (2000). A reagentless nitric oxide biosensor based on hemoglobin–DNA films. *Analytica Chimica Acta, 423*(1), 95-100.

Fei, W., Zhang, Y., Sun, X., Zhang, Y., Cao, H., Shen, H., et al. (2012). Direct electrochemistry and electrocatalysis of myoglobin immobilized on DNA-gold

nanoparticle clusters composite film. *Journal of Electroanalytical Chemistry, 675*, 5-10.

Ferreira, I., & Silva, S. (2008). Quantification of residual nitrite and nitrate in ham by reverse-phase high performance liquid chromatography/diode array detector. *Talanta, 74*(5), 1598-1602.

Frey, A., Paulus, C., Schienle, M., & Thewes, R. (2006). Circuit arrangement, electrochemical sensor, sensor arrangement, and method for processing a current signal provided via a sensor electrode: Google Patents.

G. D. Christian. (2004). *Analytical Chemistry,* (6th ed., ed.). New York: Wiley.

Gao, W., Tjiu, W. W., Wei, J., & Liu, T. (2014). Highly sensitive nonenzymatic glucose and H_2O_2 sensor based on $Ni(OH)_2$/electroreduced graphene oxide−multiwalled carbon nanotube film modified glass carbon electrode. *Talanta, 120*, 484-490.

Geim, A. K., & Novoselov, K. S. (2007). The rise of graphene. *Nature Materials, 6*(3), 183-191.

Gholivand, M.-B., Jalalvand, A. R., & Goicoechea, H. C. (2014). Computer-assisted electrochemical fabrication of a highly selective and sensitive amperometric nitrite sensor based on surface decoration of electrochemically reduced graphene oxide nanosheets with CoNi bimetallic alloy nanoparticles. *Materials Science Engineering C, 40*(0), 109-120.

Goncalves, G., Marques, P. A., Granadeiro, C. M., Nogueira, H. I., Singh, M., & Gracio, J. (2009). Surface modification of graphene nanosheets with gold nanoparticles: The role of oxygen moieties at graphene surface on gold nucleation and growth. *Chemistry of Materials, 21*(20), 4796-4802.

Gooding, J. J., Wibowo, R., Liu, J., Yang, W., Losic, D., Orbons, S., et al. (2003). Protein electrochemistry using aligned carbon nanotube arrays. *Journal of the American Chemical Society, 125*(30), 9006-9007.

Gorton, L., & Domí, E. (2002). Electrocatalytic oxidation of NAD (P) H at mediator-modified electrodes. *Reviews in Molecular Biotechnology, 82*(4), 371-392.

Griveau, S., Dumézy, C., Séguin, J., Chabot, G. G., Scherman, D., & Bedioui, F. (2007). In vivo electrochemical detection of nitric oxide in tumor-bearing mice. *Analytical Chemistry, 79*(3), 1030-1033.

Guidelli, R., Pergola, F., & Raspi, G. (1972). Voltammetric behavior of nitrite ion on platinum in neutral and weakly acidic media. *Analytical Chemistry, 44*(4), 745-755.

Guiseppi-Elie, A., Lei, C., & Baughman, R. H. (2002). Direct electron transfer of glucose oxidase on carbon nanotubes. *Nanotechnology, 13*(5), 559.

Guo, C. X., Yang, H. B., Sheng, Z. M., Lu, Z. S., Song, Q. L., & Li, C. M. (2010). Layered graphene/quantum dots for photovoltaic devices. *Angewandte Chemie International Edition, 49*(17), 3014-3017.

Guo, S., Dong, S., & Wang, E. (2009). Three-dimensional Pt-on-Pd bimetallic nanodendrites supported on graphene nanosheet: facile synthesis and used as an advanced nanoelectrocatalyst for methanol oxidation. *ACS Nano, 4*(1), 547-555.

Ha, J., Martin, S. M., Jeon, Y., Yoon, I. J., Brown, R. B., Nam, H., et al. (2005). A polymeric junction membrane for solid-state reference electrodes. *Analytica Chimica Acta, 549*(1), 59-66.

Haber, F., & Klemensiewicz, Z. (1909). Über elektrische phasengrenzkräfte. *Physik Chemistry, 67*, 385-431.

Hamachi, I., Noda, S., & Kunitake, T. (1991). Functional conversion of myoglobin bound to synthetic bilayer membranes: from dioxygen storage protein to redox enzyme. *Journal of the American Chemical Society, 113*(25), 9625-9630.

Hassan, H. M., Abdelsayed, V., Abd El Rahman, S. K., AbouZeid, K. M., Terner, J., El-Shall, M. S., et al. (2009). Microwave synthesis of graphene sheets supporting metal nanocrystals in aqueous and organic media. *Journal of Materials Chemistry, 19*(23), 3832-3837.

He, H., & Gao, C. (2010). General approach to individually dispersed, highly soluble, and conductive graphene nanosheets functionalized by nitrene chemistry. *Chemistry of Materials, 22*(17), 5054-5064.

He, X., & Zhu, L. (2006). Direct electrochemistry of hemoglobin in cetylpyridinium bromide film: redox thermodynamics and electrocatalysis to nitric oxide. *Electrochemistry Communications, 8*(4), 615-620.

Hildebrand, D. P., Tang, H.-l., Luo, Y., Hunter, C. L., Smith, M., Brayer, G. D., et al. (1996). Efficient coupled oxidation of heme by an active site variant of horse heart myoglobin. *Journal of the American Chemical Society, 118*(51), 12909-12915.

Holler, F. J., Skoog, D. A., & Crouch, S. R. (2007). *Principles of Instrumental Analysis*. Belmont: Thomson.

Hou, S., Su, S., Kasner, M. L., Shah, P., Patel, K., & Madarang, C. J. (2010). Formation of highly stable dispersions of silane-functionalized reduced graphene oxide. *Chemical Physical Letters, 501*(1), 68-74.

Huang, N. M., Lim, H. N., Chia, C. H., Yarmo, M. A., & Muhamad, M. R. (2011). Simple room-temperature preparation of high-yield large-area graphene oxide. *International Journal of Nanomedicine, 6*, 3443-3448.

Huang, X., El-Sayed, I. H., Yi, X., & El-Sayed, M. A. (2005). Gold nanoparticles: Catalyst for the oxidation of NADH to NAD+. *Journal of Photochemistry and Photobiology B: Biology, 81*(2), 76-83.

Huang, X., Li, Y., Chen, Y., & Wang, L. (2008). Electrochemical determination of nitrite and iodate by use of gold nanoparticles/poly (3-methylthiophene) composites coated glassy carbon electrode. *Sensors and Actuators B, 134*(2), 780-786.

Huang, X., Neretina, S., & El-Sayed, M. A. (2009). Gold nanorods: from synthesis and properties to biological and biomedical applications. *Advanced Materials, 21*(48), 4880.

Huang, X., Zhou, X., Wu, S., Wei, Y., Qi, X., Zhang, J., et al. (2010). Reduced graphene oxide-templated photochemical synthesis and in situ assembly of Au nanodots to orderly patterned Au nanodot chains. *Small, 6*(4), 513-516.

Hughes, M. N. (2008). Chapter one-chemistry of nitric oxide and related species. *Methods in Enzymology, 436*, 3-19.

Hwang, S., Cha, W., & Meyerhoff, M. E. (2008). Amperometric nitrosothiol sensor using immobilized organoditelluride species as selective catalytic layer. *Electroanalysis, 20*(3), 270-279.

Ignarro, L. J., Buga, G. M., Wood, K. S., Byrns, R. E., & Chaudhuri, G. (1987). Endothelium-derived relaxing factor produced and released from artery and vein is nitric oxide. *Proceedings of the National Academy of Sciences, 84*(24), 9265-9269.

Jana, N. R., Gearheart, L., & Murphy, C. J. (2001). Wet chemical synthesis of high aspect ratio cylindrical gold nanorods. *The Journal of Physical Chemistry B, 105*(19), 4065-4067.

Jasuja, K., & Berry, V. (2009). Implantation and growth of dendritic gold nanostructures on graphene derivatives: Electrical property tailoring and Raman enhancement. *ACS Nano, 3*(8), 2358-2366.

Jayabal, S., Pandikumar, A., Lim, H. N., Ramaraj, R., Sun, T., & Huang, N. M. (2015). A gold nanorod-based localized surface plasmon resonance platform for the detection of environmentally toxic metal ions. *Analyst, 140*(8), 2540-2555.

Jayabal, S., & Ramaraj, R. (2015). Amperometric sensing of NADH at gold nanorods stabilized in amine-functionalized silicate sol–gel matrix modified electrode. *Journal of Applied Electrochemistry, 45*(8), 881-888.

Jayabal, S., Viswanathan, P., & Ramaraj, R. (2014). Reduced graphene oxide–gold nanorod composite material stabilized in silicate sol–gel matrix for nitric oxide sensor. *RSC Advances, 4*(63), 33541-33548.

Jeevagan, A. J., & John, S. A. (2013). Synthesis of non-peripheral amine substituted nickel (II) phthalocyanine capped gold nanoparticles and their immobilization on electrode for the electrocatalytic oxidation of hydrazine. *RSC Advances, 3*(7), 2256-2264.

Jeevagan, A. J., Raj, M. A., & John, S. A. (2013). Growth of gold nanorods in solution and on ITO and Au substrates using non-peripheral amine functionalized nickel (II) phthalocyanine capped gold nanoparticles as a seed solution. *RSC Advances, 3*(3), 870-878.

Jena, B. K., & Raj, C. R. (2006). Electrochemical biosensor based on integrated assembly of dehydrogenase enzymes and gold nanoparticles. *Analytical Chemistry, 78*(18), 6332-6339.

Johnson, J. L., Behnam, A., Pearton, S., & Ural, A. (2010). Hydrogen sensing using Pd-functionalized multi-layer graphene nanoribbon networks. *Advanced Materials, 22*(43), 4877-4880.

Ju, Y.-W., Choi, G.-R., Jung, H.-R., & Lee, W.-J. (2008). Electrochemical properties of electrospun PAN/MWCNT carbon nanofibers electrodes coated with polypyrrole. *Electrochimica Acta, 53*(19), 5796-5803.

Kamat, P. V. (2009). Graphene-based nanoarchitectures. Anchoring semiconductor and metal nanoparticles on a two-dimensional carbon support. *The Journal of Physical Chemistry Letters, 1*(2), 520-527.

Kampouris, D. K., & Banks, C. E. (2010). Exploring the physicoelectrochemical properties of graphene. *Chemical Communications, 46*(47), 8986-8988.

Kang, X., Wang, J., Wu, H., Aksay, I. A., Liu, J., & Lin, Y. (2009). Glucose oxidase–graphene–chitosan modified electrode for direct electrochemistry and glucose sensing. *Biosensors and Bioelectronics, 25*(4), 901-905.

Kang, X., Wang, J., Wu, H., Liu, J., Aksay, I. A., & Lin, Y. (2010). A graphene-based electrochemical sensor for sensitive detection of paracetamol. *Talanta, 81*(3), 754-759.

Katz, E., & Willner, I. (2003). Probing biomolecular interactions at conductive and semiconductive surfaces by impedance spectroscopy: Routes to impedimetric immunosensors, DNA-sensors, and enzyme biosensors. *Electroanalysis, 15*(11), 913-947.

Katz, E., & Willner, I. (2004). Biomolecule-functionalized carbon nanotubes: Applications in nanobioelectronics. *Chemistry Physics Chemistry, 5*(8), 1084-1104.

Kavya, R., Saluja, R., Singh, S., & Dikshit, M. (2006). Nitric oxide synthase regulation and diversity: Implications in Parkinson's disease. *Nitric Oxide, 15*(4), 280-294.

Kim, F., Luo, J., Cruz-Silva, R., Cote, L. J., Sohn, K., & Huang, J. (2010). Self-Propagating Domino-like Reactions in Oxidized Graphite. *Advanced Functional Materials, 20*(17), 2867-2873.

Kim, L. T. T., Girard, A., Griscom, L., Razan, F., Griveau, S., & Bedioui, F. (2011). Micro-ring disc ultramicroelectrodes array for direct detection of NO-release from S-nitrosoglutathione. *Electrochemistry Communications, 13*(7), 681-684.

Kim, Y.-K., Na, H.-K., & Min, D.-H. (2010). Influence of surface functionalization on the growth of gold nanostructures on graphene thin films. *Langmuir, 26*(16), 13065-13070.

Kim, Y. T., Han, J. H., Hong, B. H., & Kwon, Y. U. (2010). Electrochemical synthesis of CdSe quantum-dot arrays on a graphene basal plane using mesoporous silica thin-film templates. *Advanced Materials, 22*(4), 515-518.

Kisiel, A., Marcisz, H., Michalska, A., & Maksymiuk, K. (2005). All solid state reference electrodes based on conducting polymers. *Analyst, 130*(12), 1655-1662.

Kissinger, P., & Heineman, W. R. (1996). *Laboratory Techniques in Electroanalytical Chemistry, Revised and Expanded*: CRC press.

Kissinger, P. T., & Heineman, W. R. (1983). Cyclic voltammetry. *Journal of Chemical Education, 60*(9), 702.

Kobayashi, H., & Hikuma, M. (2000). Determination of nitrite with a ptfe-membrane, covered electrode after reduction to nitrogen oxide, in a reagent saving flow injection system. *Analytical Letters, 33*(6), 1013- 1023.

Krylov, A. V., & Lisdat, F. (2007). Nickel hexacyanoferrate-based sensor electrode for the detection of nitric oxide at low potentials. *Electroanalysis, 19*(1), 23-29.

Kueng, A., Kranz, C., & Mizaikoff, B. (2004). Amperometric ATP biosensor based on polymer entrapped enzymes. *Biosensors and Bioelectronics, 19*(10), 1301-1307.

Kumar, S. A., Wang, S.-F., Chang, Y.-T., Lu, H.-C., & Yeh, C.-T. (2011). Electrochemical properties of myoglobin deposited on multi-walled carbon nanotube/ciprofloxacin film. *Colloids and Surfaces B: Biointerfaces, 82*(2), 526-531.

Kunimatsu, M., Qiao, H., & Okada, T. (2005). Microtubular hydrogen electrode, a reference electrode for electrochemical analyses. *Journal of the Electrochemical Society, 152*(5), E161-E166.

Lakshminarayanan, V., & Sur, U. K. (2003). Hydrophobicity-induced drying transition in alkanethiol self-assembled monolayer—water interface. *Pramana, 61*(2), 361-371.

Lee, J.-H., Ko, K.-H., & Park, B.-O. (2003). Electrical and optical properties of ZnO transparent conducting films by the sol–gel method. *Journal of Crystal Growth, 247*(1–2), 119-125.

Lee, Y., & Kim, J. (2007). Simultaneous electrochemical detection of nitric oxide and carbon monoxide generated from mouse kidney organ tissues. *Analytical Chemistry, 79*(20), 7669-7675.

Li, B., Liu, T., Wang, Y., & Wang, Z. (2012). ZnO/graphene-oxide nanocomposite with remarkably enhanced visible-light-driven photocatalytic performance. *Journal of Colloid Interface Sciences, 377*(1), 114-121.

Li, D., Mueller, M. B., Gilje, S., Kaner, R. B., & Wallace, G. G. (2008). Processable aqueous dispersions of graphene nanosheets. *Nature Nanotechnology, 3*(2), 101-105.

Li, J., Guo, S., Zhai, Y., & Wang, E. (2009). High-sensitivity determination of lead and cadmium based on the Nafion-graphene composite film. *Analytica Chimica Acta, 649*(2), 196-201.

Li, J., Guo, S., Zhai, Y., & Wang, E. (2009). Nafion–graphene nanocomposite film as enhanced sensing platform for ultrasensitive determination of cadmium. *Electrochemistry Communications, 11*(5), 1085-1088.

Li, L., Lu, H., & Deng, L. (2013). A sensitive NADH and ethanol biosensor based on graphene–Au nanorods nanocomposites. *Talanta, 113*, 1-6.

Li, L. L., Liu, K. P., Yang, G. H., Wang, C. M., Zhang, J. R., & Zhu, J. J. (2011). Fabrication of graphene–quantum dots composites for sensitive electrogenerated chemiluminescence immunosensing. *Advanced Functional Materials, 21*(5), 869-878.

Li, N., Zhao, H., Yuan, R., Peng, K., & Chai, Y. (2008). An amperometric immunosensor with a DNA polyion complex membrane/gold nanoparticles-backbone for antibody immobilisation. *Electrochimica Acta, 54*(2), 235-241.

Li, S.-J., Zhao, G.-Y., Zhang, R.-X., Hou, Y.-L., Liu, L., & Pang, H. (2013). A sensitive and selective nitrite sensor based on a glassy carbon electrode modified with gold nanoparticles and sulfonated graphene. *Microchimica Acta, 180*(9-10), 821-827.

Li, Y., Lin, X., & Jiang, C. (2006). Fabrication of a nanobiocomposite film containing heme proteins and carbon nanotubes on a choline modified glassy carbon electrode: Direct electrochemistry and electrochemical catalysis. *Electroanalysis, 18*(21), 2085-2091.

Li, Z., & Hu, N. (2003). Direct electrochemistry of heme proteins in their layer-by-layer films with clay nanoparticles. *Journal of Electroanalytical Chemistry, 558*, 155-165.

Liang, J., Xu, Y., Sui, D., Zhang, L., Huang, Y., Ma, Y., et al. (2010). Flexible, magnetic, and electrically conductive graphene/Fe_3O_4 paper and its application for magnetic-controlled switches. *The Journal of Physical Chemistry C, 114*(41), 17465-17471.

Kosel, T. H., & Kamat, P. V. (2010). Anchoring semiconductor and metal nanoparticles on a two-dimensional catalyst mat. Storing and shuttling electrons with reduced graphene oxide. *Nano Letters, 10*(2), 577-583.

Lin, K. C., Yin, C. Y., & Chen, S. M. (2012). Electrocatalytic oxidation of NADH based on polyluminol and functionalized multi-walled carbon nanotubes. *Analyst, 137*(6), 1378-1383.

Lin, W.-J., Liao, C.-S., Jhang, J.-H., & Tsai, Y.-C. (2009). Graphene modified basal and edge plane pyrolytic graphite electrodes for electrocatalytic oxidation of hydrogen peroxide and β-nicotinamide adenine dinucleotide. *Electrochemistry Communications, 11*(11), 2153-2156.

Lin, Y., Zhang, K., Chen, W., Liu, Y., Geng, Z., Zeng, J., et al. (2010). Dramatically enhanced photoresponse of reduced graphene oxide with linker-free anchored CdSe nanoparticles. *ACS Nano, 4*(6), 3033-3038.

Liu, H., Gao, J., Xue, M., Zhu, N., Zhang, M., & Cao, T. (2009). Processing of graphene for electrochemical application: noncovalently functionalize graphene sheets with water-soluble electroactive methylene green. *Langmuir, 25*(20), 12006-12010.

Liu, J., Bai, H., Wang, Y., Liu, Z., Zhang, X., & Sun, D. D. (2010). Self-assembling TiO_2 nanorods on large graphene oxide sheets at a two-phase interface and their anti-recombination in photocatalytic applications. *Advanced Functional Materials, 20*(23), 4175-4181.

Liu, J., Fu, S., Yuan, B., Li, Y., & Deng, Z. (2010). Toward a universal "adhesive nanosheet" for the assembly of multiple nanoparticles based on a protein-induced reduction/decoration of graphene oxide. *Journal of the American Chemical Society, 132*(21), 7279-7281.

Liu, Y., Han, G., Li, Y., & Jin, M. (2011). Flower-like zinc oxide deposited on the film of graphene oxide and its photoluminescence. *Materials Letters, 65*(12), 1885-1888.

Lu, G., Mao, S., Park, S., Ruoff, R. S., & Chen, J. (2009). Facile, noncovalent decoration of graphene oxide sheets with nanocrystals. *Nano Research, 2*(3), 192-200.

Lu, T., Pan, L., Li, H., Zhu, G., Lv, T., Liu, X., et al. (2011). Microwave-assisted synthesis of graphene–ZnO nanocomposite for electrochemical supercapacitors. *Journal of Alloys Compound, 509*(18), 5488-5492.

Lubert, K. H., & Kalcher, K. (2010). History of electroanalytical methods. *Electroanalysis, 22*(17-18), 1937-1946.

Madhu, R., Veeramani, V., & Chen, S.-M. (2014). Heteroatom-enriched and renewable banana-stem-derived porous carbon for the electrochemical determination of nitrite in various water samples. *Scientific Report , 4*, 4679.

Malinski, T., & Taha, Z. (1992). Nitric oxide release from a single cell measured in situ by a porphyrinic-based microsensor. *Nature, 358*(6388), 676-678.

Mani, V., Dinesh, B., Chen, S.-M., & Saraswathi, R. (2014). Direct electrochemistry of myoglobin at reduced graphene oxide-multiwalled carbon nanotubes-platinum nanoparticles nanocomposite and biosensing towards hydrogen peroxide and nitrite. *Biosensors and Bioelectronics, 53*, 420-427.

Mani, V., Periasamy, A. P., & Chen, S.-M. (2012). Highly selective amperometric nitrite sensor based on chemically reduced graphene oxide modified electrode. *Electrochemistry Communications, 17*, 75-78.

Marlinda, A. R., Huang, N. M., Muhamad, M. R., An'amt, M. N., Chang, B. Y. S., Yusoff, N., et al. (2012). Highly efficient preparation of ZnO nanorods

decorated reduced graphene oxide nanocomposites. *Materials Letters, 80*(0), 9-12.

Mastalir, Á., Király, Z., Patzko, A., Dékány, I., & L'Argentiere, P. (2008). Synthesis and catalytic application of Pd nanoparticles in graphite oxide. *Carbon, 46*(13), 1631-1637.

McCreery, R. L. (2008). Advanced carbon electrode materials for molecular electrochemistry. *Chemical Reviews, 108*(7), 2646-2687.

Meng, Y., Aldous, L., Belding, S. R., & Compton, R. G. (2012). The formal potentials and electrode kinetics of the proton/hydrogen couple in various room temperature ionic liquids. *Chemical Communications, 48*(45), 5572-5574.

Meng, Z., Liu, B., Zheng, J., Sheng, Q., & Zhang, H. (2011). Electrodeposition of cobalt oxide nanoparticles on carbon nanotubes, and their electrocatalytic properties for nitrite electrooxidation. *Microchimica Acta, 175*(3-4), 251-257.

Merkoçi, A., Aldavert, M., Marın, S., & Alegret, S. (2005). New materials for electrochemical sensing V: Nanoparticles for DNA labeling. *TrAC Trends in Analytical Chemistry, 24*(4), 341-349.

Merkoci, A., & Alegret, S. (2002). New materials for electrochemical sensing IV. Molecular imprinted polymers. *TrAC Trends in Analytical Chemistry, 21*(11), 717-725.

Morrin, A. (2012). Inkjet printed electrochemical sensors. *Inkjet-Based Micromanufacturing*, 295-311.

Muszynski, R., Seger, B., & Kamat, P. V. (2008). Decorating graphene sheets with gold nanoparticles. *The Journal of Physical Chemistry C, 112*(14), 5263-5266.

Napoli, C., & Ignarro, L. J. (2001). Nitric oxide and atherosclerosis. *Nitric Oxide, 5*(2), 88-97.

Newbery, J. E., & de Haddad, M. P. L. (1985). Amperometric determination of nitrite by oxidation at a glassy carbon electrode. *Analyst, 110*(1), 81-82.

Newman, J. D., & Turner, A. P. (2005). Home blood glucose biosensors: a commercial perspective. *Biosensors and Bioelectronics, 20*(12), 2435-2453.

Nicholson, R. S. (1965). Theory and Application of Cyclic Voltammetry for Measurement of Electrode Reaction Kinetics. *Analytical Chemistry, 37*(11), 1351-1355.

Nie, T., Zhang, O., Lu, L., Xu, J., Wen, Y., & Qiu, X. (2013). Facile synthesis of poly (3, 4-ethylenedioxythiophene)/graphene nanocomposite and its application for determination of nitrite. *International Journal of Electrochemical Sciences, 8*, 8708-8718.

Nikoobakht, B., & El-Sayed, M. A. (2003). Preparation and growth mechanism of gold nanorods (NRs) using seed-mediated growth method. *Chemistry of Materials, 15*(10), 1957-1962.

Niwa, O., Jia, J., Sato, Y., Kato, D., Kurita, R., Maruyama, K., et al. (2006). Electrochemical performance of angstrom level flat sputtered carbon film consisting of sp^2 and sp^3 mixed bonds. *Journal of the American Chemical Society, 128*(22), 7144-7145.

Novoselov, K. S., Geim, A. K., Morozov, S. V., Jiang, D., Zhang, Y., Dubonos, S. V., et al. (2004). Electric field effect in atomically thin carbon films. *Science, 306*(5696), 666-669.

Oh, B. K., Robbins, M. E., & Schoenfisch, M. H. (2006). Planar nitric oxide (NO)-selective ultramicroelectrode sensor for measuring localized NO surface concentrations at xerogel microarrays. *Analyst, 131*(1), 48-54.

Pacios, M., Del Valle, M., Bartroli, J., & Esplandiu, M. (2009). Electrocatalyzed O_2 response of myoglobin immobilized on multi-walled carbon nanotube forest electrodes. *Journal of Nanoscience and Nanotechnology, 9*(10), 6132-6138.

Pacios, M., Martín-Fernández, I., Villa, R., Godignon, P., Del Valle, M., Bartrolí, J., et al. (2011). Carbon nanotubes as suitable electrochemical platforms for metalloprotein sensors and genosensors *Carbon Nanotubes-Growth and Applications*: InTech.

Pandikumar, A., How, G. T. S., See, T. P., Omar, F. S., Jayabal, S., Kamali, K. Z., et al. (2014). Graphene and its nanocomposite material based electrochemical sensor platform for dopamine. *RSC Advances, 4*(108), 63296-63323.

Pandikumar, A., Manonmani, S., & Ramaraj, R. (2012). TiO_2-Au nanocomposite materials embedded in polymer matrices and their application in the photocatalytic reduction of nitrite to ammonia. *Catalysis Science Technology 2*(2), 345-353.

Pandikumar, A., & Ramaraj, R. (2011). Aminosilicate sol-gel embedded core-shell (TiO_2-Au) nps nanomaterials modified electrode for the electrochemical detection of nitric oxide. *Indian Journal of Chemistry, 50*(9), 1388.

Patolsky, F., Weizmann, Y., & Willner, I. (2004). Long-range electrical contacting of redox enzymes by SWCNT connectors. *Angewandte Chemie International Edition, 43*(16), 2113-2117.

Patolsky, F., Zayats, M., Katz, E., & Willner, I. (1999). Precipitation of an insoluble product on enzyme monolayer electrodes for biosensor applications: Characterization by faradaic impedance spectroscopy, cyclic voltammetry, and microgravimetric quartz crystal microbalance analyses. *Analytical Chemistry, 71*(15), 3171-3180.

Pei, R., Cheng, Z., Wang, E., & Yang, X. (2001). Amplification of antigen–antibody interactions based on biotin labeled protein–streptavidin network complex using impedance spectroscopy. *Biosensors and Bioelectronics, 16*(6), 355-361.

Peng, H.-P., Liang, R.-P., Zhang, L., & Qiu, J.-D. (2011). Sonochemical synthesis of magnetic core–shell Fe_3O_4@ZrO_2 nanoparticles and their application to the highly effective immobilization of myoglobin for direct electrochemistry. *Electrochimica Acta, 56*(11), 4231-4236.

Pérez-Juste, J., Pastoriza-Santos, I., Liz-Marzán, L. M., & Mulvaney, P. (2005). Gold nanorods: Synthesis, characterization and applications. *Coordination Chemistry Reviews, 249*(17), 1870-1901.

Petrova, H., Perez-Juste, J., Zhang, Z., Zhang, J., Kosel, T., & Hartland, G. V. (2006). Crystal structure dependence of the elastic constants of gold nanorods. *Journal of Materials Chemistry, 16*(40), 3957-3963.

Pimenta, M. A., Dresselhaus, G., Dresselhaus, M. S., Cancado, L. G., Jorio, A., & Saito, R. (2007). Studying disorder in graphite-based systems by Raman spectroscopy. *Physical Chemistry Chemical Physics, 9*(11), 1276-1290.

Pioda, L. A., Simon, W., Bosshard, H.-R., & Curtius, H. C. (1970). Determination of potassium ion concentration in serum using a highly selective liquid-membrane electrode. *Clinica Chimica Acta, 29*(2), 289-293.

Pontié, M., Gobin, C., Pauporté, T., Bedioui, F., & Devynck, J. (2000). Electrochemical nitric oxide microsensors: sensitivity and selectivity characterisation. *Analytica Chimica Acta, 411*(1), 175-185.

Pourreza, N., Fat'hi, M. R., & Hatami, A. (2012). Indirect cloud point extraction and spectrophotometric determination of nitrite in water and meat products. *Microchemical Journal, 104*, 22-25.

Pumera, M. (2010). Graphene-based nanomaterials and their electrochemistry. *Chemical Society Reviews, 39*(11), 4146-4157.

Qiu, J.-D., Peng, H.-P., Liang, R.-P., & Xia, X.-H. (2010). Facile preparation of magnetic core–shell Fe_3O_4@Au nanoparticle/myoglobin biofilm for direct electrochemistry. *Biosensors and Bioelectronics, 25*(6), 1447-1453.

Radhakrishnan, S., Krishnamoorthy, K., Sekar, C., Wilson, J., & Kim, S. J. (2014). A highly sensitive electrochemical sensor for nitrite detection based on Fe_2O_3 nanoparticles decorated reduced graphene oxide nanosheets. *Applied Catalysis B: Environmental, 148*, 22-28.

Radhakrishnan, S., Sumathi, C., Umar, A., Jae Kim, S., Wilson, J., & Dharuman, V. (2013). Polypyrrole–poly(3,4-ethylenedioxythiophene)–Ag (PPy–PEDOT–Ag) nanocomposite films for label-free electrochemical DNA sensing. *Biosensors and Bioelectronics, 47*(0), 133-140.

Rao, T. N., Yagi, I., Miwa, T., Tryk, D., & Fujishima, A. (1999). Electrochemical oxidation of NADH at highly boron-doped diamond electrodes. *Analytical Chemistry, 71*(13), 2506-2511.

Reshetilov, A., Iliasov, P., Knackmuss, H., & Boronin, A. (2000). The nitrite oxidizing activity of Nitrobacter strains as a base of microbial biosensor for nitrite detection. *Analytical Letters, 33*(1), 29-41.

Scheuermann, G. M., Rumi, L., Steurer, P., Bannwarth, W., & Mülhaupt, R. (2009). Palladium nanoparticles on graphite oxide and its functionalized graphene derivatives as highly active catalysts for the Suzuki−Miyaura coupling reaction. *Journal of the American Chemical Society, 131*(23), 8262-8270.

Schniepp, H. C., Li, J.-L., McAllister, M. J., Sai, H., Herrera-Alonso, M., Adamson, D. H., et al. (2006). Functionalized single graphene sheets derived from splitting graphite oxide. *Journal of Physical Chemistry B, 110*(17), 8535-8539.

Schwarz, J., Kaden, H., & Enseleit, U. (2000). Voltammetric examinations of ferrocene on microelectrodes and microarrayelectrodes. *Electrochemistry Communications, 2*(8), 606-611.

Shah, B., & Chen, A. (2012). Novel electrochemical approach for the monitoring of biodegradation of phenolic pollutants and determination of enzyme activity. *Electrochemistry Communications, 25*, 79-82.

Shan, C., Yang, H., Han, D., Zhang, Q., Ivaska, A., & Niu, L. (2010). Graphene/AuNPs/chitosan nanocomposites film for glucose biosensing. *Biosensors and Bioelectronics, 25*(5), 1070-1074.

Shan, C., Yang, H., Song, J., Han, D., Ivaska, A., & Niu, L. (2009). Direct electrochemistry of glucose oxidase and biosensing for glucose based on graphene. *Analytical Chemistry, 81*(6), 2378-2382.

Shang, N. G., Papakonstantinou, P., McMullan, M., Chu, M., Stamboulis, A., Potenza, A., et al. (2008). Catalyst-free efficient growth, orientation and biosensing properties of multilayer graphene nanoflake films with sharp edge planes. *Advanced Functional Materials, 18*(21), 3506-3514.

Shen, J., Hu, Y., Shi, M., Li, N., Ma, H., & Ye, M. (2010). One step synthesis of graphene oxide−magnetic nanoparticle composite. *The Journal of Physical Chemistry C, 114*(3), 1498-1503.

Shen, J., Shi, M., Li, N., Yan, B., Ma, H., Hu, Y., et al. (2010). Facile synthesis and application of Ag-chemically converted graphene nanocomposite. *Nano Research, 3*(5), 339-349.

Sheppard, S., Lambert, R., & Walker, R. (1939). Optical sensitizing of silver halides by dyes I. Adsorption of sensitizing dyes. *Journal of Chemical Physics, 7*(4), 265-273.

Shi, A. W., Qu, F. L., Yang, M. H., Shen, G. L., & Yu, R. Q. (2008). Amperometric H_2O_2 biosensor based on poly-thionine nanowire/HRP/nano-Au-modified glassy carbon electrode. *Sensors and Actuators B: Chemical, 129*(2), 779-783.

Shi, F., Xi, J., Hou, F., Han, L., Li, G., Gong, S., et al. (2016). Application of three-dimensional reduced graphene oxide-gold composite modified electrode for

direct electrochemistry and electrocatalysis of myoglobin. *Materials Science and Engineering C, 58*, 450-457.

Shibata, M., Yoshida, K., & Furuya, N. (1995). Electrochemical synthesis of urea on reduction of carbon dioxide with nitrate and nitrite ions using Cu-loaded gas-diffusion electrode. *Journal of Electroanalytical Chemistry, 387*(1), 143-145.

Shibuki, K. (1990). An electrochemical microprobe for detecting nitric oxide release in brain tissue. *Neuroscience Research, 9*(1), 69-76.

Si, Y., & Samulski, E. T. (2008). Exfoliated graphene separated by platinum nanoparticles. *Chemistry of Materials, 20*(21), 6792-6797.

Singh, V., Patra, M., Manoth, M., Gowd, G., Vadera, S., & Kumar, N. (2009). In situ synthesis of graphene oxide and its composites with iron oxide. *New Carbon Materials, 24*(2), 147-152.

Solé, S., Merkoçi, A., & Alegret, S. (2001). New materials for electrochemical sensing III. Beads. *TrAC Trends in Analytical Chemistry, 20*(2), 102-110.

Son, J. Y., Shin, Y.-H., Kim, H., & Jang, H. M. (2010). NiO resistive random access memory nanocapacitor array on graphene. *ACS Nano, 4*(5), 2655-2658.

Stankovich, S., Dikin, D. A., Piner, R. D., Kohlhaas, K. A., Kleinhammes, A., Jia, Y., et al. (2007). Synthesis of graphene-based nanosheets via chemical reduction of exfoliated graphite oxide. *Carbon, 45*(7), 1558-1565.

Stankovich, S., Piner, R. D., Nguyen, S. T., & Ruoff, R. S. (2006). Synthesis and exfoliation of isocyanate-treated graphene oxide nanoplatelets. *Carbon, 44*(15), 3342-3347.

Stetter, J. R. (2004). Chemical sensing apparatus and methods: Google Patents.

Strom, T. A., Dillon, E. P., Hamilton, C. E., & Barron, A. R. (2010). Nitrene addition to exfoliated graphene: A one-step route to highly functionalized graphene. *Chemical Communications, 46*(23), 4097-4099.

Sun, W., Zhang, S., Liu, H., Jin, L., & Kong, J. (1999). Electrocatalytic reduction of nitrite at a glassy carbon electrode surface modified with palladium (II)-substituted Keggin type heteropolytungstate. *Analytica Chimica Acta, 388*(1), 103-110.

Suni, I. I. (2008). Impedance methods for electrochemical sensors using nanomaterials. *TrAC Trends in Analytical Chemistry, 27*(7), 604-611.

Suresh, S., Pandikumar, A., Murugesan, S., Ramaraj, R., & Paul Raj, S. (2011). Metal-free low-cost organic dye-sensitized ZnO-nanorod photoanode for solid-state solar cell. *Materials Express, 1*(4), 307-314.

Tabrizi, M. A., & Zand, Z. (2014). A facile one-step method for the synthesis of reduced graphene oxide nanocomposites by NADH as reducing agent and its application in NADH sensing. *Electroanalysis, 26*(1), 171-177.

Tang, L., Wang, Y., Li, Y., Feng, H., Lu, J., & Li, J. (2009). Preparation, structure, and electrochemical properties of reduced graphene sheet films. *Advanced Functional Materials, 19*(17), 2782-2789.

Tang, L., Zeng, G.-M., Wang, H., Shen, G.-L., & Huang, D.-L. (2005). Amperometric detection of lignin-degrading peroxidase activities from Phanerochaetechrysosporium. *Enzyme and Microbial Technology, 36*(7), 960-966.

Tang, L., Zeng, G., Shen, G., Zhang, Y., Li, Y., Fan, C., et al. (2009). Highly sensitive sensor for detection of NADH based on catalytic growth of Au nanoparticles on glassy carbon electrode. *Analytical and Bioanalytical Chemistry, 393*(6-7), 1677-1684.

Thangavel, S., & Ramaraj, R. (2008). Polymer membrane stabilized gold nanostructures modified electrode and its application in nitric oxide detection. *The Journal of Physical Chemistry C, 112*(50), 19825-19830.

Thejass, P., & Kuttan, G. (2007). Allyl isothiocyanate (AITC) and phenyl isothiocyanate (PITC) inhibit tumour-specific angiogenesis by downregulating nitric oxide (NO) and tumour necrosis factor-α (TNF-α) production. *Nitric Oxide, 16*(2), 247-257.

Thévenot, D. R., Toth, K., Durst, R. A., & Wilson, G. S. (2001). Electrochemical biosensors: recommended definitions and classification. *Biosensors and Bioelectronics, 16*(1), 121-131.

Traub, O., & Van Bibber, R. (1995). Role of nitric oxide in insulin-dependent diabetes mellitus-related vascular complications. *Western journal of medicine, 162*(5), 439.

Valentini, F., Salis, A., Curulli, A., & Palleschi, G. (2004). Chemical reversibility and stable low-potential NADH detection with nonconventional conducting polymer nanotubule modified glassy carbon electrodes. *Analytical Chemistry, 76*(11), 3244-3248.

Veerapandian, M., Seo, Y.-T., Shin, H., Yun, K., & Lee, M.-H. (2012). Functionalized graphene oxide for clinical glucose biosensing in urine and serum samples. *International Journal of Nanomedicine, 7*, 6123.

Vijay Kumar, S., Huang, N. M., Lim, H. N., Marlinda, A., Harrison, I., & Chia, C. H. (2013). One-step size-controlled synthesis of functional graphene oxide/silver nanocomposites at room temperature. *Chemical Engineering Journal, 219*, 217-224.

Vishnuvardhan, V., Kala, R., & Rao, T. P. (2008). Chemical switch based reusable dual optoelectronic sensor for nitrite. *Analytica Chimica Acta, 623*(1), 53-58.

Wang, C., Ma, Z., Wang, T., & Su, Z. (2006). Synthesis, assembly, and biofunctionalization of silica-coated gold nanorods for colorimetric biosensing. *Advanced Functional Materials, 16*(13), 1673-1678.

Wang, D., Choi, D., Li, J., Yang, Z., Nie, Z., Kou, R., et al. (2009). Self-assembled TiO_2–graphene hybrid nanostructures for enhanced Li-ion insertion. *ACS Nano, 3*(4), 907-914.

Wang, D., Kou, R., Choi, D., Yang, Z., Nie, Z., Li, J., et al. (2010). Ternary self-assembly of ordered metal oxide−graphene nanocomposites for electrochemical energy storage. *ACS Nano, 4*(3), 1587-1595.

Wang, G., Wang, B., Park, J., Yang, J., Shen, X., & Yao, J. (2009). Synthesis of enhanced hydrophilic and hydrophobic graphene oxide nanosheets by a solvothermal method. *Carbon, 47*(1), 68-72.

Wang, H., Robinson, J. T., Diankov, G., & Dai, H. (2010). Nanocrystal growth on graphene with various degrees of oxidation. *Journal of the American Chemical Society, 132*(10), 3270-3271.

Wang, J. (2005). Carbon-nanotube based electrochemical biosensors: A review. *Electroanalysis, 17*(1), 7-14.

Wang, J., & Musameh, M. (2003). Carbon nanotube/teflon composite electrochemical sensors and biosensors. *Analytical Chemistry, 75*(9), 2075-2079.

Wang, J., Yang, S., Guo, D., Yu, P., Li, D., Ye, J., et al. (2009). Comparative studies on electrochemical activity of graphene nanosheets and carbon nanotubes. *Electrochemistry Communications, 11*(10), 1892-1895.

Wang, J., Zhao, D., Zhang, Y., Li, J., & Xu, C. (2014). A highly sensitive sensor for the detection of nitrite based on a nanoporous Fe_2O_3–CoO composite. *Analytical Methods, 6*(9), 3147-3151.

Wang, P., Jiang, T., Zhu, C., Zhai, Y., Wang, D., & Dong, S. (2010). One-step, solvothermal synthesis of graphene-CdS and graphene-ZnS quantum dot nanocomposites and their interesting photovoltaic properties. *Nano Research, 3*(11), 794-799.

Wang, Q., & Yun, Y. (2012). A nanomaterial composed of cobalt nanoparticles, poly (3, 4-ethylenedioxythiophene) and graphene with high electrocatalytic activity for nitrite oxidation. *Microchimica Acta, 177*(3-4), 411-418.

Wang, X., Adams, E., & Van Schepdael, A. (2012). A fast and sensitive method for the determination of nitrite in human plasma by capillary electrophoresis with fluorescence detection. *Talanta, 97*, 142-144.

Wang, X., Zhou, X., Yao, K., Zhang, J., & Liu, Z. (2011). A SnO_2/graphene composite as a high stability electrode for lithium ion batteries. *Carbon, 49*(1), 133-139.

Wang, Y., Song, B., Xu, J., & Hu, S. (2015). An amperometric sensor for nitric oxide based on a glassy carbon electrode modified with graphene, Nafion, and electrodeposited gold nanoparticles. *Microchimica Acta, 182*(3-4), 711-718.

Wen, W., Chen, W., Ren, Q.-Q., Hu, X.-Y., Xiong, H.-Y., Zhang, X.-H., et al. (2012). A highly sensitive nitric oxide biosensor based on hemoglobin–

chitosan/graphene–hexadecyltrimethylammonium bromide nanomatrix. *Sensors and Actuators B: Chemical, 166*, 444-450.

WookáLee, Y., & WooáHan, S. (2010). The direct growth of gold rods on graphene thin films. *Chemical Communications, 46*(18), 3185-3187.

Wu, H., Wang, J., Kang, X., Wang, C., Wang, D., Liu, J., et al. (2009). Glucose biosensor based on immobilization of glucose oxidase in platinum nanoparticles/graphene/chitosan nanocomposite film. *Talanta, 80*(1), 403-406.

Wu, J., Shen, X., Jiang, L., Wang, K., & Chen, K. (2010). Solvothermal synthesis and characterization of sandwich-like graphene/ZnO nanocomposites. *Applied Surface Science, 256*(9), 2826-2830.

Wu, L., Camacho-Alanis, F., Castaneda, H., Zangari, G., & Swami, N. (2010). Electrochemical impedance spectroscopy of carboxylic-acid terminal alkanethiol self assembled monolayers on GaAs substrates. *Electrochimica Acta, 55*(28), 8758-8765.

Wu, S., He, Q., Tan, C., Wang, Y., & Zhang, H. (2013). Graphene-based electrochemical sensors. *Small, 9*(8), 1160-1172.

Wu, S., Yin, Z., He, Q., Huang, X., Zhou, X., & Zhang, H. (2010). Electrochemical deposition of semiconductor oxides on reduced graphene oxide-based flexible, transparent, and conductive electrodes. *The Journal of Physical Chemistry C, 114*(27), 11816-11821.

Wu, S., Yin, Z., He, Q., Lu, G., Zhou, X., & Zhang, H. (2011). Electrochemical deposition of Cl-doped n-type Cu_2O on reduced graphene oxide electrodes. *Journal of Materials Chemistry, 21*(10), 3467-3470.

Wu, Z.-S., Ren, W., Wang, D.-W., Li, F., Liu, B., & Cheng, H.-M. (2010). High-energy MnO_2 nanowire/graphene and graphene asymmetric electrochemical capacitors. *ACS Nano, 4*(10), 5835-5842.

Xiang, Q., Yu, J., & Jaroniec, M. (2011). Enhanced photocatalytic H_2-production activity of graphene-modified titania nanosheets. *Nanoscale, 3*(9), 3670-3678.

Xu, C., Wang, X., & Zhu, J. (2008). Graphene−metal particle nanocomposites. *The Journal of Physical Chemistry C, 112*(50), 19841-19845.

Yan, J., Fan, Z., Wei, T., Qian, W., Zhang, M., & Wei, F. (2010). Fast and reversible surface redox reaction of graphene–MnO_2 composites as supercapacitor electrodes. *Carbon, 48*(13), 3825-3833.

Yan, J., Wei, T., Qiao, W., Shao, B., Zhao, Q., Zhang, L., et al. (2010). Rapid microwave-assisted synthesis of graphene nanosheet/Co_3O_4 composite for supercapacitors. *Electrochimica Acta, 55*(23), 6973-6978.

Yang, N., Zhai, J., Wang, D., Chen, Y., & Jiang, L. (2010). Two-dimensional graphene bridges enhanced photoinduced charge transport in dye-sensitized solar cells. *ACS Nano, 4*(2), 887-894.

Yang, S., Feng, X., Ivanovici, S., & Müllen, K. (2010). Fabrication of graphene-encapsulated oxide nanoparticles: towards high-performance anode materials for lithium storage. *Angewandte Chemie, 122*(45), 8586-8589.

Yang, S., Guo, D., Su, L., Yu, P., Li, D., Ye, J., et al. (2009). A facile method for preparation of graphene film electrodes with tailor-made dimensions with Vaseline as the insulating binder. *Electrochemistry Communications, 11*(10), 1912-1915.

Ye, D., Luo, L., Ding, Y., Chen, Q., & Liu, X. (2011). A novel nitrite sensor based on graphene/polypyrrole/chitosan nanocomposite modified glassy carbon electrode. *Analyst, 136*(21), 4563-4569.

Yen, H.-F., Horng, Y.-Y., Hu, M.-S., Yang, W.-H., Wen, J.-R., Ganguly, A., et al. (2015). Vertically aligned epitaxial graphene nanowalls with dominated nitrogen doping for superior supercapacitors. *Carbon, 82*, 124-134.

Yin, Z., Wu, S., Zhou, X., Huang, X., Zhang, Q., Boey, F., et al. (2010). Electrochemical deposition of ZnO nanorods on transparent reduced graphene oxide electrodes for hybrid solar cells. *Small, 6*(2), 307-312.

Yogeswaran, U., & Chen, S.-M. (2008). A Review on the electrochemical sensors and biosensors composed of nanowires as sensing material. *Sensors, 8*(1), 290.

Yu, A., Liang, Z., Cho, J., & Caruso, F. (2003). Nanostructured electrochemical sensor based on dense gold nanoparticle films. *Nano Letters, 3*(9), 1203-1207.

Yuan, W., Zhou, Y., Li, Y., Li, C., Peng, H., Zhang, J., et al. (2013). The edge-and basal-plane-specific electrochemistry of a single-layer graphene sheet. *Scientific Reports, 3*, 2248.

Yue, R., Lu, Q., & Zhou, Y. (2011). A novel nitrite biosensor based on single-layer graphene nanoplatelet–protein composite film. *Biosensors and Bioelectronics, 26*(11), 4436-4441.

Yusoff, N., Pandikumar, A., Huang, N. M., & Lim, H. N. (2015). Facile synthesis of nanosized graphene/Nafion hybrid materials and their application in electrochemical sensing of nitric oxide. *Analytical Methods, 7*(8), 3537-3544.

Yusoff, N., Pandikumar, A., Ramaraj, R., Lim, H. N., & Huang, N. M. (2015). Gold nanoparticle based optical and electrochemical sensing of dopamine. *Microchimica Acta, 182*(13-14), 2091-2114.

Zhang, D., Fang, Y., Miao, Z., Ma, M., Du, X., Takahashi, S., et al. (2013). Direct electrodeposion of reduced graphene oxide and dendritic copper nanoclusters on glassy carbon electrode for electrochemical detection of nitrite. *Electrochimica Acta, 107*, 656-663.

Zhang, H., Lu, H., & Hu, N. (2006). Fabrication of electroactive layer-by-layer films of myoglobin with gold nanoparticles of different sizes. *The Journal of Physical Chemistry B, 110*(5), 2171-2179.

Zhang, J., & Oyama, M. (2005). Gold nanoparticle-attached ITO as a biocompatible matrix for myoglobin immobilization: direct electrochemistry and catalysis to hydrogen peroxide. *Journal of Electroanalytical Chemistry, 577*(2), 273-279.

Zhang, L.-S., Jiang, L.-Y., Yan, H.-J., Wang, W. D., Wang, W., Song, W.-G., et al. (2010). Mono dispersed SnO_2 nanoparticles on both sides of single layer graphene sheets as anode materials in Li-ion batteries. *Journal of Materials Chemistry, 20*(26), 5462-5467.

Zhang, L., Zhang, Q., & Li, J. (2007). Layered titanate nanosheets intercalated with myoglobin for direct electrochemistry. *Advanced Functional Materials, 17*(12), 1958-1965.

Zhang, L., Zhao, G.-C., Wei, X.-W., & Yang, Z.-S. (2003). Electroreduction of oxygen by myoglobin on multi-walled carbon nanotube-modified glassy carbon electrode. *Chemistry Letters, 33*(2), 86-87.

Zhang, L. L., Zhou, R., & Zhao, X. S. (2010). Graphene-based materials as supercapacitor electrodes. *Journal of Materials Chemistry, 20*(29), 5983-5992.

Zhang, P., Zhang, X., Zhang, S., Lu, X., Li, Q., Su, Z., et al. (2013). One-pot green synthesis, characterizations, and biosensor application of self-assembled reduced graphene oxide–gold nanoparticle hybrid membranes. *Journal of Materials Chemistry B, 1*(47), 6525-6531.

Zhang, Q., Wei, W., & Zhao, G. C. (2008). Direct electrochemistry of myoglobin on a room temperature ionic liquid modified electrode and its application to nitric oxide biosensing. *Electroanalysis, 20*(9), 1002-1007.

Zhang, Q., Xie, C., Zhang, S., Wang, A., Zhu, B., Wang, L., et al. (2005). Identification and pattern recognition analysis of Chinese liquors by doped nano ZnO gas sensor array. *Sensors and Actuators B, 110*(2), 370-376.

Zhang, X.-Y., Li, H.-P., Cui, X.-L., & Lin, Y. (2010). Graphene/TiO_2 nanocomposites: Synthesis, characterization and application in hydrogen evolution from water photocatalytic splitting. *Journal of Materials Chemistry, 20*(14), 2801-2806.

Zhang, Y., Zeng, G.-M., Tang, L., Huang, D.-L., Jiang, X.-Y., & Chen, Y.-N. (2007). A hydroquinone biosensor using modified core–shell magnetic nanoparticles supported on carbon paste electrode. *Biosensors and Bioelectronics, 22*(9), 2121-2126.

Zhao, L., Liu, H., & Hu, N. (2006). Electroactive films of heme protein-coated multiwalled carbon nanotubes. *Journal of Colloid and Interface Science, 296*(1), 204-211.

Zhao, X., Mai, Z., Kang, X., Dai, Z., & Zou, X. (2008). Clay–chitosan–gold nanoparticle nanohybrid: Preparation and application for assembly and direct electrochemistry of myoglobin. *Electrochimica Acta, 53*(14), 4732-4739.

Zhou, H., Qiu, C., Liu, Z., Yang, H., Hu, L., Liu, J., et al. (2009). Thickness-dependent morphologies of gold on N-layer graphenes. *Journal of the American Chemical Society*, *132*(3), 944-946.

Zhou, K., Zhu, Y., Yang, X., Jiang, X., & Li, C. (2011). Preparation of graphene-TiO_2 composites with enhanced photocatalytic activity. *New Journal Chemistry*, *35*(2), 353-359.

Zhou, M., Zhai, Y., & Dong, S. (2009). Electrochemical sensing and biosensing platform based on chemically reduced graphene oxide. *Analytical chemistry*, *81*(14), 5603-5613.

Zhou, X., Huang, X., Qi, X., Wu, S., Xue, C., Boey, F. Y., et al. (2009). In situ synthesis of metal nanoparticles on single-layer graphene oxide and reduced graphene oxide surfaces. *The Journal of Physical Chemistry C*, *113*(25), 10842-10846.

Zhu, C., Guo, S., Fang, Y., & Dong, S. (2010). Reducing sugar: New functional molecules for the green synthesis of graphene nanosheets. *ACS Nano*, *4*(4), 2429-2437.

Zhu, J., Zhu, T., Zhou, X., Zhang, Y., Lou, X. W., Chen, X., et al. (2011). Facile synthesis of metal oxide/reduced graphene oxide hybrids with high lithium storage capacity and stable cyclability. *Nanoscale*, *3*(3), 1084-1089.

Zhu, Y., Murali, S., Cai, W., Li, X., Suk, J. W., Potts, J. R., et al. (2010). Graphene and graphene oxide: Synthesis, properties, and applications. *Advanced Materials*, *22*(35), 3906-3924.

LIST OF PUBLICATIONS AND PAPERS PRESENTED

Publications

1. **Marlinda, A.R**., Pandikumar, A., Jayabal, S., Yusoff, N., Suriani, A.B., & Huang, N. M., (2016). Voltammetric determination of nitric oxide using a glassy carbon electrode modified with a nanohybrid consisting of myoglobin, gold nanorods, and reduced graphene oxide. *Microchimica Acta*, *183:* 3077–3085.
2. **Marlinda, A.R**., Pandikumar, A., Yusoff, N., Huang, N. M., & Lim, H.N., (2015). Electrochemical sensing of nitrite using a glassy carbon electrode modified with reduced functionalized graphene oxide decorated with flower-like zinc oxide. *Microchimica Acta*, *182:* 1113–1122.

Paper presented in international conference

1. **Marlinda, A.R**., Pandikumar, A., Yusoff, N., Huang, N. M., & Lim, H.N., (2015). "Electrochemical sensing of nitrite using a glassy carbon electrode modified with reduced functionalized graphene oxide decorated with flower-like zinc oxide" in *International Conference On Recent Advances In Materials And Chemical Sciences*, 14-15 December 2015, Department of Chemistry, Gandhigram Rural Institute, Dindigul District, Tamil Nadu, India. **(Poster Presentation)**.